Inaugural-Dissertation

zur
Erlangung der Doktorwürde
der
Naturwissenschaftlich-Mathematischen Gesamtfakultät
der
Ruprecht-Karls-Universität
Heidelberg

vorgelegt von
Master of Engineering Tomohiro Hayashi
aus Tokyo
Tag der mündlichen Prüfung: 26. Mai 2003

Computer simulations of water near model organic surfaces: interfacial behavior and hydration forces

Gutachter: Prof. Dr. Michael Grunze
Prof. Dr. Joachim P. Spatz

Contents

Introduction

Water is the most abundant compound on earth, existing naturally in the forms of vapor, liquid and solid. Seventy per cent of the surface of the planet is covered by oceans. In addition, living tissue is composed mainly of water, and cells, organs, and organisms are constantly bathed in an aqueous environment. Without water, many chemical reactions could not take place, and biological systems would not function. Thus, it is clear that without a fundamental and detailed knowledge of water, many phenomena in nature would be difficult if not impossible to understand.[1-6]

Compared to other molecules with similar molecular weight, water has an unusually high heat capacity, interfacial tension, cohesive energy, and dielectric permittivity, as well as exceptionally high melting, boiling, and critical temperatures. The origin of the unusual properties of water is a unique combination of its small molecular size with strong and highly oriented intermolecular interaction due to hydrogen bonding.[7,8] A manifestation of this interaction in water is a specific short-range order, which is characterized by a distorted tetrahedral arrangement with a coordination number not too far away from four.[9] The strong orientation dependence of the water-water interactions complicates substantially the theoretical treatment of water, for instance, in terms of the well-developed theories of simple liquids.[10]

The behavior of water near solid surfaces is one of the most challenging aspects of its physico-chemical behavior. The interest in this area of water science is mainly associated with forces that operate between surfaces and colloid particles in water.[3,4,11-13] These forces play an important role in colloid chemistry, biology and other areas. In particular, they are responsible for colloidal stability, micelle formation, biomembrane fusion, and the resistance of surfaces to protein adsorption.[3,12,14-17]

A first explanation of the water-mediated forces was given by the DLVO theory in terms of direct van der Waals attraction between the surfaces and screened electrostatic mean-field repulsion between ions adsorbed on or concentrated near the surfaces.[18] As the experimental techniques for measuring surface forces become available, forces of different nature have been found. These non-DLVO forces, which are usually referred as hydration forces, have nothing to do with the presence of ions and so they would occur even in ideally deionized water. The source of hydration forces is the surface induced changes in the structure and density of the adjacent water. Hydrophobic surfaces usually attract each other in water, whereas hydrophilic ones show water-mediated repulsion. For this reason, the attractive and repulsive water-mediated forces are frequently referred to as “hydrophobic attraction” and “hydrophilic repulsion”, respectively.[3]

The focus of the present work is on organic surfaces, whose interaction with water is of particular interest in biology and biomedical applications. Ideal models for studying organic surfaces are provided by self-assembled monolayers (SAMs), as formed by chemisorption of long-chain organic molecules on the surface of solid substrates. Unlike most organic compounds, whose surfaces suffer from chemical and structural imperfection, SAMs possess stable and controllable surface chemical functionality and a nearly perfect surface structure. In addition to being good models of organic surfaces, SAMs are promising systems for practical use in chemical sensing, thin-film non-linear optics, biocompatibility, and lithography.[19-22] Of direct relevance to the interaction of water with SAMs is the outstanding resistance of some of them to adsorption of proteins from aqueous solutions.[23] This resistance is frequently ascribed to a specific surface-induced water structuring leading to the water-mediated repulsion of protein from the SAM surface. The best protein resistance is exhibited by alkanethiol SAMs terminated by oligo-ethylene glycol (OEG) moieties. The interest in these particular SAMs is further stimulated by a strong dependence of their protein resistance and water-mediated interaction on the substrate used.[24,25] Thus, the Au-supported SAMs repel each other in water, whereas the SAMs on Ag show attraction. Also, the SAMs prepared on Au are resistant to protein adsorption, while those on Ag are not. The existence of these differences offers a good opportunity to gain a better insight into the nature of protein resistance.

Unfortunately, experimental studies of the interfaces formed by water and organic surfaces in general and SAM surfaces in particular involve serious difficulties, which arise eventually from an extremely small thickness of the interfacial region. This imparts importance to the methods of computer simulation, which allow direct modeling of the interface based on the principles of statistical mechanics and an assumed form of the water-water and water-surface interaction potentials. Despite a large body of literature on computer simulation of water in contact with solid surfaces, the number of simulations concerned with water-mediated forces is very limited. The reason has to do with the necessity of simulating an open confined system that is allowed to exchange molecules and is in chemical equilibrium with a bulk water reservoir. The standard molecular dynamics (MD) technique is not well suited for such simulations because it requires an explicit simulation of both confined water region and the bulk water reservoir. In this respect, the Monte Carlo technique in its grand canonical ensemble version (hereafter, GCMC) has a great advantage because the bulk water reservoir is present in it implicitly.[26] An alternative to the GCMC technique is provided by isotension ensemble Monte Carlo (IEMC) simulations.[27] Unlike GCMC, where the density fluctuations are simulated through particle insertion and deletion attempts, the IEMC technique implements density fluctuations by allowing area fluctuations parallel to the confining walls at a fixed lateral pressure. A disadvantage of the IEMC technique is that it cannot be applied to simulation of water near structured organic substrates because the area fluctuations are inconsistent with the condition that the lateral dimensions of the simulation cell must be commensurate with the substrate lattice.

All of the few reported simulations of water-mediated forces were concerned with ideally smooth, structureless surfaces, such that the water-surface interaction potential was independent of the lateral position of the water molecule over the surface. Nearly all of these simulations dealt with hydrophobic attraction.[28,29] Thus, Wallqvist and Berne used the MD technique to simulate the hydration force between two large hydrophobic ellipsoids interacting with water through a repulsive inverse power potential.[30] The simulations were restricted to very short separations: The largest width of the slit between the ellipsoids was about 10 Å. As the ellipsoids were moved together, an oscillating hydration force was observed, until the constrained water between the ellipsoids underwent capillary evaporation (cavitation) leading to attraction between the ellipsoids due to the pressure imbalance. The interpretation of hydrophobic attraction in terms of capillary evaporation (or “drying”) can also be found in recent publications by Chandler and *et al.*.[31] By contrast, the IEMC simulation by Forsman *et al.* of water confined between two hard walls at separations ranging from 10 to 23 Å revealed a strong hydrophobic attraction due to a density depression between the walls, with no cavitation observed.[29] Similar results were obtained in an early study by Luzar *et al.* for a simple one-site model of water confined between hard walls.[32]

To the best of our knowledge, the only published computer simulation of hydration forces on hydrophilic surfaces is the one reported by Forsman *et al.*.[33] The water-surface interaction potential comprised a short-range exponential attractive term and an inverse 9-th power repulsion term. An orientation dependent potential was also tried, which included an additional term proportional to the cosine of the angle between the molecular dipole moment and the surface normal. The authors concluded that the hydration force was mainly determined by the range of the water-surface potential: A strong repulsion was only observed when the potential decay length was greater than about half the molecular diameter. The inclusion of the orientation dependent term in the potential made the hydration interaction more repulsive, though this effect was asserted to be of minor importance.

The fewness and limitations of the above discussed simulation studies of water-solid interfaces have given impetus to the work described in the subsequent chapters. This work extends the computer simulations of water-solid interfaces in the following directions. First, the simulations of hydration forces between structureless surfaces are extended to the range of large wall-to-wall separations (4 nm and more), where the oscillations of the hydration force have decayed and the sign of the hydration force reflects the thermodynamic affinity of the walls for water. Both hydrophobic and hydrophilic walls will be considered. Similar to the Forsman's *et al*. study, the walls will be described using both non-orienting and orienting potentials. In the latter case, however, more realistic potentials, which reflect the preference of water for tetrahedral hydrogen bonding coordination, will be used, including potentials which model proton-acceptor surfaces and also surfaces bearing both proton acceptors and proton donors in equal amounts. In this way, the most important types of organic surfaces will be covered. For each particular surface type, several discrete values of the potential well depth will be tried to follow the effect of the surface-water interaction strength on the hydration force. In addition to changes in the hydration force, the behavior of various distribution functions and order parameters will be monitored to see how the changes in the water-surface interaction potential affect the structure of the adjoining water layers. Of particular interest will be the behavior of the average density of confined water. Since the position of a water molecule close to a hydrophilic surface is favorable, it can intuitively be expected that the average water density between two such surfaces will be always enhanced. Reciprocally, the average water density between two hydrophobic surfaces can be expected to be always depressed.

The simulation studies of water-solid interfaces will be further extended to cover structured organic surfaces, as formed by OEG terminated alkanethiol SAMs on the surface of gold and silver. The chains constituting the SAMs will be treated in the full-atom representation, with all conformational degrees of freedom, except for bond lengths, considered as variables. As far as we know, this is the first computer simulation of a so complicated interfacial system formed by water and organic surfaces. The simulations will be preceded by a test of the atomistic force field describing the interaction of water with OEG terminated OEG molecules. The test will be accomplished through a comparison of the force field results for the OEG-water binding energy with the respective predictions of *ab initio* electronic structure calculations based on density functional theory (DFT).[34] The results of our computer simulations of the SAM-water interface will be discussed in the context of the experimentally observed differences in surface force behavior and protein adsorption properties between the gold and silver supported SAMs.

The structure of the thesis is the following. **Chapter 1** represents a literature overview of the experimental and theoretical work on water-solid interfaces. The emphasis is placed on hydration forces and protein adsorption, mainly in relation to OEG terminated alkanethiol SAMs. An analysis of the terminology used in the literature in characterizing the affinity of solid surfaces for water is also presented to avoid ambiguities involved in the terms “hydrophilic” and “hydrophobic”. **Chapter 2** provides a full account of the simulation method used in our work. It includes both the fundamentals of the GCMC technique and some specific details associated with the particular systems studied in our work. **Chapter 3** describes the force fields used in our simulations to evaluate the potential energy of the system as a function of its configuration. New analytical potentials are introduced, which mimic the hydrogen bonding of water to structureless surfaces bearing proton acceptors, proton donors or both. The test of the OEG-water potentials against *ab initio* DFT results is also included in this chapter. **Chapter 4** comprises two parts. In the first part, we present our simulation results for bulk water, which are then used as a reference in the subsequent simulations of confined water. In the second part of the chapter, the simulations results for structureless surfaces are described and discussed. **Chapter 5** is devoted to the investigation of the behavior of water near the OEG terminated SAMs on the gold and silver substrates. Based on the simulation results, a likely explanation of the effect of substrate on the properties of the SAMs is put forward. The last section of the thesis, **Conclusions**, summarizes and generalizes the results of our work.

Chapter 1: Water-solid interfaces. A literature review.

Interfacial phenomena concerning water and surfaces have been of interest for a long time.[2,3,11,14] Water near a surface differs from that in the bulk phase, both thermodynamically and molecularly. There exists a thin transition zone which makes a small but sometimes perceptible contribution to the mechanical, thermodynamic, and chemical behavior of the system. In subsequent sections, we introduce previous works investigating the interfacial behavior of water. Although our interests are focused mainly on the works with the methods of computer simulation, several examples of comparison of simulation and experimental results are also discussed.

1.1 “hydrophobic” and “hydrophilic”

As far as the interaction of solid surfaces with water will be concerned, we will inevitably have to employ the terms "hydrophilic" and "hydrophobic". Despite the widespread use of these terms in surface science, colloid chemistry, biology, and other areas, their meaning involves ambiguity because of the lack of a well-defined and commonly accepted criterion that distinguishes surfaces into hydrophilic and hydrophobic. For a detailed analysis of the hydrophilic/hydrophobic terminology, we refer the reader to a recent review by Vogler[3] and here we only make few comments necessary to avoid confusion in the subsequent discussion.

The customary understanding of the terms hydrophilic and hydrophobic is associated with the strength of the interaction of a surface, colloid particle or solute with water. Thus, "hydrophilic (hydrophobic) solute" is usually understood as a solute which attracts water molecules more (less) strongly than water molecules attract one another. A similar criterion is frequently applied to surfaces: A surface is referred to as being hydrophilic (hydrophobic) if it is capable (incapable) of forming strong hydrogen bonds with water. It is clear, however, that the hydrogen bond strength is not the only factor responsible for the affinity of the surface for water. Equally important are the areal density, lateral arrangement, orientation, and flexibility of the surface groups involved in the hydrogen bonding with water. Similar arguments apply to hydrophobic surfaces, whose effect upon the adjacent water may substantially differ from that of small hydrophobic solutes.[31]

A thermodynamically sound criterion for the hydrophilicity of a surface is the condition that the water-surface interfacial tension, γ_{ws}, is negative, *i.e.* that an increase in the area of the water-surface interface lowers the free energy of the system. The criterion for hydrophobicity is opposite: $\gamma_{ws} > 0$. To relate γ_{ws} to the hydration pressure, p_h, consider two parallel plates of an area A, which are immersed in a water reservoir of volume V and held in equilibrium at a separation H apart by an external force f (**Figure 1-1**).[35] The hydration pressure experienced by the plates can be expressed in terms of the tension of the water film between the plates, γ. If the system is treated using the grand canonical ($\mu VT = \text{const}$) ensemble, then $\gamma = \Delta\Omega/A$, where $\Omega = U - TS - \mu N$ is the grand potential and Δ denotes the difference between the systems with and without plates. The hydration pressure is then given by differentiation, $p_h = -(\partial\gamma/\partial H)_{\mu T}$.[35] When the surfaces are in contact ($H = 0$), there is no water tension, $\gamma(0) = 0$, while at $H \rightarrow \infty$, $\gamma(H) \rightarrow 2\gamma_{ws}$. If $\gamma_{ws} < 0$ and γ is a monotonic function of separation, then $p_h > 0$, *i.e.* the plates repel each other. That is the hydrophilicity criterion $\gamma_{ws} < 0$ is equivalent to the condition that p_h is repulsive. Similarly, the hydrophobicity criterion $\gamma_{ws} > 0$ reduces to the condition that p_h is attractive.

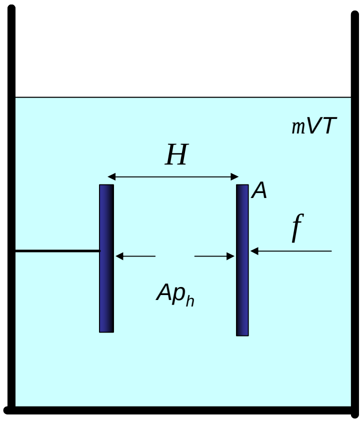

Figure 1-1 System of two parallel plates of area *A*, which are immersed in water and repel each other with force Ap_h ; p_h is the hydration pressure and at a given separation *H* apart.

At short separations, the monotonicity of $\gamma(H)$ can be violated due to water layering effects, which may lead to oscillations in p_h.[12] In this case, however, the sign of p_h can still be used as a hydrophilicity/hydrophobicity criterion provided that H is large enough for the oscillations in p_h to decay.[i]

Based on an analysis of the available surface force literature, Vogler[3] suggested to include the reference to the sign of p_h in the definition of hydrophilicity and hydrophobicity. Considering however that the true hydration contribution to the surface force may be masked by forces due to the presence of ions and impurities, p_h can hardly serve as a practical criterion for hydrophilicity/hydrophobicity. By contrast, it can well be used as such a criterion in computer simulations, which deal with ideally pure and ion-free water.

The hydration pressure can also be related to the water contact angle, θ, based on the Young equation, $\gamma_{wv}\cos(\theta) = \gamma_{sv} - \gamma_{ws}$, where the subscript "$v$" refers to water vapor. When employing θ or the so-called "adhesion tension" $\gamma_{wv}\cos(\theta)$ as a hydrophilicity/hydrophobicity criterion, the dividing line between hydrophilic and hydrophobic is usually taken to be $\theta = 90°$ or $\gamma_{wv}\cos(\theta) = 0$ (see Vogler's review[3] for discussion of alternative choices), which corresponds to the null change in free energy upon immersing the surface in water. The offset of this dividing line from that based on γ_{ws} or p_h is equal to γ_{sv}. Since γ_{sv} is always positive, the hydrophilicity/hydrophobicity criteria based on θ and $\gamma_{wv}\cos(\theta)$ overestimate the surface's hydrophilicity compared to the γ_{ws}- and p_h-based criteria: In the interval $0 < \gamma_{wv}\cos(\theta) < \gamma_{sv}$, θ and $\gamma_{wv}\cos(\theta)$ show that the surface is already hydrophilic, while it is still hydrophobic from the viewpoint of γ_{ws} and p_h ($\gamma_{ws} > 0$, $p_h < 0$). In this interval, the terms "hydrophilic repulsion" and "hydrophobic attraction" make no sense if the hydrophilicity/ hydrophobicity of the surface is understood in terms of the water contact angle.

---

[i] As shown by Besseling[36] in his mean-field lattice theory of hydration forces, $\gamma(H)$ may have a extremum regardless of the presence of layering effects. Such a situation, which does not allow the use of p_h as a hydrophilicity/hydrophobicity criterion at long separations, can however be readily recognized both in real and computer experiments.

The occurrence of an offset between the different hydrophilicity/hydrophobicity criteria can well seen in the plot discussed by Vogler,[3] where the characteristic decay length of surface force for partially silanized silica was depicted as a function of θ. In this plot, the change-over from attractive to repulsive forces occurred at $\theta \cong 62°$ ($\gamma_{wv}\cos(\theta) = 34$ dyn cm^{-1}). That is in the range between 62° and 90° the surface was hydrophilic with regard to θ, while being hydrophobic with regard to p_h. Similar examples were found by Besseling[36] in his theoretical treatment of hydration forces.

In the simulations described in the following sections, the direct interaction between the constraining walls is neglected, so that no work is required to spread the walls in vacuum from contact to infinity. Hence the term γ_{sv} in the Young equation vanishes. That is for the walls studied in our work, the hydrophilicity/hydrophobicity dividing lines based on p_h and θ are coincident.

1.2 The properties of water at water-solid interfaces

In computer simulations, it is impossible to simulate an infinity thick water layer in contact with a solid surface. One possible solution is to confine water at the top with a hard wall. In this case, however, the behavior of water at the interface may be distorted by the structuring effect of the wall.[37,38] Therefore, in most studies, simulation cells were mirrored at the top of the cell or water was confined between two surfaces. To the best of our knowledge, the first computer simulation of water between hard walls was initiated by Joensson[39] and Marchesi[40]. They used the Monte Carlo (MC) technique and MYC water model[41] and the molecular dynamics (MD) method with the ST2 water model[42], respectively. These authors found that there exists a preferential orientation of the molecules at the interfaces. Lee *et al.* also employed the ST2 model to represent water near idealized hydrocarbon walls.[43] In their work, the liquid structure nearest the surface was characterized by “dangling” hydrogen bonds, giving a good agreement with the results of Sum Frequency Generation (SFG) measurements[44,45].

The first MD simulation of water in close proximity to a polar interface was reported by Kjellander *et al.*.[46] They showed that electric fields associated with discrete surface charges strongly orient neighboring water molecules and weaken the hydrogen bond network. Later, Lee *et al.* simulated water in contact with a fully hydrated silica surface.[47] In their work, it was found that the surface-water bond is stronger than the interactions in the bulk. As a result, distinct structural perturbation of the water extends up to 10 Å from the surface. The perturbed hydrogen bond network at water-solid interfaces is also confirmed by other computer simulations.[47,48] To sum up the above studies, the common conclusion is that water-water interaction at the interfaces is perturbed due to the loss of hydrogen bonding between water molecules, and the increase of the energy is partly compensated by reorientation of adjacent water molecules. As a result, there exists a preferential orientation of the water molecules in the vicinity of the surface (even near a hard wall[40]).

The change in water density at solid-water interface is also an important issue to understand the effect of a surface on the interfacial behavior of water. As to experimental investigations studying the density profile of water in vicinity of a surface, we can find only two publications. Cheng *et al*. reported the water density profiles as a function of a distance from an atomically flat mica surface using the X-ray reflectivity technique.[49] The authors observed the oscillations in water oxygen density at a water-mica interface in the surface-normal direction, giving the evidence of the interfacial water (**Figure 1-2**). The oscillation of the oxygen density extends only to 10 Å and do not strictly maintain a solvent-size periodicity, suggesting that the effect of the solid surface on water structure vanishes within a few molecular layers. Recently, neutron reflectivity measurements by Schwendel *et al*. revealed the water density depletion near hydrophobic surfaces.[50]

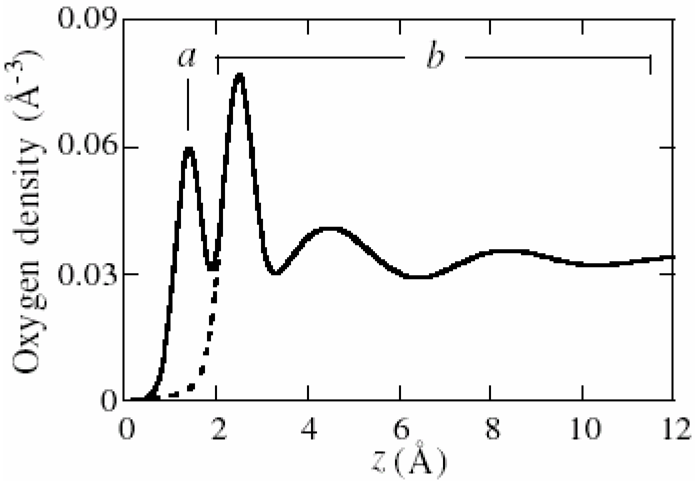

Figure 1-2 Derived density profile of interfacial water near the mica-water interface by Cheng *et al.*. The first and second peaks are adsorption and hydration layer, respectively.[49]

As to the first density profiles of water in vicinity of solid surfaces obtained with computer simulations, we refer the reader to the work of Joensson *et al.* again.[39] The authors reported that oscillatory density profiles were observed between two surfaces and water density was depressed near the hard wall. Later, similar results were obtained in several other simulations.[32,40,43,48]. Unfortunately, these were performed at rather small wall-to-wall separations (below 20 Å) and water formed a layered-structure due to the packing effect. Therefore it makes no sense to compare these results with the experimental results[49,50]. Recent several computer simulations of water near solid surfaces were carried out with a relatively large wall-to-wall separation (40 Å ~ 60 Å).[28,47,51-54] The important finding is, that the propagation length of the density oscillation from the surface into bulk is only 10-12 Å, although there is local density enhancement (depletion) near hydrophilic (hydrophobic) surfaces, giving an agreement with the experimental results by Cheng *et al.*[49].

1.3 Hydration forces

Although indirect, the force between solid surfaces in water provides information of interfacial properties of water as reviewed by Israelachvili[12,14,55] and Vogler.[3] The first attempt to measure force between solid surfaces immersed in water was performed by Israelachvili *et al.*[56] They investigated the forces between molecularly smooth mica surfaces in aqueous electrolyte solutions at different ion concentrations. At low ion concentrations, the forces were well described by the Poisson-Boltzmann equation for two double-layers interacting at constant surface potential. On the other hand, at high ion concentrations, an additional repulsive force, which is independent of the type and concentration of electrolyte, was observed. This is the first evidence of the force that cannot be explained by the DLVO theory[18]. Later, they found that forces at small surface-to-surface separations oscillate with a molecular diameter of a water molecule (about 2.5 Å).[12,55] Their results suggested that the confined water molecules form a layered-structure at small separations.

With further development of the surface force studies of water, it was found that the sign and magnitude of the forces correlate well with the wettability of the surface, *i.e.* hydrophobic surfaces attract each other in water,[57,58] while hydrophilic ones interact repulsively.[59,60] By analyzing the correlation between water contact angles and the forces, Vogler found that the forces change from attractive to repulsive at water contact angle around 65° (**Figure 1-3**). The author suggested that hydration force can serve as a practical criterion for hydrophilicity/hydrophobicity.[3]

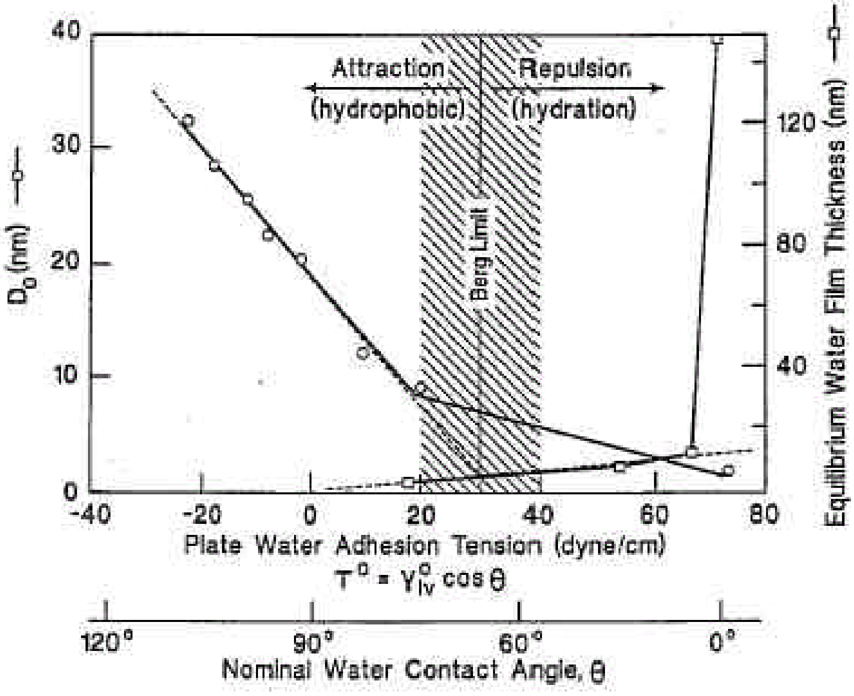

Figure 1-3 Decay length of surface forces measured by surface force apparatus as a function of water adhesion tension and water contact angle.[3]

As mentioned in the introductory part, there are only a limited number of theoretical studies on hydration forces between two plates, and most of the literature on hydration forces dealt with hydrophobic attractions. There have mainly two interpretations of hydrophobic attraction been suggested, *i.e.* one is the interpretation in terms of "drying" or "capillary evaporation", and the other is attraction due to the depletion of water density. Lum *et al.* suggested from the analysis of free energy of the system with mean field theory that the confined water between two hydrophobic plates experiences drying provided that the wall-to-wall separation is below a critical value.[31] The drying phenomenon was observed in the MD simulations by Wallqvist *et al.* considering with two large hydrophobic ellipsoids interacting with water through a repulsive inverse power potential.[30] Unfortunately, the simulations were restricted to very short separations (below 10 Å). Nevertheless, they observed an oscillating hydration force at the separation above 3.5 Å, and capillary evaporation at smaller separations. They also found that the entropic part is dominant in the change of free energy, which determines the sign and magnitude of hydration force.

On the other hand, the interpretation of hydrophobic attraction in terms of depletion of water density is suggested by Yaminsky *et al.*[61] Their studies applying modified classical nucleation theory showed that hydrophobic attraction or hydrophilic repulsion is explained by fluctuation of water density. A similar interpretation can also be found in publications by Forsman *et al.*[28,29] Both density functional theory and MC simulations using the isotension ensemble showed that the density depression in the slit gives rise to a strong attractive interaction exceeding the standard van der Waals force by an order of magnitude.

As to hydration forces acting between hydrophilic surfaces, Besseling investigated the relationship between the water-surface interaction strength, hydration pressure, and average density in his treatment of hydration forces, based on a kind of self-consistent field lattice theory.[36] Despite the well-known weaknesses of lattice theories in describing the properties of liquids, Besseling's calculations provide good qualitative examples of how water structuring may affect the hydration pressure. It was found, in particular, that two parallel confining surfaces, which were hydrophilic from the viewpoint of the water-surface interaction energy and the density of the surface interaction sites, might exhibit, along with an expectedly enhanced adsorption of water, an attractive hydration force. This was observed with surfaces which beared an equal number of proton donors and proton acceptors. Such surfaces affected mainly the local density near the wall, while retaining the orientational distribution of water molecules unchanged. Repulsive hydration forces were only observed with surfaces that carried either proton donors or proton acceptors only. These surfaces induced orientational ordering in the adjoining water layers, thereby disturbing the typical hydrogen bonding network of bulk water.

To the best of our knowledge, the only published computer simulation of hydration forces on hydrophilic surfaces is the one reported by Forsman *et al.* [33] using the SPC water model[62]. The water-surface interaction potential comprised a short-range exponential attractive term and an inverse 9-th power repulsion term. An orientation dependent potential was also tried, which included simply an additional term proportional to the cosine of the angle between the molecular dipole moment and the surface normal. Although their simulation results of hydration force suffer from statistical noise at large separations (in the separation interval (10 Å < H <15 Å)), the authors concluded that the hydration force was mainly affected by the range of the water-surface potential at short separations (below 10 Å): A strong repulsion was only observed when the potential decay length was greater than about half the molecular diameter. The inclusion of the orientation dependent term in the potential made the hydration interaction more repulsive, though this effect was found to be of secondary importance.

1.4 Surfaces resistant to protein adsorption

The resistance of surfaces coated with poly(ethylene glycol) (PEG) towards non-specific protein and cell adsorption has been explained by the “steric repulsion” theory,[63] which associates the inertness of the polymer brushes with their high conformational freedom and with the unfavorable free energy change of the system when the polymer brushes are compressed and dehydrated. This perception is, however, challenged by the ability of oligo(ethylene glycol) (OEG) terminated alkanethiol self-assembled monolayers (SAMs), because the surfaces are not very hydrophilic and comprise densely packed molecules with constrained conformational freedom.[23]

The interesting feature of methoxy tri(ethylene glycol) (EG3-OMe) terminated alkanethiol SAMs is a strong dependence of their protein resistance on the substrate used.[24] The IR measurements by Harder *et al.* revealed that SAMs exhibiting an the helical or amorphous conformation of the oligo(ethylene oxide) moiety EG part, which forms on gold surfaces, showed protein resistance, whereas the more densely packed planar phase, which is observed on silver, adsorbed up to 60 % of a monolayer of fibrinogen.[24]

To explain the dependence of protein resistance on the substrate, Wang *et al.* studied the interaction of water with OEG moieties in the helical and the planar "all-trans" conformations based on *ab initio* calculations.[64] They found that the helical conformation adsorbs water strongly and serves as a template for water, whereas the all-trans conformation interacts only weakly with water molecules. Based on this result, they speculated that the stability of the water interface with helical OEG prevents proteins and other molecules from adsorbing irreversibly on the OEG surface.

To acquire direct information of the interaction between the SAMs and protein molecules, Feldmann *et al.* employed the atomic force microscope (AFM) technique. In their work, the AFM tip was covered with fibrinogen molecules. A long-range repulsion was observed for gold-supported SAMs and a short-range attractive force was observed between protein and silver-supported SAMs. Further AFM measurements were performed by Dicke *et al.*[65] They measured the force between EG3-OMe terminated alkanethiol SAMs on gold and hydrophobic probes in solution with different electrolytes. Their results showed that there is no difference in the decay length in the force-distance curves for different electrolytes. In addition, they measured the interaction of a gold-supported EG3-OMe SAM with positively (AlO_x) and negatively (Si_3N_4) charged AFM tips and concluded that the surface of the SAM is negatively charged.[66] The authors also measured the force-distance curves at different pH values and found the strong dependence of the force on pH values. That is, long-range repulsive forces were observed at high pH values and the force vanished, with decreasing pH. At $pH < 4.4$, the repulsive interaction turned from repulsive to attractive. Their results imply that the origin of the long range repulsion between EG3-OMe and the hydrophobic probe comes from electrostatic interaction between hydroxide ions adsorbed on the surfaces and not from the interaction between electrolytes adsorbed on the SAM and AFM tip.

The presences of negative surface charges on the SAM were recently confirmed with electrokinetic measurements by Chan *et al*..[67] The zeta potentials measured on EG3-OMe SAMs, both on gold and glass substrates, indicate preferential hydroxide ion adsorption from the aqueous phase resulting in a net negative surface charge at pH > 4. In addition, the authors showed that EG3-OMe SAMs are not unique in exhibiting preferential hydroxide ion adsorption. Although the preferential hydroxide ion adsorption was found also on octadecanethiol and mercaptoundecanol SAMs formed on gold, these SAMs interact with the hydrophobic AFM tip in an aqueous environment quite differently from gold-supported EG3-OMe SAMs. To answer this question, Kreuzer *et al*. proposed a model based on *ab initio* calculation using density functional theory.[68] The authors reported that water molecules trapped in the EG chains form hydrogen bonds with the hydroxide ions concentrated at the SAM-water interface and reduce their mobility, as a result, the surface repels a negatively charged hydrophobic tip or protein molecules due to electrostatic repulsion. On the other hand, hydroxide ions on SAMs that are not penetrable for water are mobile and easily displaced. In such cases, other forces, such as hydration forces or van der Waals attraction, becomes dominant, as a consequence, these surfaces attract the AFM tip and adsorb protein molecules.

Chapter 2: Simulation method

The simulations described in the subsequent chapters were all carried out using the Monte Carlo (MC) technique. Unlike the more widely used molecular dynamics (MD) method, which simulates the movement of a system along the phase trajectory by direct solution of Newton’s equations of motion, the MC technique represents in fact a mathematical method for evaluation of thermodynamic averages by judiciously sampling a sequence of trial configurations in the configurational space. The key advantage of the MC technique is that the moves of particles in the system need not be physical (*i.e.* satisfying the classical equation of motion), which provides a lot of freedom for organization of efficient sampling. The possibility of using non-physical moves is of particular importance for the systems studied in the present work. Thus, in sampling the trial configurations of the SAMs, the dimensionality of the problem can be substantially reduced by treating the bond lengths of their constituent molecules as rigid. The use of non-physical “rotational displacement” coordinates (Sect. 2.2.1) allows the implementation of the bond length constraints in a much easier and computationally cheaper way compared to what is practiced in MD simulations.[26] Even more important is that the MC technique allows non-physical creation and deletion (annihilation) moves. This makes it possible to simulate fluctuations of density, as occur in open confined systems considered in our study.

2.1 Thermodynamic averages

For a closed system (N = const) at a constant temperature and volume, the evaluation of thermodynamic quantities is reduced to calculation of ensemble averages of the form

$$\langle f \rangle_{NVT} = Q^{-1} \int_{\Omega} f(q) \exp\left(-\frac{U(q)}{kT} \right) dq \qquad (2.1)$$

In this equation U is the potential energy of the system at configuration q, and Q is the so-called configurational integral,

$$Q = \int_{\Omega} \exp\left(-\frac{U(q)}{kT} \right) dq \qquad (2.2)$$

The choice of $f(q)$ in eq. (2.1) depends on what particular thermodynamic quantity is to be calculated. Thus, for evaluation of the internal energy E, one needs to calculate the average potential energy $\langle U \rangle$, which is calculated from eq. (2.1) by setting $f(q) = U(q)$. For a system containing N particles with three translational and three rotational degrees of freedom, q represents a $6N$-dimensional vector and $\Omega = \left(8p^{2}V\right)^{N}$.

In principle, the integrals in eqs. (2.1, 2.2) can be calculated by randomly sampling a sequence of k trial configurations $q^{(m)}$ in Ω and then averaging the respective integrands,

$$Q = \frac{1}{k}\sum_{i=1}^{k} \exp\left(-\frac{U(q^{(m)})}{kT}\right); \ \langle f \rangle_{NVT} = \frac{1}{Q}\frac{1}{k}\sum_{i=1}^{k} f(q^{(m)}) \exp\left(-\frac{U(q^{(m)})}{kT}\right). \tag{2.3}$$

Such a calculation method is however highly inefficient because the overwhelming majority of the randomly sampled configurations $q^{(m)}$ will have a too high potential energy and hence a negligible statistical weight. To improve the sampling efficiency, $q^{(m)}$ should be preferentially sampled in low-energy regions of Ω, which provide the major contribution to the ensemble averages and are hence of most importance. Sampling methods improved in such a way are usually referred to as the importance sampling methods. One of possible implementations of importance sampling is to sample the trial configurations with a probability proportional to the probability density distribution

$$r_{NVT}(q) = Q^{-1} \exp\left(-\frac{U(q)}{kT}\right) \tag{2.4}$$

2.2 Markov chains and the Metropolis method

A sequence of random configurations $q^{(m)}$ distributed in the configurational space with the probability density distribution r_{NVT} is usually generated in the form of a Markov chain, so that every consecutive configuration $q^{(m+1)}$ depends only on the previous one, $q^{(m)}$. Consider two arbitrary configurations, $q^{(m)}$ and $q^{(n)}$, with the associated probabilities r_m and r_n. The configurations are linked by the transition probability p_{mn}, which represents the probability of going from configuration m to n. The transition probability satisfies the conditions

$$\sum_m r_m p_{mn} = r_n \ , \tag{2.5}$$

$$\sum_n p_{mn} = 1 \qquad . \tag{2.6}$$

To construct a sequence of states such that $r_m = r_{NVT}\left(q^{(m)}\right)$, it is useful (though not necessarily) to impose on p_{nm} the condition of 'microscopic reversibility'.[26]

$$p_{mn} r_m = p_{nm} r_n \tag{2.7}$$

With this condition we regain Eq.(2.5),

$$\sum_m r_m p_{mn} = \sum_m r_n p_{nm} = r_n \sum_m p_{nm} = r_n \ . \tag{2.8}$$

In typical Monte Carlo simulations, p_{mn} is taken to be in the form

$$p_{mn} = a_{mn} f_{mn} \, , \tag{2.9}$$

where a_{mn} is the probability of attempting a certain move and f_{mn} is the probability of accepting that move. Combining Eqs. (2.7) and (2.9) gives

$$\frac{f_{mn}}{f_{nm}} = \frac{a_{nm} r_n}{a_{mn} r_m} \ . \tag{2.10}$$

To insure that this condition is satisfied, Metropolis *et al.* employed a condition equivalent to

$$f_{mn} = \min\left(1, \frac{f_{mn}}{f_{nm}}\right).\text{(Ref. 69)}. \tag{2.11}$$

In practice, the evaluation of the ratio f_{mn}/f_{nm} reduces to calculation of the energy change $\Delta U_{nm} = U(q^{(n)}) - U(q^{(m)})$ associated with the transition from a given configuration *m* to a trial configuration *n*. If $\Delta U_{nm} < 0$, then the new configuration is accepted; otherwise the Boltzmann factor of the energy difference, $\exp(-\Delta U_{mn})/kT)$ is calculated and compared with a random number γ uniformly distributed in the interval (0, 1). If the latter is less than the former, then the trial move is accepted; otherwise it is rejected (*i.e.* the system remains in configuration *m*). The implementation of the Metropolis procedure in the canonical (*NVT* = const) ensemble is described in detail in many textbooks and monographs (see, for example [26,70-72]), here we will pay more attention to grand canonical ensemble simulations used in our work.

2.3 Grand canonical Monte Carlo simulations

In grand canonical Monte-Carlo (GCMC) simulations, the number of particles N is allowed to fluctuate, whereas the chemical potential m is kept fixed. The respective probability density distribution differs from r_{NVT} by the factor exp(Nm/kT) and the integration over q in eq. (2.2) is complemented by the summation over N.[26] The fluctuation of N is accomplished through particle insertion and deletion (annihilation) attempts.

In simulations of water confined between OEG terminated SAMs, an GCMC run consists of n passes, each composed of $N + N_s$ moves, where N is now the current number of water molecules and N_s is the number of the alkanethiol molecules in the SAM. There are a total of four types of moves: (1) A displacement of a water molecule, which combines a translational and rotational displacement, (2) An insertion of a water molecule, (3) A deletion of a water molecule, and (4) A move of a SAM molecule, which changes both the position and all the conformational parameters of the molecule using a rotational displacement procedure[73,74] described in the next subsection. The number of molecules in the SAM is fixed, N_s = const, so that no attempt to delete or create a molecule comprising the SAM is undertaken. The four allowed types of moves are attempted with probabilities P_w, P_i, P_d, and P_s, respectively, such that

$$P_w + P_i + P_d + P_s = 1 \quad . \tag{2.12}$$

The probabilities P's are calculated from the following input parameters:

$$R_{w/s} = (P_w + P_i + P_d)/P_s \quad , \tag{2.13}$$

$$R_i = P_i/(P_w + P_i + P_d)\,, \tag{2.14}$$

$$R_{i/d} = P_i/P_d \quad . \tag{2.15}$$

The meaning of these parameters is apparent: $R_{w/s}$ specifies the distribution of attempted moves between the water and SAM molecules, R_i presets the fraction of insertions among all moves of the water molecules, and $R_{i/d}$ specifies the ratio between water insertion and deletion attempts. The numerical values used for these parameters are: $R_{w/s}$ = 10, R_i = 0.7-0.8, $R_{i/d}$ = 15.

2.3.1 Displacements.

The displacement of a water molecule is performed using a combination of translation of its center of mass by a random vector $\delta\mathbf{r}$ and then rotation by a random angle $\delta\gamma$ about one of the three-fixed axis chosen at random. In most of simulations, the maximum displacement and rotation angle are 0.16 Å and 10° respectively.

The SAMs modeled in our simulation are all composed of EG3-OMe terminated alkanethiol molecules, $S(CH_2)_n$-$(OCH_2CH_2)_3OCH_3$. For the sake of computational simplicity, the alkane chain is taken short, $n = 3$. (A few comparative simulations of the SAMs with $n = 3$ and $n = 10$ did not reveal a perceptible effect of the alkane chain length on the behavior of the EG_3-OMe tails.) The chains constituting the SAMs are treated as being flexible but subject to bond length constraint. In addition, the positions of the two hydrogen atoms attached to a carbon atom, X_j, is constrained by maintaining the H-H vector perpendicular to the X_i-X_j-X_k plane and the midpoint of this vector on the bisector of X_i-X_j-X_k angle (X= S, C, O, or H). The conformational displacement of the molecule is accomplished by using the rotational displacement procedure (**Figure 2-2**).[73,74] In this procedure, an elementary displacement represents a rotation of a chain backbone atom X_j, around the virtual bond linking the two neighboring two backbone atoms, X_i and X_k. For actual simulations, the one displacement is defined as follows: 1. one of the molecules constituting the SAM is randomly selected. 2. Rotational displacements, whose magnitude and direction are determined by random number for each X_i-X_j-X_k unit (its maximum is 1.15° in this work), are performed, starting from the headgroup sulfur atom and ending with the terminal X atom of the molecule.

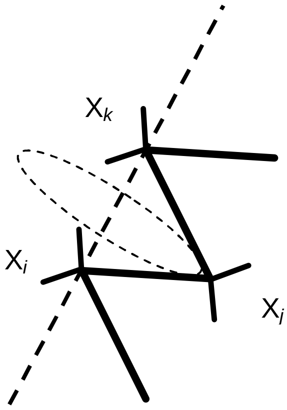

Figure 2-2 Rotational displacement procedure.

Unlike rotations around single bonds, which result in large displacements of the molecular tails and in intermolecular overlaps, rotations around the above-defined virtual bonds affect the structure of a long chain only locally. The rotational displacement procedure is therefore particularly suitable for dense systems such as SAMs.[73].

2.3.2 Insertions and deletions.

In the conventional GCMC technique,[26] as applied to a system of N rigid molecules, an insertion move is accepted with a probability given by

$$\min\left(1,\frac{N\exp[(m'+U_N-U_{N+1})/kT]}{R_{i/d}(N+1)}\right) \quad . \tag{2.16}$$

In this equation, m' is the excess (nonideal) part of the chemical potential, $m'=m-m_0$, where m_0 is the contribution to m due to the translational and rotational degrees of freedom of the water molecules (with the intermolecular interactions switched off). The explicit expression for m_0 in terms of the mass, m, and the moments of inertia of the water molecule, I_i (i = 1,...,3), is

$$m_0 = kT\ln\left[\frac{N}{8p^2V}\left(\frac{h}{\sqrt{2pmkT}}\right)^3\left(\frac{h}{\sqrt{2pkT\sqrt[3]{I_1I_2I_3}}}\right)^3\right] \quad . \tag{2.17}$$

A deletion attempt is accepted with a probability given by

$$\min\left(1,R_{i/d}\exp[(-m'+U_N-U_{N-1})/kT]\right) \quad . \tag{2.18}$$

In our simulations we basically followed the above described procedure, except for the use of two special techniques intended for improving the sampling efficiency. These techniques are discussed in the next subsection.

2.3.3 Improving the sampling efficiency.

For dense systems, one of the main difficulties encountered in GCMC simulations is that the insertion and deletion moves have typically low acceptance because random insertions and deletions often result in high energy loss. To overcome this problem, we resort to the excluded volume mapping (EVM) technique[75] and the Swendsen-Wang (SW) filter[76]. The former directs the insertion of a water molecule, into the vacancy, which has enough space to accommodate it, whereas the latter enables one to reject improbable insertions or deletions using computationally cheap energy predictors

As a simulation starts, the EVM method begins constructing the excluded volume map for the initial configuration of the system. The whole volume accessible to the system is divided into a large number of small cubes (~8 × 10^{-3} Å^3 in volume). A cube is considered to be forbidden for insertion of a water molecule if there is an oxygen or a carbon atom closer than a specified distance to all points within the cube. (The particular distances used are 2.5 Å for O and 2.8 Å for C.)

After the position for the insertion or deletion of the new molecule is determined, the SW-filter is applied. In our simulations, we use an SW filter based on evaluation of the Lennard-Jones contribution to the potential energy of the system, as described in detail by Shelley and Patey[77]. For the inserted molecule or the molecule chosen to be deleted, we first calculate its Lennard-Jones interaction energy with all the surrounding, U^{LJ}, and then the quantity

$$\Delta U^{SW} / kT = \begin{cases} \exp(t\,(U^{LJ} - U^{LJ0}) - 1, & \text{for}\, U^{LJ} > 0 \\ 0, & \text{otherwise} \end{cases}, \tag{2.19}$$

where τ and U^{LJ0} are constants (0.327 and 12 kcal/mole, as recommended by Shelley and Patey). Thereafter $\exp(-\Delta U^{SW})$ is compared with a random number γ in the same way as described in Sect. 2.2 for the Metropolis algorithm. If $\exp(-\Delta U^{SW}) < \gamma$, then the trial move is rejected. Otherwise, the total (exact) interaction energy of the particle with its surroundings is calculated and the move is accepted or rejected in accordance with the conventional GCMC algorithm.

To correct for the bias introduced by the EVM technique and SW filter into the sampling, we resort to a general formula for a_{mn} in eq. (2.9, 2.10),[77]

$$a_{mn} = a^{\mathrm{p}}_{mn} a^{0}_{mn} a^{\mathrm{SW}}_{mn} a^{\mathrm{EVM}}_{mn} \tag{2.20}$$

where a^{p}_{mn} is the probability of attempting a particular move in a particular direction, a^{0}_{mn} is the probability that a move from state m to n will be attempted once the type of move has been selected, a^{SW}_{mn} and a^{EVM}_{mn} are the correction factors for the SW filter and EVM technique. The bias due to the different frequencies of attempting insertions and deletions has been already taken into account in eq. (2.16, 2.18) by the factor $R_{i/d}$.

The probability a_{mn}^{0} is assumed to be equal to unity. As follows from the above description of the SW filter used, the respective correction is given by

$$\begin{aligned} a_{mn}^{\mathrm{SW}} &= 1, \text{ if } \Delta U^{\mathrm{SW}} \le 0 \\ &= \exp(-\Delta U^{\mathrm{SW}} / kT), \text{ if } \Delta U^{\mathrm{SW}} > 0 \end{aligned} . \tag{2.21}$$

At last, the correction for the EVM leads to the appearance in eq. (2.16, 2.18) of the probability of finding a cavity, f_N, which is simply equal to the fraction of cubes allowed for insertion. The final expression for the probability of insertion takes thus the form

$$P_{\mathrm{i}} = \min\left(1, \frac{N f_N}{(N+1) a^{SW} R_{i/d}} \exp\left[m_{ex} + U(\mathbf{r}^N) - U(\mathbf{r}^{N+1}) / kT\right]\right) \tag{2.22}$$

where f_{N} is the fraction of cubes allowed for insertion corresponding to the probability of finding a cavity and $R_{\mathrm{i/d}}$ is the factor that corrects for the bias when insertions and deletions are attempted with different frequencies (see Section 2.3). A deletion attempt is accepted by the probability given by

$$P_i = \min\left(1, \frac{R_{i/d}}{a^{SW} f_{N-1}} \exp\left[m_{ex} + U(\mathbf{r}^N) - U(\mathbf{r}^{N+1}) / kT\right]\right) \tag{2.23}$$

Compared to the case of insertion, deletion of a water molecule requires the estimation of f_{N-1} prior to the deletion attempt. The problem arises when no state with N-1 water molecules has not been sampled. In such a situation $f_{N\text{-}1}$ is estimated by linear extrapolation from the equation

$$f_{N-1} = f_N - < f_N > + < f_{N+1} >, \tag{2.24}$$

where the bracket denotes ensemble averages. The event when $f_{N\text{-}1}$ and $< f_{N+1} >$ are not available may happen only once in the beginning of the simulation. In that event, $f_{N\text{-}1}$ is simply equal to f_N.

To summarize the sampling procedure, an explicit description of the procedure is as follows.

(1) Select a position for the new water molecule randomly.

(2) Check if the new position is allowed to insert the new water molecule. (in the case of deletion, this step is skipped.)

(3) Calculate the Lennard-Jones energy of the new water molecule and determine if the insertion (or deletion) is to be rejected.

(4) Calculate the true change in the total energy and decide if the insertion (or deletion) is accepted or not (Eqs. (2.22) and (2.23)).

2.3.4 Boundary conditions

The simulation box represents a rectangular cell with dimensions L_x, L_y, and L_z. The substrate of the lower SAM or structureless model surfaces are placed at $z = 0$ parallel to the x-y plane. In the x and y directions, standard periodic boundary conditions are used. The lateral dimensions L_x and L_y were taken to be multiples of the SAM lattice periods a and b conform to the periodic boundary conditions. The particular dimensions used were $L_x = 6a$ and $L_y = 3b = 3\sqrt{3}a$, where $a = 5.01$ and 4.6 Å for the gold and silver substrate, respectively.[78,79]

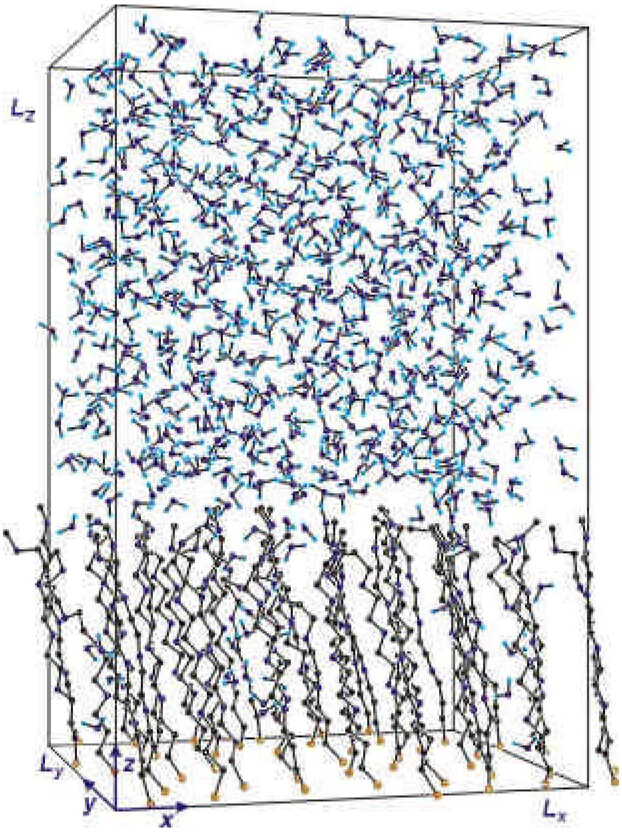

Figure 2-3 The simulation cell used and a typical configuration of the system for the Au-supported SAM. For clarity, the hydrogen atoms in the molecular chain are not shown.

Along the z axis, the gliding boundary conditions[80], which combines a mirror plane at $z = L_z$ with a half-period translation along x, were used. This shift is necessary to avoid highly correlated moves of a particle and its image across the mirror plane. Because of the mirror plane at $z = L_z$, the substrate of the upper confining SAM occurs at $z = H = 2L_z$. The transformation of the x and z coordinates by the GPB condition is:

$$x' = x + kL_x / 2 \; (k = 1 \text{ for } x < L_x / 2 \text{ and } k = -1 \text{ otherwise}), \qquad (2.25)$$

$$z' = 2L_z - z, \qquad (2.26)$$

while the y coordinate remains unchanged. As a molecule leaves the simulations cell through the top face, its image, whose coordinates are given by Eqs. (2.25) and (2.26), enters the cell through the other half of the top face.

Although the GPB conditions save nearly half the CPU time, they may, in principle, affect the simulation results because of the artificial correlations induced by Eqs (2.25) and (2.26) in the configuration of the system near the mid-plane $z = L_z$. To assess the importance of these correlations, we made a comparative simulation of two bulk water systems. One system was simulated using the usual periodic boundary conditions in all three dimensions. In the other system, the periodic boundary conditions were only applied along the x and y axis, while along the z axis the system was replicated by applying the GPB conditions at $z = 0$ and $z = L_z$. The three lengths of the simulation box were set equal to 30 Å. The thermodynamic and structural quantities proved to be practically independent on whether the periodic or GPB conditions were used along the z axis.

2.4 Quantities calculated

In the course of GCMC run, we calculated the following quantities.

- The average potential energy of the system $<U>$.
- The average water density in the confined region r.
- Hydration pressure p^h.
- The orientational order parameter of water molecules Ξ.

The average water density in the confined region was calculated in a straightforward way as $\bar{r} = <N> / V_c$, where $V_c = L_x L_y L_z$ is the volume of the cell. For the system containing a SAM, because of some penetration of water in the near-surface region of the SAMs, there was no clear-cut interface between the SAM and water, and so the volume occupied by water remained uncertain. As a consequence, we could not calculate the average water density between the SAMs based on the ensemble average number of water molecules in the confined region, $<N>$. As an alternative measure of the overall density depression or enhancement, the water density at the mid-point between the walls, $\rho_{H/2}$, was used. To smooth the statistical noise, the density distribution $\rho(z)$ near the mid-point was averaged over a certain interval Δ (typically, 3–5 Å), so that the exact definition for $\rho_{H/2}$ was

$$\rho_{H/2} = \Delta^{-1} \int_{H/2-\Delta}^{H/2} dz \rho(z) \quad . \tag{2.27}$$

Clearly, the use of $\rho_{H/2}$ as a measure of density changes in the confined region made sense only when H was large enough for the water density oscillations near $H/2$ to decay.

Hydration pressure p^h was calculated by

$$p^h = \bar{f} / A - p^b , \tag{2.28}$$

where p^b is the bulk water pressure, A is the surface area, $A = L_x L_y$, and $\bar{f}$ is the mean force exerted by the water molecules upon the lower confining wall. In the separation range studied, the direct interaction between the SAMs did not exceed 3 % of the solvent contribution to p^h,[ii] and so this interaction was neglected. In the case of the water/SAM systems, the mean force in Eq. (2.28) is given by the equation

$$\bar{f} = \left\langle -\sum_I f_z^I \right\rangle = \left\langle \sum_{I,J} \sum_{i,j} \frac{\partial u(\boldsymbol{r}^{\boldsymbol{I},\boldsymbol{i}}, \boldsymbol{r}^{J,j})}{\partial z_c^{\boldsymbol{I}}} \right\rangle , \tag{2.29}$$

where the angular brackets denote ensemble averaging, f_z^I is the z-component of the force experienced by the I-th water molecule due to its interactions with the confining SAMs, $u(\boldsymbol{r}^{\boldsymbol{I},\boldsymbol{i}}, \boldsymbol{r}^{J,j})$ is the interaction energy between the i-th force site on the I-th water molecule and the j-th atom in the J-th chain molecule in the SAM; the differentiation was performed with respect to the z coordinate of the center-of-mass of

---

[ii] In the calculation of the direct interaction between the SAMs, the simulation cell was mirrored at the top of the cell without the GPB condition. The force was calculated using the SJY force field (see Chapter 3).

the I-th water molecule. In cases of water confined between structureless walls, $\overline{f}$ was calculated from

$$\overline{f} = \left\langle \sum_i \frac{\partial u}{\partial z_c^i} \right\rangle, \tag{2.30}$$

where u is the wall-water potential whose detail is discussed in Chapter 3. We will hereafter refer to the values of p^h on the upper confining surface, so that positive p^h will correspond to repulsion, while negative p^h to attraction.

The orientational structure of water at different separations from the wall was monitored by calculating the distribution of the angles, θ_μ and θ_{OH}, formed by the molecular dipole moments and O–H bonds with the z axis, respectively. Also calculated were the orientational order parameter,

$$S_0^1(z) = \left\langle \cos\theta_\mu(z) \right\rangle, \tag{2.31}$$

and the integrated density-weighted order parameter

$$\Xi = \left(\int_0^{H/2} dz\, \rho(z) \right)^{-1} \int_0^{H/2} dz\; S_0^1(z)\, \rho(z) \ . \tag{2.32}$$

While $S_0^1(z)$ is the average of $\cos\theta_\mu$ over the molecules lying at distance z from the wall, Ξ represents the average of $\cos\theta_\mu$ over all molecules between the wall and the mid-plane at $z = H/2$.

In addition to the above quantities, in order to monitor quantities dependent on the distance from the wall, the simulation box was divided into 100 slices of thickness $\Delta z = L_z/100$ lying parallel to the wall. During the GCMC run, the following z-dependent quantities were averaged within each individual slice and then referred to the z coordinate of its center.

- Water density based on the number of water O atoms
- The orientational order parameter.
- Pair distribution function of water O atoms.
- The radial distribution functions of the water O and H atoms around the different O atoms of the SAM molecule (if the system contains a SAM)
- Average water-surface and water-water interaction energies

In the case of the water/SAM systems, the radial distribution functions of the water O and H atoms around the different O atoms of the SAM molecule were also investigated.

In order to analyze the structure of SAM molecules, the following quantities were also monitored

- the distribution of the dihedral angles
- density distribution of non-hydrogen atoms of the SAM

Chapter 3: Evaluation of potential energy

For computer simulations, which deal with systems of 10^2-10^4 particles and involve sampling of 10^7-10^9 distinct configurations, simple atomistic force fields have been the only feasible methods of calculating the potential energy, because of their computational simplicity, despite a few conceptual drawbacks of the atomistic approach.[81] With this method, intra- and inter molecular potentials are calculated with simple analytical functions. In the evaluation of potential energy, the geometry of a system is specified by a vector $\boldsymbol{r}^N = \{\boldsymbol{r}_m\}$, where N is the total number of molecules in the system (both in water and in the SAM) and $\boldsymbol{r}_m$ ($m = 1,...N$) is a vector specifying the position, orientation, and (for the molecules making up the SAM) conformation of molecule m. The total potential energy of the system, $U(\boldsymbol{r}^N)$, is assumed to include only one- and two-body terms,

$$U(\boldsymbol{r}^N) = \sum_m u_m(\boldsymbol{r}_m) + \sum_{n>m} u_{mn}(\boldsymbol{r}_m, \boldsymbol{r}_n) \,. \tag{3.1}$$

All three-body and higher terms, such as the polarization energy, are thus neglected[iii]. In this approximation, the total potential energy of the system can be broken down into four independent contributions and described as

$$U(\mathbf{r}^{\mathbf{N}}) = U^{\mathrm{W}} + U^{\mathrm{S}} + U^{\mathrm{W-S}} + U^{\mathrm{S-M}} \,, \tag{3.2}$$

where U^{W}, U^{S}, $U^{\mathrm{W\text{-}S}}$, and $U^{\mathrm{S\text{-}M}}$ are the energy contributions from the water subsystem, from the molecules making up the SAM, from the SAM-water interactions, and from the interactions of the SAM with its metal substrate, respectively. Considering a fairly large thickness of the SAM, the interactions of water molecules with the SAM substrate are neglected. In studies of water confined between structureless surfaces, the potential energy comprises only two contributions: from the water-water and water-surface interactions. In the subsequent sections, we consider the individual contributions to the potential energy in detail.

[iii] The effect of the polarization on water-water and water-SAM interaction energies will be explained in Section 3.1 and 3.3.

3.1 Water-water interactions

In the calculations of the potential energy of the water subsystem, we treat the water molecules as rigid, and so the potential energy comprises only intermolecular water-water interactions. These interactions are described using the four-site TIP4P model,[82] which is perhaps the most reliable of rigid non-polarizable water models.[iv] The TIP4P water molecule comprises four interaction sites corresponding to the oxygen, two hydrogen atoms, and a quasi-atom located 0.15 Å away from the oxygen atom along the bisector of the H-O-H bond angle (**Figure 3-1**). The two hydrogen atoms carry a charge of 0.52e each, while the quasi-atom carries a balancing charge of -1.04e. The oxygen atoms are considered to be electrically neutral and to interact through a Lennard-Jones potential. The total interaction energy of molecules *m* and *n* is thus the sum of the Coulomb and Lennard-Jones terms,

$$E_{mn}(\text{kcal/mole}) = \sum_{i \in m} \sum_{j \in n} \frac{332.08 q_i q_j}{r_{ij}} + \frac{60000}{r^{12}{}_{OO}} - \frac{610}{r^{6}{}_{OO}}, \tag{3.3}$$

where q_i denote the partial charges(atomic units) on the hydrogens and quasi-atom , and r_{OO} is the distance between oxygens(Å).[82]

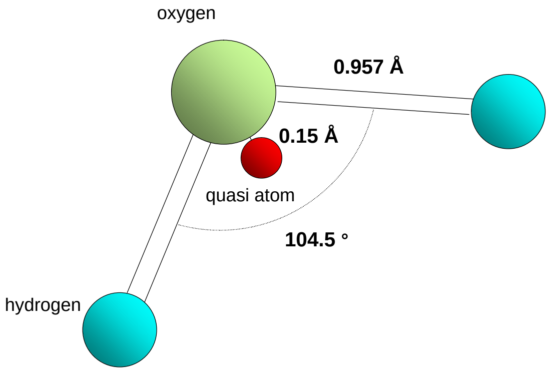

Figure 3-1 TIP4P water model. Two hydrogens and a quasi atom carry positive and negative partial charges respectively. The oxygens interact with themselves through Lennard-Jones potential.

In the evaluation of U^{W}, we have to choose an appropriate summation scheme and to restrict the summation with an appropriate cut-off in order to reduce the

---

[iv] The effect of the assumed non-polarizability on the behavior of water near solid surfaces was studied by Wallqvist.[48]

computational cost. The dependence of simulation results on the summation schemes applied was investigated by Shelley and Patey.[83] They simulated 216 TIP4P water molecules confined between two hydrophobic surfaces using four different summation schemes, namely, the Ewald,[84] minimum image (MI),[26] cylindrical cut-off (CC)[2] as well as the spherical cut-off (SC)[2] ones. In all these simulations, periodic boundary condition is employed in *x* and *y* directions. Their results showed that CC and MI schemes induce orientational ordering of molecular dipoles. As a result, the water molecules form a liquid-crystal-like structure, whereas there were not such phenomena observed in the simulations with SC and Ewald schemes. These two simulations provided nearly the same results. Because the computational cost of simulations with the SC scheme is much lower than that with the Ewald scheme, we employed the former.

In our simulations the SC scheme was employed based on the distance between oxygens, i.e. the charges on a water molecule are not split in the summation. The cut-off radius is fixed at 7.5 Å. To check the effect of the cut-off radius on simulation results, we performed bulk water simulations with two different cut-off radii of 7.5 and 8.5 Å. In these simulations, the periodic boundary conditions were used in all three dimensions. The simulation results showed that the deviations for the pressure and average density were within the statistical uncertainty of the calculations.

3.2 Intra- and intermolecular interactions within SAM

3.2.1 Potential functions and parameters

In our simulations, the bond lengths in the molecules making up the SAM were kept fixed at the respective average values taken from the results of relevant *ab initio* results (TABLE 3-1 (a)) ,[34] i.e. the potential energy due to bond stretching was neglected. The intra- and intermolecular interactions within the SAM, U^{S} is of the form

$$U^{S} = \sum_{i<j} E^{n.b.}(r_{ij}) + \sum_{ijk} E^{b}(q_{ijk}) + \sum_{ijkl} E^{t}(f_{ijkl}) \,, \tag{3.4}$$

where $E^{n.b.}(r_{ij})$ is the nonbonded energy associated with the atom pair *i* and *j*. A pair of atoms *i* and *j* is considered nonbonded if they are in different molecules or they are atoms in the same molecule separated by two or more atoms. $E^{b}(q_{ijk})$ is the potential energy due to bending of the bond angle defined by atoms *i*, *j*, and *k*, and $E^t(f_{ijkl})$ is the potential energy due to twisting of the dihedral angle defined by atoms *i*, *j*, *k*, and *l*.

We chose the analytical forms of potential functions and empirical parameters were adopted from the force field developed by Smith, Jaffe, and Yoon (denoted as an SJY force field hereafter).[85] The nonbonded potential $E^{n.b.}$ is described in terms of dispersion and repulsion using the Buckingham 6-exp potential, and Coulombic interactions.

$$E^{n.b.}(r) = A\ \exp(-r B) - C\, r^{-6} + \frac{332.08qq'}{r}, \tag{3.5}$$

where *A*, *B*, and *C* are empirical constants, *r* is the distance between two nonbonded atoms, and *q* is the partial charge the atoms *i* and *j* carry. The bond angle bending energy E^b is of the form

$$E^b(q) = \frac{1}{2}k^b(q - q^o)^2, \tag{3.6}$$

where k^b and *q* are a force constant and the bond angle, respectively, and q^o is the ideal bond angle. The torsional potential function E^t is represented by a sum of 1-, 2-, and 3-fold terms, given as

$$E^t(f) = \sum_n^3 \frac{1}{2}k_n^t\left[\cos n\left(f - f^o\right)\right], \tag{3.7}$$

where k^t, *f*, and f^0 are a force constant, the dihedral angle, and the function minimum angle, respectively.

The partial charges *q* and force constants were parameterized by Smith *et al.* as follows.[85] First, the partial atomic charges were calculated from the Mulliken population analysis of diethylether (DEE) (**Figure 3-2** (a)) and then proportionally scaled to reproduce the dipole moment of the all-trans conformer of DEE. The empirical parameters *A*, *B*, and *C* were adopted from the Sorensen's work.[86] The other parameters of force field (bond angle bending and torsional) were adjusted so as to attain the best agreement between the force field and MP2 level *ab initio* results for the energies and geometries of 1,2-dimethoxyethane (EG1) (**Figure 3-2** (b))and DEE. The resulting force field was finally tested in a stochastic dynamics simulation of gas-phase EG1 by comparing the calculated conformer populations and pair distribution functions with those deduced from an electron diffraction experiment. For the C-C-C-C and C-C-C-O torsions and for the C-C-C bend, which are absent in the SJY force filed but are required to treat the alkane chain and its junction with the methoxy tri(ethylene glycol) (EG3-OMe) tail, we use the analytical potential from Sorensen's force field[86]. The parameters used in our simulations are summarized in TABLE 3-1.

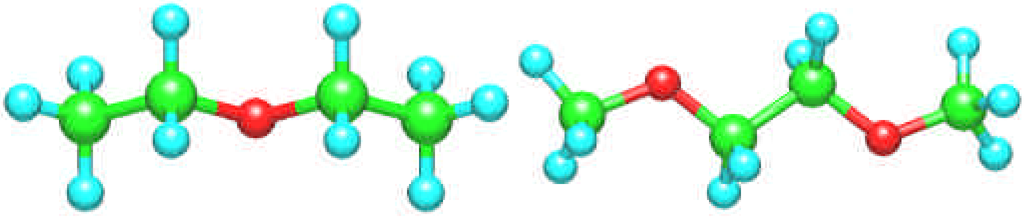

(a) (b)

Figure 3-2 All trans conformers of DEE (a) and EG1 (b).

TABLE 3-1 Force field parameters for U^S

(a) Bond lengths

Bond	length(Å)
S-C[a]	1.82
C-C	1.52
C-O	1.43
C-H	1.11

(b) Nonbonded dispersion and repulsion parameters[b]

interacting pair	A(kcal/mole)	B(Å^{-1})	C(Å^{6}kcal/mole)
C…C	14976.0	3.090	640.8
O…O	75845.0	4.063	398.9
H…H	2650.0	3.740	27.4
C…H	4320.0	3.415	138.2
O…C	33702.0	3.577	505.6
O…H	14176.0	3.902	104.5

(c) Partial atomic charges in EG1 and DEE[c]

atom(i)	charge(q)[d]
methyl carbon	-0.163
methylene carbon	-0.066
methyl hydrogen	0.097
methylene hydrogen	0.097
oxygen	-0.256

(d) Bonded parameters: bends

Bend	q^0(radians)	k^b(kcal/mole)
S-C-C[a]	1.9967	107.0
C-C-C[b]	1.9373	107.0
O-C-C[d]	1.9031	172
C-O-C[b]	1.9471	149

(e) Bonded parameters: torsions

torsion	n	ϕ^o(radians)	k^t(kcal/mole)
O-C-C-H[b]	3	0	0.28
C-C-C-H[b]	3	0	0.28
H-C-C-H[b]	3	0	0.28
C-O-C-H[b]	3	0	0.81
O-C-C-O[d]	1	π	0.05
O-C-C-O[d]	2	$\pi/2$	2.55
O-C-C-O[d]	3	0	0.00
C-O-C-C[d]	1	0	1.00
C-O-C-C[d]	2	$\pi/2$	0.70
C-O-C-C[d]	3	0	0.32
S-C-C-C and O-C-C-C[a]	3	0	0.417

[a] Taken from ref. [87]. [b] From the Sorensen's work.[86] [C] The hydrogens and carbons in the alkyl chains are considered to carry no partial charges. They interact only through the non-bonded potentials shown in (b). [d] From Smith's work.[85]

3.2.2 The force field testing

Prior to our GCMC simulations, the SJY force field were tested for the transferability to methoxy terminated tri(ethylene glycol) (EG3) (**Figure 3-3**). The test was performed by a straightforward comparison of the force field energies and conformations with the relevant results of *ab initio* calculation using density functional theory with gradient corrections and large basis set (BP86/6-311G**).[34]

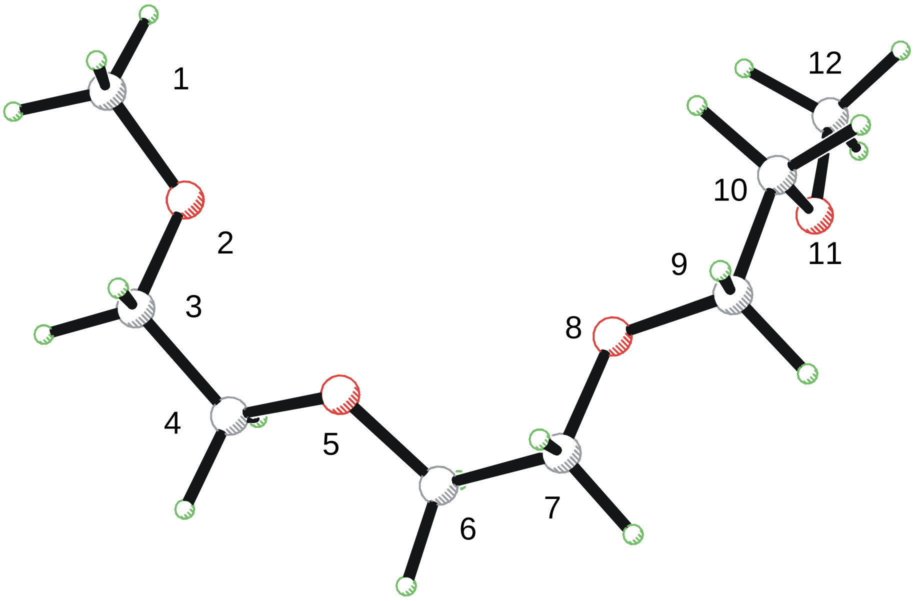

Figure 3-3 The ($g^+|g^+|g^-$) configuration of a EG3 molecule. The carbon and oxygen atoms are numbered to define dihedral angles.

Figure 3-4 compares the *ab initio* and force field energies for ten low energy conformers of the lone EG3-OMe molecule. The energies are given relative to that of the lowest energy conformer *tgt-tgt-tgt* usually referred to as helical.[v] One can see that the SJY force field well reproduces the stability sequence of the conformers.

---

[v] In the notation *tgt* the *t*'s refer to the two C-O bonds being in the *trans* configuration with a dihedral angle of about 180°; the *g* indicates that the C-C bond is in a gauche conformation with either a clockwise (+) or anticlockwise (-) sense of rotation. As long as the C-O bond is nearly in the *trans* configuration, we adopt a notation where we omit this information. As examples the all-*trans* and helical conformers of $(EG)_3$ we denote by ($t|t|t$)=(ttt-ttt-ttt) and ($g^+|g^+|g^+$)=(tg^+t-tg^+t-tg^+t).

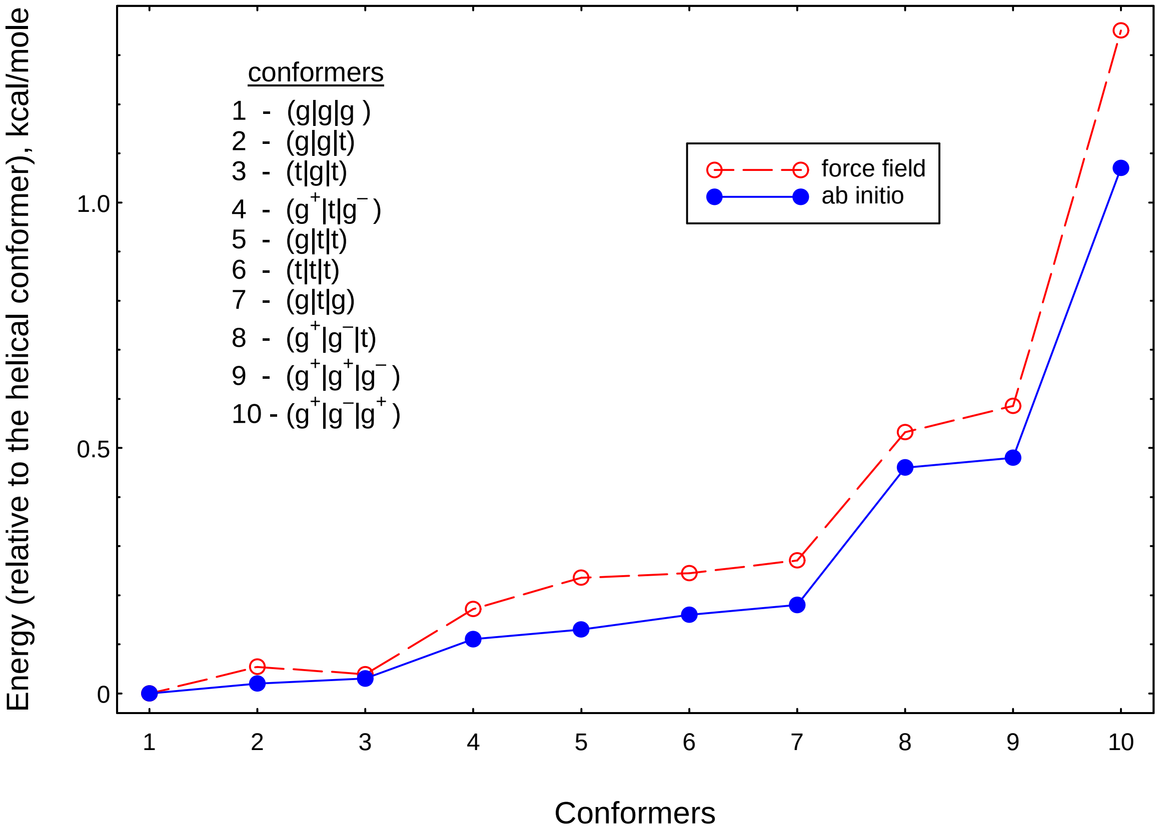

Figure 3-4 Comparison of the *ab initio* and force field energies for ten low-energy conformers of a lone EG3 molecule

The only disagreement in the sequence of stability is observed with conformers 2 and 3, which are very close in energy: The *ab initio* calculation predicts the energy difference to be 0.01 kcal/mole, while the force field prediction is –0.01 kcal/mole. It can also be seen from **Figure 3-4** that the force field well reproduces the general shape of the stability curve, correctly predicting the presence of four energetically distinct groups of conformers (1-3, 4-7, 8-9, and 10). The overall standard deviation of the force field predictions from the *ab initio* energies is as small as 0.12 kcal/mole. For the bond and dihedral angles, the deviations are within 0.6° and 4°, respectively.

The ability of the SJY force field to correctly describe the rotation barriers in the EG3 molecule can be appreciated from **Figure 3-5** and **3-6**. Depicted with a dashed line in **Figure 3-5** is the energy of the helical conformer, calculated using the SJY force field as a function of the –C6–C7– dihedral angle (with all the other conformational parameters adjusted to minimize the energy). A comparison with the respective *ab initio* data (full circles) reveals a remarkable agreement in both the location and magnitude of the energy maxima and minima. Similar comparisons are made in **Figure 3-6**, which shows the magnitudes of the energy minima and maxima for some other conformers and/or another dihedral angle (–O3–C6–). The agreement is in general good except perhaps for a noticeably underestimated energy barrier predicted for the rotation around the O3–C6 bond in the (*tgt*–*tgt*–*ttt*) conformer.

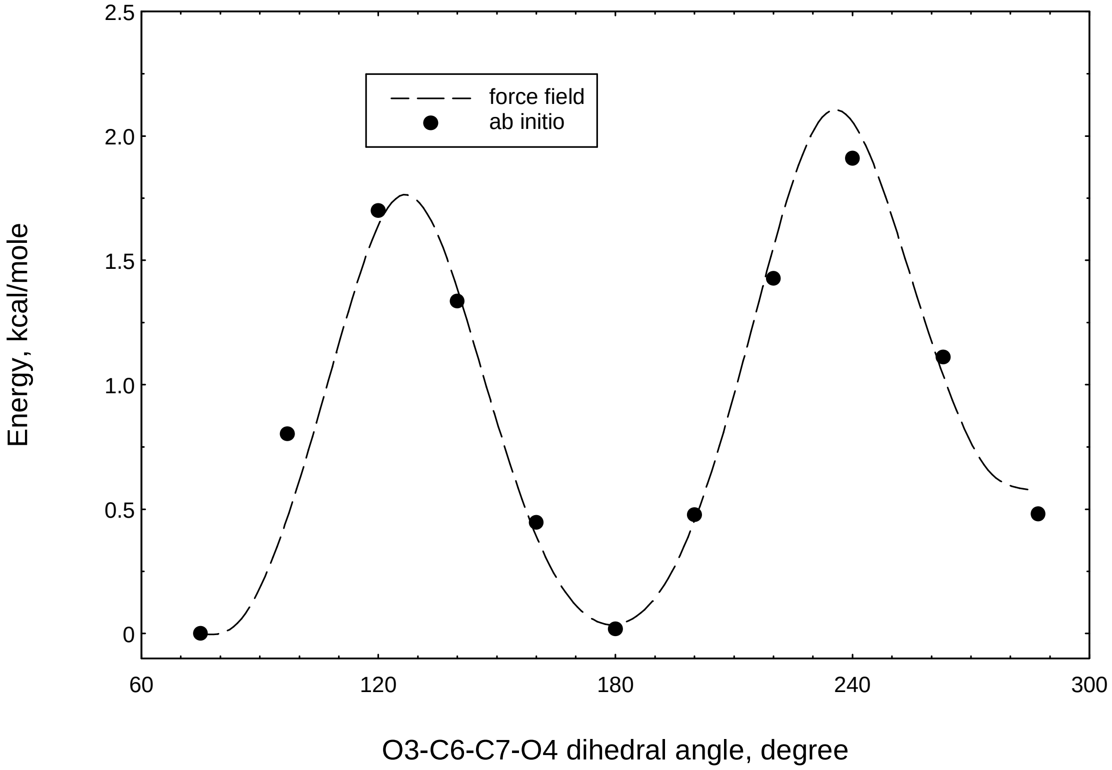

Figure 3-5 Energy of the helical conformers as a function of rotation about the C6-C7 bond.

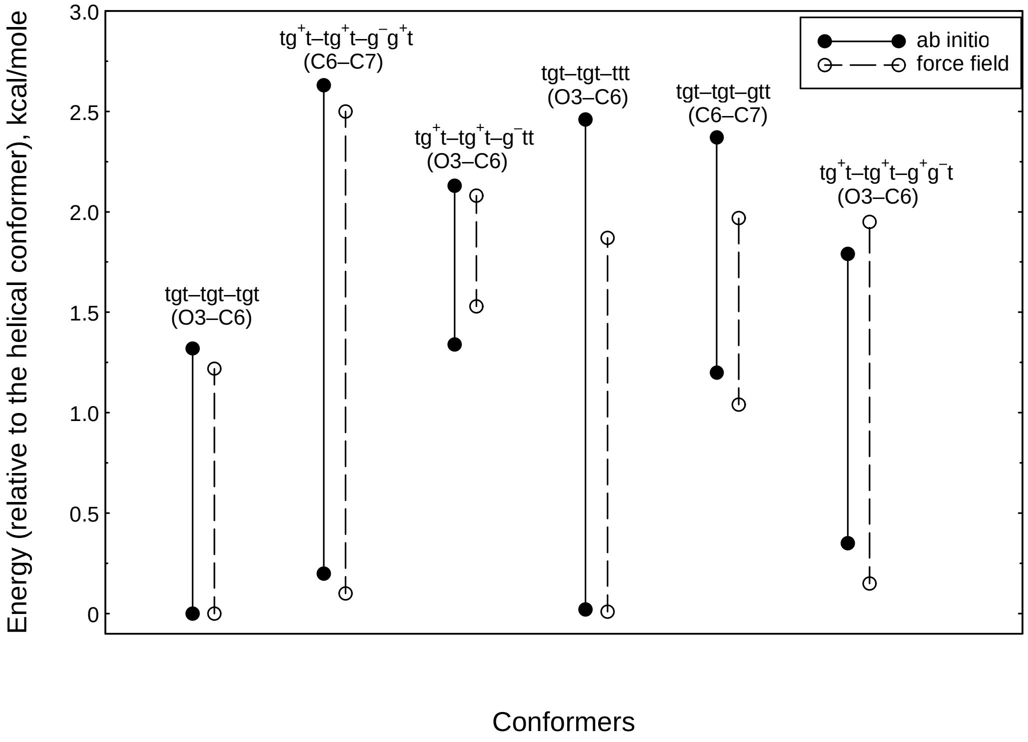

Figure 3-6 Energy minima and maxima for some selected EG3 conformers, as a function of rotation around O3-C6 and C6-C7 bonds.

3.2.3 Evaluation of Coulomb lattice sums

Since the force field used in calculation of the potential energy of the SAM contains Coulombic terms, which are characterized by a slow distance dependence (~r^{-1}), the problem of efficient summation of the electrostatic interaction takes on great importance. In systems with three-dimensional periodic boundary conditions, a number of “accelerated convergence” techniques have been proposed.[81] Most of these techniques involve a replacement of the original summation by two rapidly conversing sums, one in real space and the other in reciprocal one.

The convergence problem becomes particularly difficult to cope with when the system is periodic in two dimensions, while being of a finite thickness in the third dimension. The pertinent formulas are rather complicated and provide a satisfactory convergence only when the system size in the “nonperiodic” dimension is much less than the lattice period in the other two dimensions.[88] This condition obviously fails in SAMs, where the length of the molecules is greater than the lattice spacing of the monolayer. Fortunately, it turned out that quite reliable estimates for the electrostatic lattice energy of EG3-OMe terminated alkanethiol SAMs can be obtained in a comparatively simple way using a modified direct summation method suggested by Heyes and van Swol.[89] In this method, the electrostatic potential at a point $\mathbf{r} = \{X, Y, Z\}$ from a system of N charges q_j replicated in two dimensions with periods $\mathbf{L}_x$ and $\mathbf{L}_y$ is represented by a truncated direct sum

$$\sum_{j=1}^{N} q_j \sum_{i_1, i_2 (i_1^2 + i_2^2 \leq i_c^2)} \left| \mathbf{r} - \mathbf{r}_j - i_1 \mathbf{L}_x - i_2 \mathbf{L}_y \right|^{-1} \tag{3.8}$$

and a correction term, $C(i_c)$, which provides an approximate estimate for the discarded long-range contributions ($i_1^2 + i_2^2 > i_c^2$). The approximation involves, in particular, the replacement of the discrete charges in each jth sublattice by a uniform two-dimensional distribution of density $q_j / \left| \mathbf{L}_x \times \mathbf{L}_y \right|$. The final equation for the correction term is

$$C(i_c) = -\frac{1}{2 L_y i_c} \sum_{j=1}^{N} q_j \left[C_x (x - x_j)^2 + C_y (y - y_j) + C_z (z - z_j)^2 \right] \tag{3.9}$$

where the coefficients C_x, C_y, C_z are expressed in terms of complete elliptical integrals of the first and second kind, $K(\varepsilon^2)$ $E(\varepsilon^2)$, with $\varepsilon = (L_x^2 + L_y^2)^{1/2} / L_x$. The efficiency of the Heyes-van Swol scheme was demonstrated by Pertsin *et al.*[90], who showed that the long-range correction given by Eq. (3.9) allows one to obtain quite reliable estimates for the electrostatic lattice energy at small i_c.

3.3 Water-SAM interactions

3.3.1 Potential functions and parameters

The water-SAM interaction energy $U^{W\text{-}S}$ was evaluated using the force field developed by Bedrov, Pekny, and Smith (denoted as an BPS force field hereafter).[91] The analytic form of BPS force field is essentially the same as that of the TIP4P model *i.e.* $U^{W\text{-}S}$ consists of the electrostatic and Lennard-Jones parts (the parameters are summarized in TABLE 3-2). The partial charges are fixed as shown in TABLE 3-1 (c). The fitting of the parameters was performed in two different ways. The first method involved adjusting the parameters, so as to reproduce the experimental density of EG1-water as a function of composition and temperature from molecular dynamics simulations. The second involved fitting the values of e and σ (see TABLE 3-2) so as to reproduce the binding energy[vi] and the complex geometries obtained from the MP2 level *ab initio* calculation (the parameters are summarized in TABLE 3-2).[vii] We employed the latter, because we particularly investigate short-range ordering of water molecules near the SAMs.

In our simulations the interaction of a water molecule with the atoms in the SAM was cut off if the distance between the oxygen atom and the nearest atom of the chain exceeded 15 Å, whereas the Lennard-Jones potential is spherically cut off with a radius 7.2 Å.

TABLE 3-2 The Lennard-Jones parameters (*e*: potential well depth and *s*: equilibrium separation) for SAM-water interactions.[91]

Interaction	*e*(kcal/mole)	*s* (Å)
water-carbon	0.2405	3.2665
water-oxygen	0.3490	2.9704
water-hydrogen	0.0772	3.0484

3.3.2 The force field testing

The BPS force field was also tested for the transferability to the EG3's complexes with water. The test was performed by a straightforward comparison of the force field energies and conformations with the relevant results of *ab initio* calculation.[34] **Figure 3-7** compares the *ab initio* and force field energies for ten low-energy complex conformations studied by Wang *et al.* As with pure EG3 (**Figure 3-4**), there is only one difference in the stability sequence which is again associated with a too low energy of the ($t|g|t$) conformer (no. 8 in **Figure 3-7** and no.3 in **Figure 3-4**) The force field result is that this conformer is 0.25 kcal/mole lower in energy than the preceding one, while the *ab initio* calculation[34] predicts it to be 0.08 kcal/mole less stable. Considering the accuracy of the *ab initio* calculations themselves (see below), this discrepancy can hardly be given much significance. Also, it should be taken into

---

[vi] Based on the *ab initio* calculation results, Bedrov *et al.* concluded that polarization effects do not play an important role in the interaction of EG1 and water.[91]

[vii] Recently, Smith *et al.* performed the *ab initio* calculation of EG1/water systems with a larger basis set and they modified the force field. Their new force field can well describe the binding energy of high energy conformers, in which only weak hydrogen bonds are formed between EG1 and water.[92]

account that at room temperature the population of the $(t\,|\,g\,|\,t)$ conformer and its neighbors in the stability series is very small (less than 1 % of the population of the lowest energy conformers).

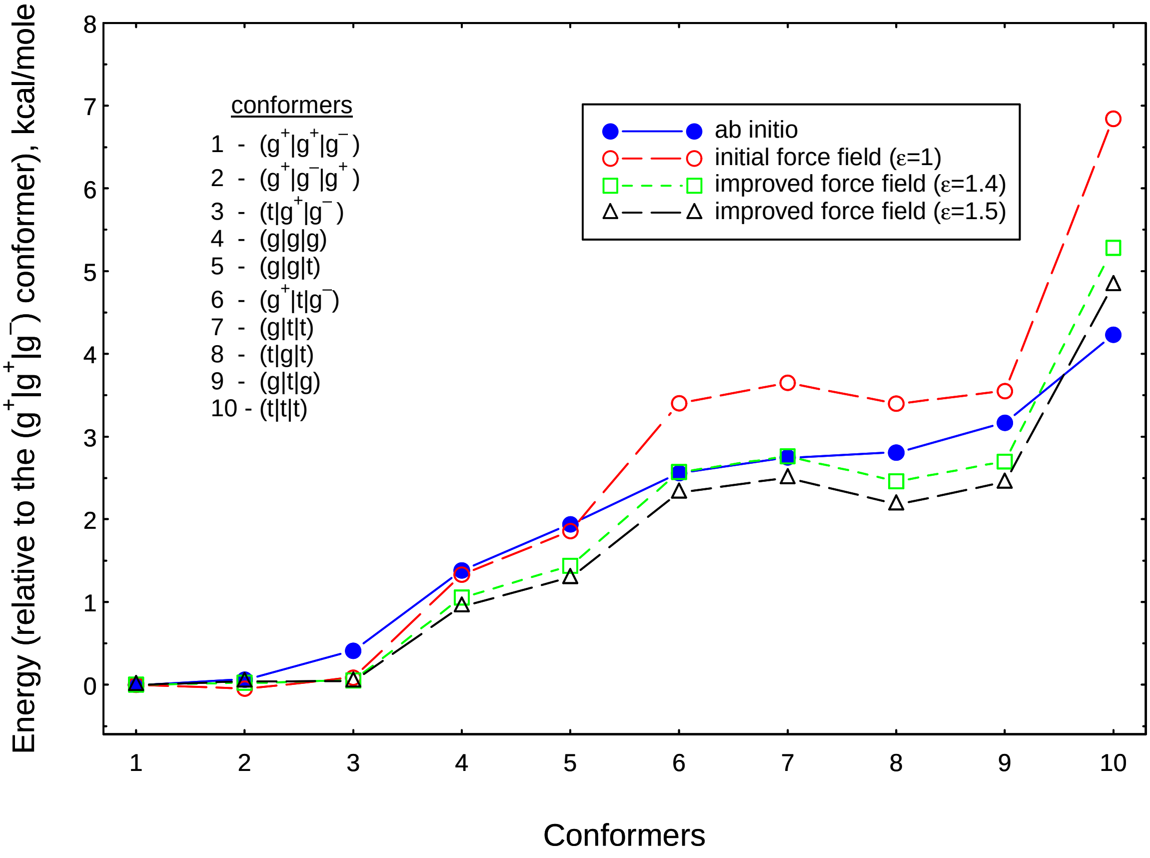

Figure 3-7 Comparison of *ab initio* and force field energies for ten low energy EG3/water complex conformations.

In full agreement with the *ab initio* results,[34] the force field calculations correctly predict that the helical conformer $(g\,|g\,|g)$, which is the lowest energy one for the lone EG3 molecule, gives place to the $(g^{+}|g^{+}|g^{-})$ conformer upon interaction with water. The latter conformer is stabilized by a water molecule due to formation of a triple hydrogen bond which involves two water hydrogen atoms interacting with three oxygen atoms of EG3. A similar stabilization is observed with the $(g^{+}|g^{-}|g^{+})$ and $(t\,|g^{+}|g^{-})$ conformations (conformers 2 and 3 in **Figure 3-7**). In the next two conformers (4 and 5), one of the three oxygen atoms involved in the hydrogen bond becomes further and further removed from the water molecule, which makes the complex less and less stable.

The next four conformers, 6 to 9, form a pure double hydrogen bond with water, O...H–O–H...O, in which the water molecule forms as if a bridge between two neighboring oxygen atoms of EG3. Finally, the all-*trans* conformer 10 is capable of forming with water only a single hydrogen bond, O...H–O. The presence of three more or less distinct steps in the stability curve (**Figure 3-7**), corresponding to triple, double and single hydrogen bonds, is well reproduced by the BPS force field. Although the force field noticeably exaggerates the loss in stability associated with the transition from the double to single hydrogen bond conformers, this disadvantage is of minor significance for computer simulations of OEG/water systems because the statistical weight of single hydrogen bonds in such systems is negligible.[80,93]

An important requirement for a force field intended for calculating OEG/water interactions is that it accurately reproduces not only the relative energies of various complex configurations but also the absolute magnitudes of the OEG/water binding energies. This requirement is necessary to attain a proper balance of the OEG/water and water/water interactions, which is essential, in particular, for correctly describing OEG/water miscibility as well as hydrophilicity of OEG-containing surfaces. A comparison of the force field and *ab initio* DFT predictions for the EG3/water binding energy is given in **Figure 3-8**. For each particular EG3 conformer *i*, the binding energy is calculated as

$$E_i^{bind} = E_i(EG3) - E_i(EG3/water)\,, \tag{3.10}$$

where E_i (EG3/water) is the optimized energy of the complex of conformer i with water, and E_i (EG3) is the optimized energy of the lone conformer *i.* Inasmuch as the TIP4P and BPS models treat the water molecule as rigid, its internal energy in the isolated state and in the complex is the same and hence cancels out in Eq. (3.10). So, our definition of the binding energy is equivalent to that used by Wang *et al.*.[34]

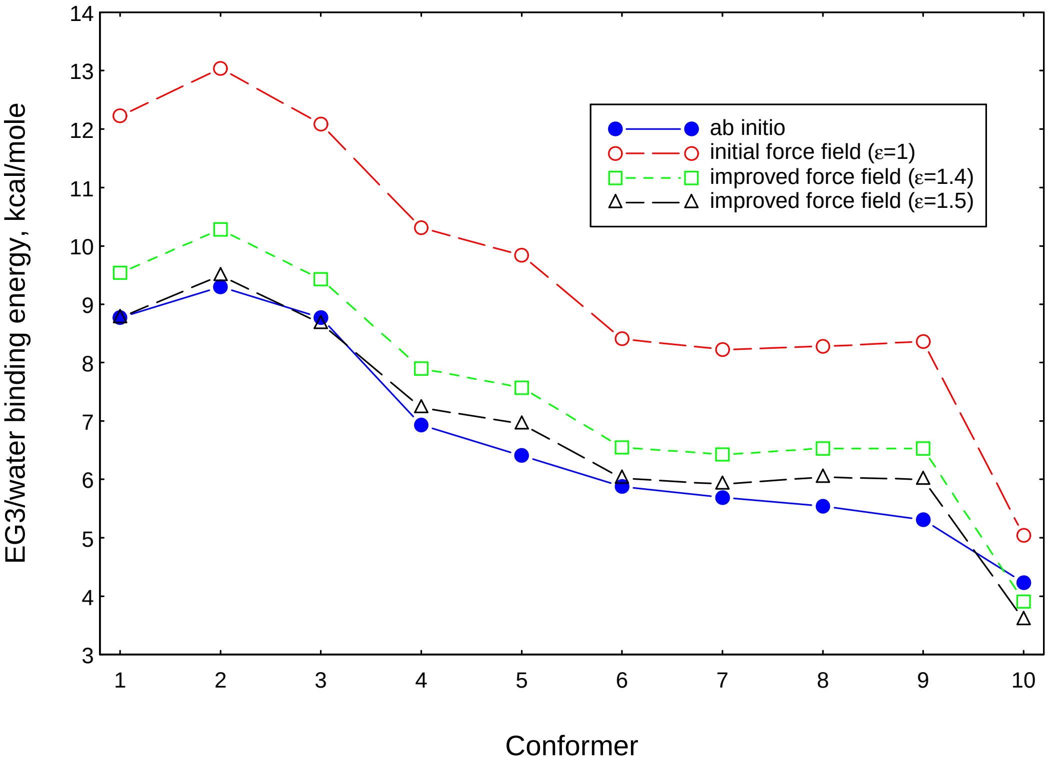

Figure 3-8 Comparison of *ab initio* and force field binding energies for ten low-energy EG3/water complex conformations (the numbering of conformers is the same as in **Figure 3-7**).

As seen from **Figure 3-8**, the BPS force field provides a reasonable description for the general behavior of the binding energy curve. At the same time, the *ab initio* binding energies are, on the average, ~30 % lower than the BPS force field predictions. The observed shift can, for the most part, be ascribed to the difference between the MP2[85] and DFT[34] estimates for the OEG/water binding energy. This follows from a comparison reported by Wang *et al.*[34] for the EG1/water complexes, which shows that the MP2 binding energies are about 20 % higher than the respective DFT results. The remaining 10 % of the difference between the force field and *ab initio* DFT energies in **Figure 3-8** is most likely associated with the "excessive" additivity inherent in all atomistic force fields without polarization terms.[81] Since the OEG/water interaction energy is treated as the sum of interactions of the water molecule with the individual units of OEG, the "many-body" effects associated with the polarization of the water molecule by the individual units are neglected. As a result, a force field fitted to the interaction energy of a short molecule (e.g. EG1) will usually exaggerate the interaction energy of its longer homologue (e.g. EG3). In our particular case, the associated error is estimated to be about 10 %, which is quite a small price to pay for the computational simplicity of the force field.

In principle, the BPS force field can be easily modified to fit the *ab initio* DFT calculation results.[34] Considering that the OEG/water interactions are dominated by the Coulomb interactions between the partial atomic charges on OEG and the TIP4P charges on water, the OEG/water interaction can be attenuated by introducing a formal dielectric permittivity, ε, into the Coulomb site-site potentials. It should be emphasized that ε introduced in such a way has no physical meaning and represents just an additional fitting parameter to make the force field more flexible. This parameter enters the OEG/water interaction potential only and not the potentials describing the interactions within the OEG molecule and between the water molecules.

The calculation results using the modified force field and two trial values for ε are shown in **Figure 3-7** and **3-8** with squares and triangles. At $\varepsilon = 1.4$, the agreement between the force field and DFT predictions markedly improves. Although the sequence of the conformers in stability still shows one disturbance (**Figure 3-7**), the standard deviation of the force field energies from their *ab initio* counterparts reduces from 1.3 to 0.7 kcal/mole. The bias in the binding energies (**Figure 3-8**) decreases, on the average, from ~3 to 0.9 kcal/mole. As ε is increased to 1.5, the agreement between the force field and DFT binding energies further improves (**Figure 3-8**). The conformer energies, however, become too low (**Figure 3-7**) and the O...O separations too long. So, the value of 1.4 can well be taken as an acceptable compromise for ε.

Although the BPS force field can readily be adjusted to reproduce the results of the *ab initio* DFT calculations,[34] the reasonableness of such an adjustment still remains to be seen because no straightforward experimental data on the EG3/water binding energy is available and hence there are no firm grounds to prefer the DFT[34] over MP2[91] calculation results. In their paper, Wang *et al.*[34] criticize the MP2 calculations[93] based on the MP2 prediction that a single O-H...O bond in the EG1/water complex is slightly stronger than that between two water molecules. In their view,[34] this can hardly be so because the electrostatic field around the oxygen atom of an isolated EG1 molecule is weaker than that around the water oxygen. Although such an argument is physically sound, it should be taken into account that an estimate of the interaction energy of two molecules in terms of the electrostatic field created by one molecule and the charge distribution on the other is very approximate and can hardly be a reliable criterion to judge the accuracy of a straightforward *ab initio* calculation.[94]

A weighty argument in favor of the original (non-attenuated) force field based on the MP2 calculations[91] is that the use of a slightly weaker EG1/water interaction potential (*viz.* the one with the geometric mean approximation for the potential parameters) in MD simulations of the EG1/water solutions yields an immiscible system, contrary to experimental evidence.[91] Based on this result, we incline to give some preference to the original force field, at least, when used in combination with the TIP4P potential.

3.5 SAM-substrate interactions

The interactions of the oxygen atoms, and CH_2 and CH_3 groups with the metal surfaces are treated same as those in the work of Hautman *et al.*[95,96]. In their force field, the oxygens and groups are represented by single sites which interact with a surface via a (3-12) potential function,

$$f_z = \frac{e}{3}\left[\left(\frac{z_m}{z}\right)^{12} - 4\left(\frac{z_m}{z}\right)^{3}\right] \tag{3.11}$$

where ε is the potential well depth and z_m is the equilibrium separation. The values of e and z_m are summarized in TABLE 3-3.

TABLE 3-3 Parameters used in the evaluation of the SAM-metal interaction energy (see Eq. (3.11)).

	CH_2	CH_3	O	S
z_m (Å)	3.51	3.51	3.51	2.4
ε (kcal/mole)	1.36	1.65	1.36	27.82*

* estimated form the desorption measurements by Nuzzo *et al.*[97]

The interaction of the sulfur head group with the gold surface is described by the sum of two contributions,[viii]

$$f_{S-Au} = f_z(z) + f_c(x,y)\,. \tag{3.12}$$

The first contribution $f_z(z)$ is responsible for the distance dependence of the interaction energy and is taken in the same form as Eq. (3.12) (the parameters are shown in TABLE 3-3). The next contribution $f_c(x,y)$ is a surface corrugation potential, which is taken in form similar to that used by Hautman *et al.*

$$f_c(x,y) = b\left[3 - \sum_{i=1}^{3} \cos(\mathbf{s}\cdot\mathbf{k}_i)\right] / 4.5 \tag{3.13}$$

where $\mathbf{s} = (x,y)$ is the position vector of the sulfur atom in the surface plane; the reciprocal lattice vectors k_i are $k_1 = k_0(\sqrt{3}/2, -1/2)$, $k_2 = k_0(-\sqrt{3}/2, -1/2)$, $k_3 = k_0(0,1)$ with $k_0 = 4p / a\sqrt{3}$ and a = 5.01 and 4.60 Å for a gold and silver substrate, respectively [78,79]. The height of the barrier for lateral movement is given by b, somewhat arbitrarily taken to be 2 kcal/mole.

3.6 The interaction of water with structureless model surfaces

The water-wall interaction potentials are all constructed based on a (9-3) inverse power function,

$$u(z) = \frac{\varepsilon}{2}\left[\left(\frac{z_m}{z}\right)^9 - 3\left(\frac{z_m}{z}\right)^3\right], \tag{3.14}$$

where z is the separation of the water oxygen atom from the wall, ε is the potential well depth, and z_m is the equilibrium separation, i.e. $\varphi'(z_m) = 0$. In all potentials, z_m is fixed at 2.97 Å,[98] a typical O...O separation in the O–H...O hydrogen bond. It is to be noted that the individual terms of the (9-3) potential, as derived from the (12-6) Lennard-Jones potential by integration,[81] are usually associated with the exchange repulsion and dispersion attraction, respectively. We will however treat the (9-3) potential in a purely formal way, without assigning the original physical meaning to its individual terms.

[viii] The head-group surface potential (Eq. (3.12)) comprises no explicit terms dependent on the orientation of the S-C bond.

Both non-orienting and orienting walls are considered. In describing non-orienting walls, isotropic water-wall potentials are used. For these walls, hereafter referred to as walls of the I-type, ε is treated as a constant. A total of four distinct values are tried for ε. One value, $\varepsilon = \varepsilon_0 = 0.46$ kcal/mole, represents a typical interaction energy of a water molecule with hydrophobic paraffin-like surfaces.[43] For walls capable of forming hydrogen bonds with water, ε is assigned the meaning of the hydrogen bond energy between a water molecule and the wall, $\varepsilon = \varepsilon_H$. Three discrete values are tried for ε_H: 6.24, 10 and 15 kcal/mole. The first value is the binding energy of a linear TIP4P water dimer,[98] whereas the two higher values are selected somewhat arbitrarily just to follow the effect of the water-wall bond strength on the hydration force. From the standpoint of the water-wall interaction energy, all the three non-orienting walls with $\varepsilon = \varepsilon_H$ can be regarded as hydrophilic.

For orienting walls, ε is considered to be dependent on the orientation of the water molecule. In constructing an appropriate model for ε, we assume that the preferred hydrogen bonding coordination of the water molecule is tetrahedral. With this choice, ε is represented as the sum of orientation-dependent contributions from the individual water protons and lone electron pairs:

$$\varepsilon = \varepsilon_0 + \varepsilon_\mathrm{H} \sum_i h_i(\theta_i) \ . \tag{3.15}$$

In this equation $h_i(\theta_i)$ varies from 0 to 1 and describes the orientation dependence of the energy of the hydrogen bond formed by the i-th water proton or lone electron pair and the surface; θ_i is the angle between the O–H bond or O–lone pair vector and the outward-pointing vector normal to the wall surface ($0 \le \theta_i \le 180°$, see **Figure 3-9**). It is assumed, for simplicity, that the angle between the two O–lone pair vectors in the water molecule is the same as between the O–H bonds (104.52° for the TIP4P model, see **Figure 3-1**).[98] The numerical values of the potential parameters ε_0 and ε_H in Eq. (3.15) are taken to be the same as discussed above for the non-orienting walls. For the orienting walls, ε_H takes on the meaning of the energy of a single hydrogen bond formed by a water molecule with the wall. The parameter ε_0 is introduced in the expression for ε to avoid penetration of the water molecule into the wall when no hydrogen bonds are formed, *i.e.* when all $h_i(\theta_i) = 0$. In modeling proton acceptor walls (hereafter, the walls of the A-type), the summation in Eq. (3.15) is performed over the two water protons, while for the walls bearing both proton acceptors and proton donors (hereafter, the AD-type walls), the lone electron pairs are included as well. In this way, the ability of the wall to carry either proton acceptors only or both proton acceptors and proton donors is modeled.

The function $h(\theta)$ in Eq. (3.15) is in essence a somewhat smoothed on-or-off function. As seen from **Figure 3-9**, where $h(\theta)$ is depicted, the hydrogen bond forms only if the direction of the O–H bond or O–lone pair vector is partly down, *i.e.* $\theta > 90°$. In the transition range, $90° < \theta \leq 180° - \Theta$, $h(\theta)$ is represented by a cosine function and it rapidly increases from 0 to 1 as the hydrogen bond geometry becomes closer to linear. At $\theta > 180° - \Theta$, $h(\theta) = 1$, so that the hydrogen bond energy is independent of θ and takes its maximum value, ε_H. The width of the latter interval, Θ, is an important parameter which specifies the directionality of the hydrogen bond and also the relationship between the binding energies of single, double and triple hydrogen bonds formed by the water molecule with the wall. The presence of an orientation independent range in $\varepsilon(\theta)$ at $180° - \Theta < \theta < 180°$ formally reflects the flexibility of the surface groups, which allows them to adjust their orientations so as to meet water molecules at the most favorable angles for the formation of hydrogen bonds. The more flexible the surface groups, the greater Θ. For this reason, Θ will hereafter be referred to as the flexibility parameter. As Θ is decreased, the orientation independent range in $\varepsilon(\theta)$ becomes narrower and the orienting effect of the wall is enhanced.

For walls of the A type, the energies of the strongest double and single hydrogen bonds can be easily shown to be in the ratio $2:1$ when $\Theta > \angle HOH/2 \cong 52°$. At $\Theta = 30°$, this ratio reduces to $1.4:1$, which is close to the *ab initio* electronic structure calculation results for the double and single hydrogen bonds formed by water with the oxygen atoms of an oligo(ethylene oxide) chain.[34,64] For walls of the AD type, the ratio $3:2:1$ for the triple, double, and single hydrogen bond energies is attained when Θ is chosen to be greater than ~70°.

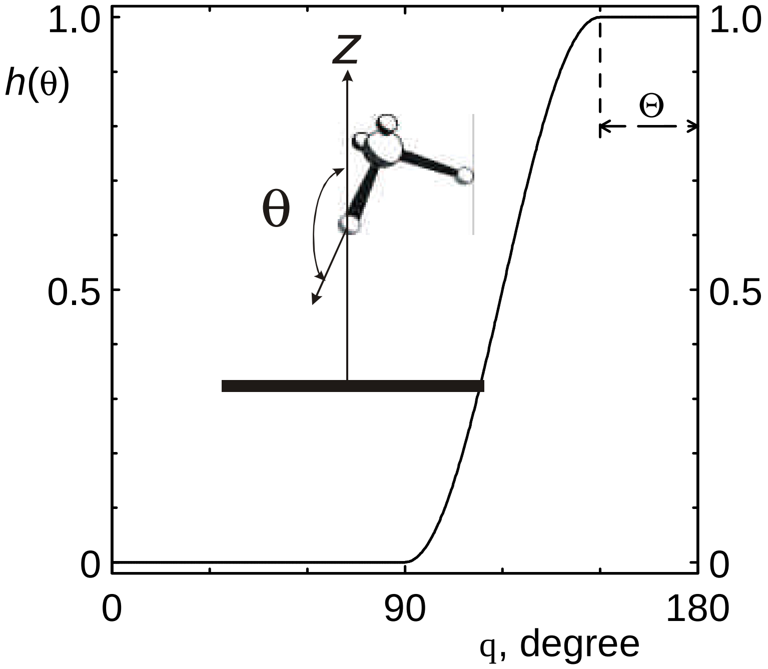

Figure 3-9 Orientation dependence of the hydrogen bond potential, as specified by $h(\theta)$ in Eq. (3.15).

Chapter 4: Water confined between structureless walls

4.1 Bulk water

The knowledge of the chemical potential of bulk water is a prerequisite of simulating confined water in the chemical equilibrium with the bulk water reservoir (**Figure 1-1** in **Chapter 1**). For rigid water models, such as TIP4P, only the excess (non-ideal) part of the chemical potential, μ', is required. An early MD simulation by Hermans *et al.*[99] using the thermodynamic integration method resulted – for the TIP4P model at room temperature – in a value of –5.3 kcal mole^{-1}, in satisfactory agreement with an experimental estimate of –5.7 kcal mole^{-1} based on the known ratio between the molar volumes of water vapor and liquid. Note that the Herman's *et al*. simulations[99] were made with a very small periodic system (N = 80) and a fairly short cut-off distance (6 Å). More recently, Shelley and Patey[83] reported a value of –6.0 kcal mole^{-1} as best reproducing the room-temperature bulk water density when the TIP4P model and Ewald summation method were employed.

To find μ' suited to the particular summation scheme, cut-off distance, and typical system size used in our simulations of confined water, we performed a series of bulk water simulations as a function of μ'. In these simulations, the periodic boundary conditions were used in all three dimensions. The experimental bulk water density at room temperature, ρ_b = 0.997 g cm^{-3}, was reproduced at μ' = –6.10 kcal mole^{-1}, close to the Shelley and Patey result.[83] However, the respective bulk pressure, as calculated from the virial formula, proved to be 0.13 ± 0.03 kbar higher than the atmospheric pressure. The desired pressure was obtained at μ' = –6.15 kcal mole^{-1}. The corresponding equilibrium density was 0.991 g cm^{-3}, 0.6 % lower than required. The observed small inconsistency between the calculated equilibrium pressure and density of TIP4P water is hardly surprising because the original fitting of the TIP4P model to the experimental properties of water employed a different cut-off distance, number of molecules in the simulation cell, and statistical ensemble (NPT)[ix] than our simulations. In deciding between the two alternative values found for μ', our reasoning was that the

---

[ix] The difference in the statistical ensembles could introduce some discrepancy in view of the relatively small system size used in deriving the TIP4P model (N = 125).[98]

"overpressure" of 0.13 kbar could be readily compensated for through Eq. (2.28), unlike the shift in density, which might have an unpredictable effect on the structural organization of water near confining surfaces. So, the excess chemical potential of –6.10 kcal mole^{-1}, which exactly reproduced ρ_b, and somewhat overestimated p_b was adopted in all subsequent calculations.

4.2 Non-orienting walls

We begin the discussion of the I-type walls with the one characterized by the most shallow potential ($\varepsilon = \varepsilon_0$). The behavior of water between two such walls was studied in the separation range 30 Å ≤ H ≤ 65 Å. At the wall-to-wall separations less than a critical separation H_c = 58.4 Å, the confined water experienced capillary evaporation (cavitation), typical of hydrophobic confining surfaces: Starting with a certain length of the MC run, the number of water molecules rapidly decreased until nearly all of the molecules left the confined region. At separations in a ~0.5 Å range below H_c, the state of the system was dependent on the starting configuration used to initiate the MC run: Some configurations resulted in cavitation, while the other remained liquid up to 10^7 MC passes. It is therefore quite likely that H_c would shift to larger separations if the MC runs would be longer. Note that the observed H_c = 58.4 Å agrees with a theoretical mean-field estimate of the limit of metastability reported by Lum *et al.*[31] for water confined between two hard walls (~50 Å). On the other hand, H_c is about an order of magnitude larger than the critical slit width found by Wallqvist and Berne[30] for two hydrophobic ellipsoids (~6.4 Å). A likely reason is a comparatively small size and large curvature of the ellipsoids, as well as the absence of an attractive contribution in the water-ellipsoid interaction potential.

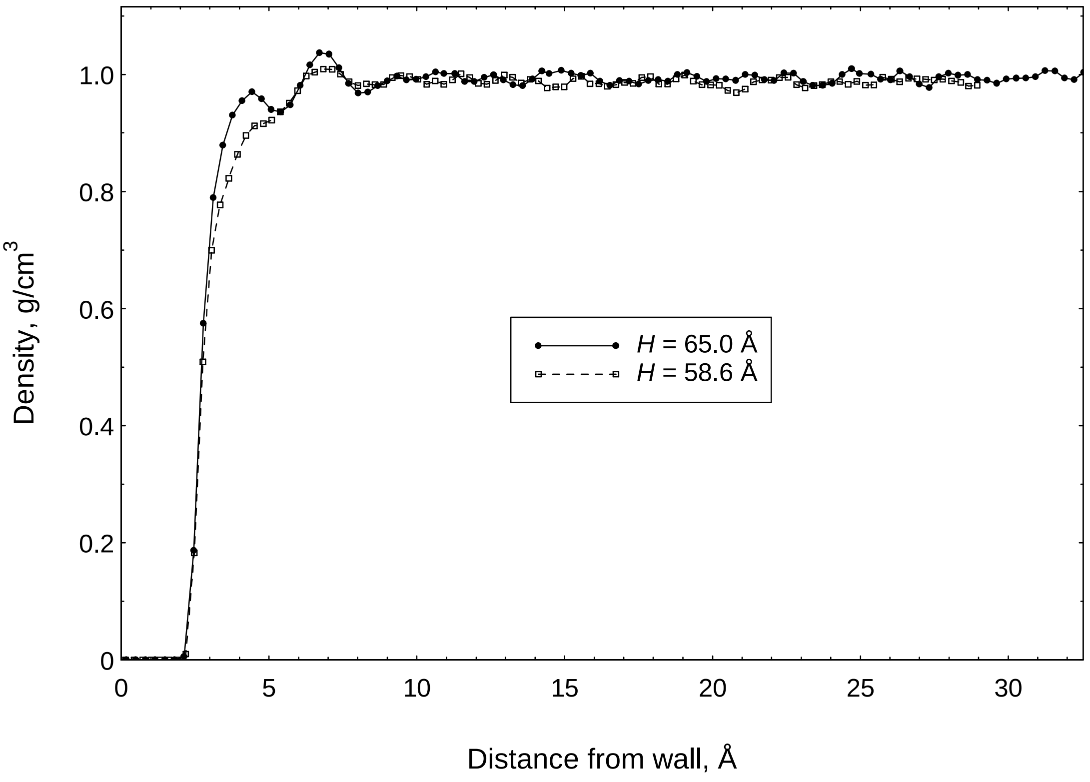

Figure 4-1 Water density distributions for the hydrophobic I-type wall at two wall-to-wall separations *H*.

The water density distribution ρ(*z*) near the $\varepsilon = \varepsilon_0$ wall is shown in **Figure 4-1** for the largest separation tried (65 Å) and also for a separation of 58.6 Å just beyond H_c. The vanishing density at $z < 2$ Å is associated with the sharply ascending water-wall repulsion and it is observed for all the walls studied in this work. By contrast, the substantially depressed density in the range 3 Å < z < 6 Å is a distinguishing feature of the $\varepsilon = \varepsilon_0$ I-type wall, which can be compared with the theoretical predictions by Lum *et al.*[31] for water in contact with hydrophobic walls. As H approaches H_c, the density depression progresses. The average water density between the walls is also substantially depressed (Table 4-1).

TABLE 4-1. Average density, hydration pressure and integrated order parameter for water confined between I-type walls

ε, kcal mole^{-1}	H, Å	$\bar{\rho}$, g cm^{-3}	p_h, kbar	Ξ
0.46	65	0.898	-0.51	0.011
0.46	58.6	0.885	-0.53	0.010
6.24	40	0.980	-0.12	0.018
10	40	1.013	0.13	0.017
15	40	1.040	0.28	0.018

Although the water-wall interaction potential for the I-type surfaces contains no explicit orientation-dependent terms, the $\varepsilon = \varepsilon_0$ wall does have a perceptible orienting effect on the neighboring water molecules. This can be seen from **Figure 4-2**, which shows the distribution of angles formed by the O–H bond vector and the *z*-axis for different separations from the wall. The orientation of a typical water molecule at the wall is such that one of its O–H bonds is preferentially directed toward the surface ($\theta_{OH} = 180°$), in agreement with the results of MD simulations by Lee and Rossky[47] who used the same potential model for water and the wall. With increasing separation, the molecules reorient so that one of their O–H vectors look preferentially outward the surface ($\theta_{OH} = 0$). The orientational ordering near the $\varepsilon = \varepsilon_0$ wall was found to be short range and lost almost completely at separations greater than two molecular diameters.

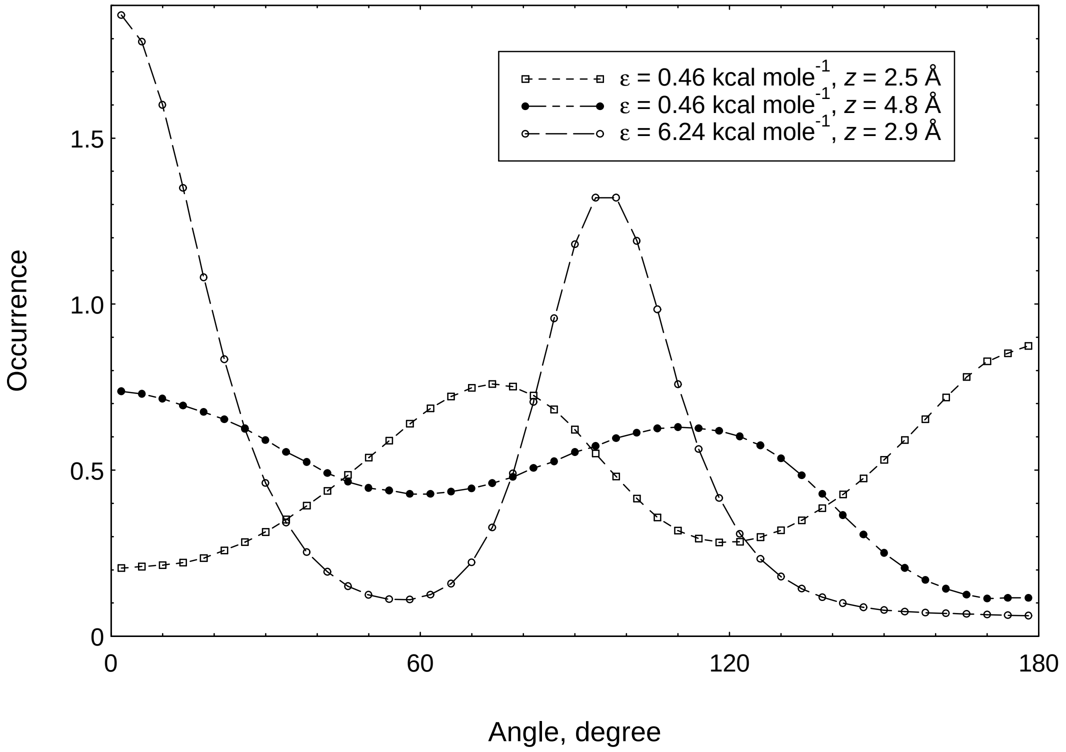

Figure 4-2 Orientational distribution of O-H bonds for some selected separations from I-type walls with ε = 0.46 and 6.24 kcal mole^{-1}.

The simulation results for p_h at $H > H_c$ (Table 4-1) show a strong hydrophobic attraction between the $\varepsilon = \varepsilon_0$ walls, which can be associated with the reduction in water density. That is, as the separation between the walls is increased, the driving force behind the hydrophobic attraction changes from cavitation to density depression. Importantly, the magnitude of p_h due to the density depression substantially exceeds the upper limiting value of p_h due to cavitation, $p_h < p_b$ (0.13 kbar in our case). This result can be roughly understood in terms of the fact that the compressibility of liquid water is very low, so that a small reduction in the water density may result in a significant stretching of the confined water. The substantial exceeding of p_h over p_b also means that the treatment of the hydrophobic attraction solely in terms of cavitation or “drying” can hardly provide a comprehensive description of this phenomenon.

The increase in the wall-water interaction strength on going from the $\varepsilon = \varepsilon_0$ to $\varepsilon = \varepsilon_H$ walls is accompanied by substantial changes in the structure and properties of confined water. Already at ε_H = 6.24 kcal mole^{-1}, the water density distribution becomes sharply structured and shows two distinct hydration layers next to the wall (**Figure 4-3**). The orientational ordering perceptibly increases, which can be judged from the increase of the density-weighted order parameter Ξ in Table 4-1. A typical water molecule in the first hydration layer now has one of its O–H bonds directed outward the wall (**Figure 4-2**).

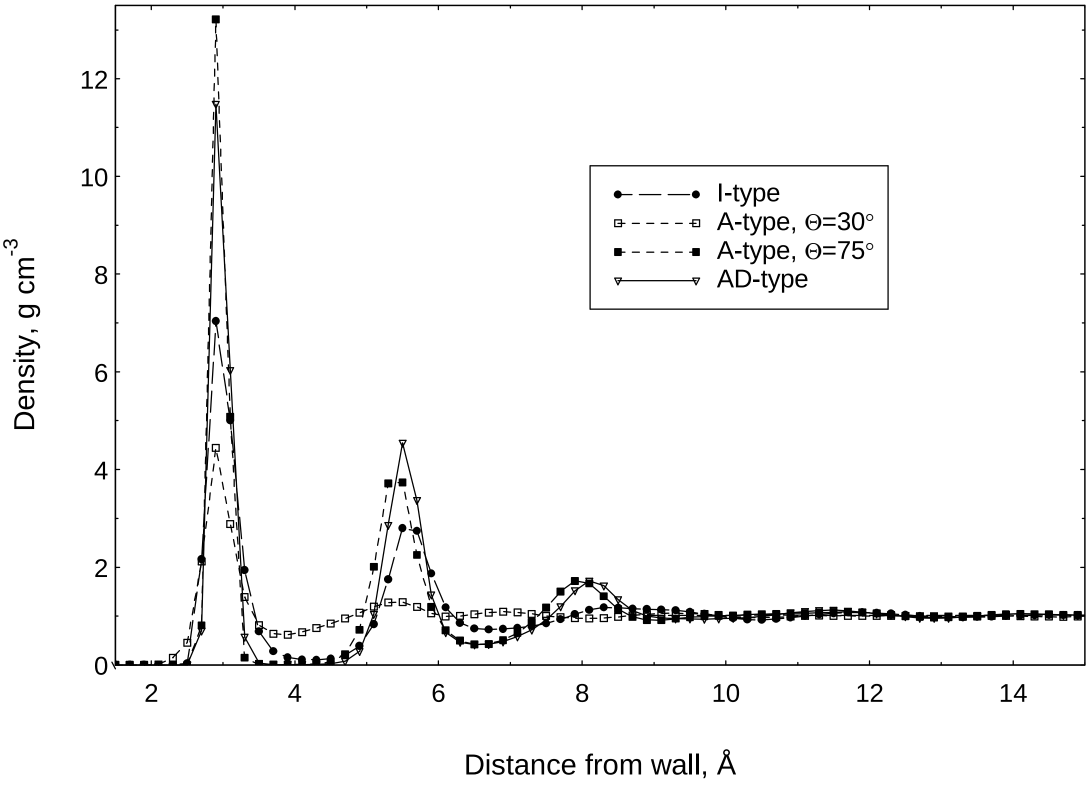

Figure 4-3 Water density distribution for the I-, A- and AD-type walls with ε_H = 6.24 kcal mole^{-1}.

The behavior of p_h as a function of H is shown in **Figure 4-4** together with the data for the ε_H = 6.24 kcal mole^{-1} walls of the other types. Because of the high computational cost of these simulations, we restricted ourselves only to few selected separations and did not undertake calculation of the detailed profile $p_h(H)$. It can nevertheless be seen that p_h ceases changing its sign at $H \approx 18$ Å, long before the separation of 40 Å used in most our simulations. (Note that at ε_H = 6.24 kcal/mole, all the walls showed no cavitation at all separations tried.)

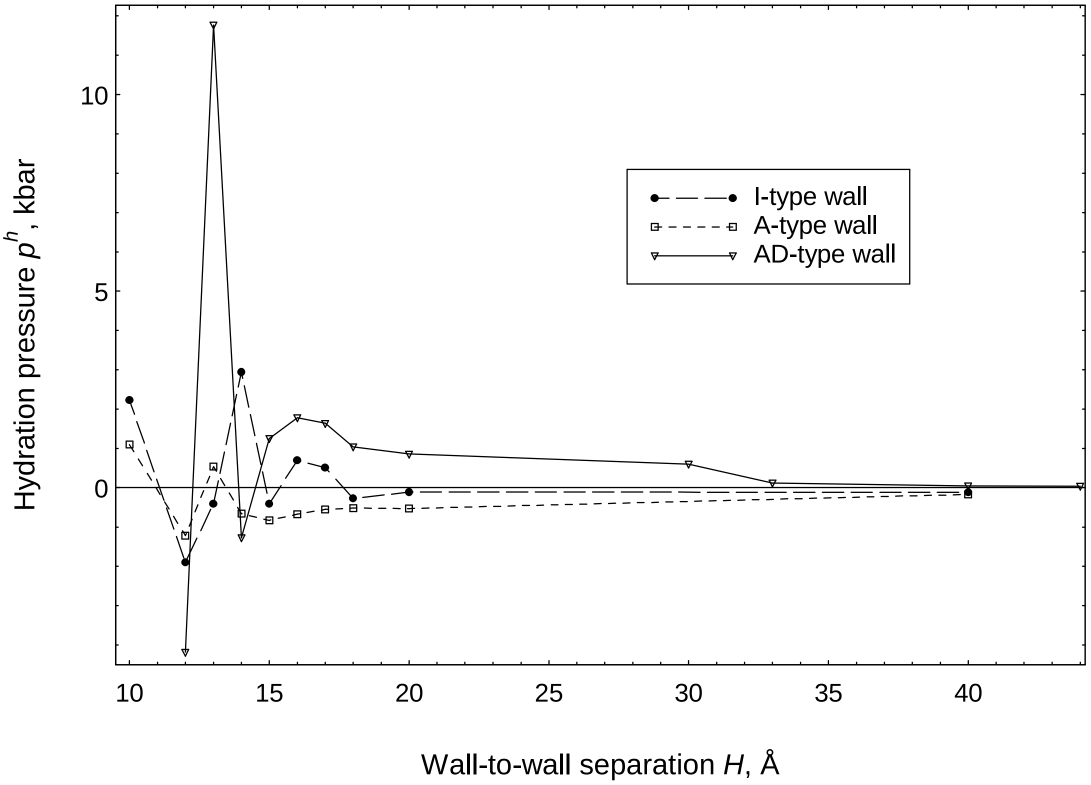

Figure 4-4 Hydration pressure as a function of wall-to-wall separation for the I-, A- (Θ = 30°) and AD-type walls with ε_H = 6.24 kcal mole^{-1}.

From the negative sign of p_h exhibited by the I-type ε_H = 6.24 kcal mole^{-1} wall at large separations, we conclude that it is hydrophobic. The origin of its hydrophobicity can be understood from a simple analysis of the individual components of the water film tension, $\gamma = (\Delta U - T\Delta S - \mu\Delta N)/A$. At the given ε_H and H = 40 Å, $\overline{\rho}$ is fairly close to ρ^b (see Table 4-1) and hence ΔN vanishes. For the ensemble-averaged potential energy, the simulations give –11.4 kcal mole^{-1}, which is substantially lower than that for bulk water (–10.1 kcal mole^{-1}). Considering that these energies refer to the systems with nearly the same N, we obtain that $\Delta U < 0$. Thus we can conclude that the positive sign of γ can only result from a negative ΔS. The obvious cause of the entropy loss in the confined region is the surface-induced ordering. The entropic factor was earlier found to be dominant for water confined between hydrophobic ellipsoids[30] and it turns out to be important in our case, too.

As ε_H is increased to 10 and then 15 kcal mole^{-1}, the average potential energy decreases to –12.3 and –13.5 kcal mole^{-1}, respectively. This more than compensates for the loss in entropy with the result that p_h goes repulsive and the wall becomes hydrophilic (Table 4-1). Simultaneously, $\overline{\rho}$ becomes greater than ρ_b, as intuitively expected.

4.3 Proton-acceptor walls

The simulations of water near the walls of the A-type were performed for two different flexibility parameters, $\Theta = 30°$ and 75°. We first discuss the results for $\Theta = 30°$, which correspond to a stiffer hydrogen bond and hence a stronger orienting effect of the wall on the neighboring water molecules. Compared to the I-type wall with $\varepsilon_H = 6.24$ kcal mole^{-1}, the water density distribution near the A-type wall with the same ε_H is less structured (**Figure 4-3**). Both the first and second density maxima of $\rho(z)$ are substantially lower in intensity and the gap between them is partly filled. An analysis of the angular distribution of the molecular dipole moments and O–H vectors shows that the water molecules near the wall of the A-type have two distinct preferred orientations associated with the formation of double and single hydrogen bonds with the wall. The presence of two kinds of hydrogen bonds, which differ noticeably in strength, leads to a wide variation in the wall-water bond lengths and the associated smearing of $\rho(z)$ between the first and second maxima.

The property of the A-type wall to bind water molecules in a highly asymmetric way, with their O–H bonds directed preferentially towards the wall, brings about strong and fairly long-ranged orientational ordering. This can be appreciated from **Figure 4-5**, which compares the order parameters $S_0^1(z)$ for water in contact with the I-, A- and AD-type walls. In the case of the I-type walls, which are characterized by oscillations of $S_0^1(z)$ about zero, Ξ is fairly small, positive and practically independent of the strength of the water-wall interactions, as specified by the magnitude of ε_H (Table 4-1). By contrast, water in contact with the A-type walls shows large negative Ξ, strongly dependent on ε_H (Table 4-2).

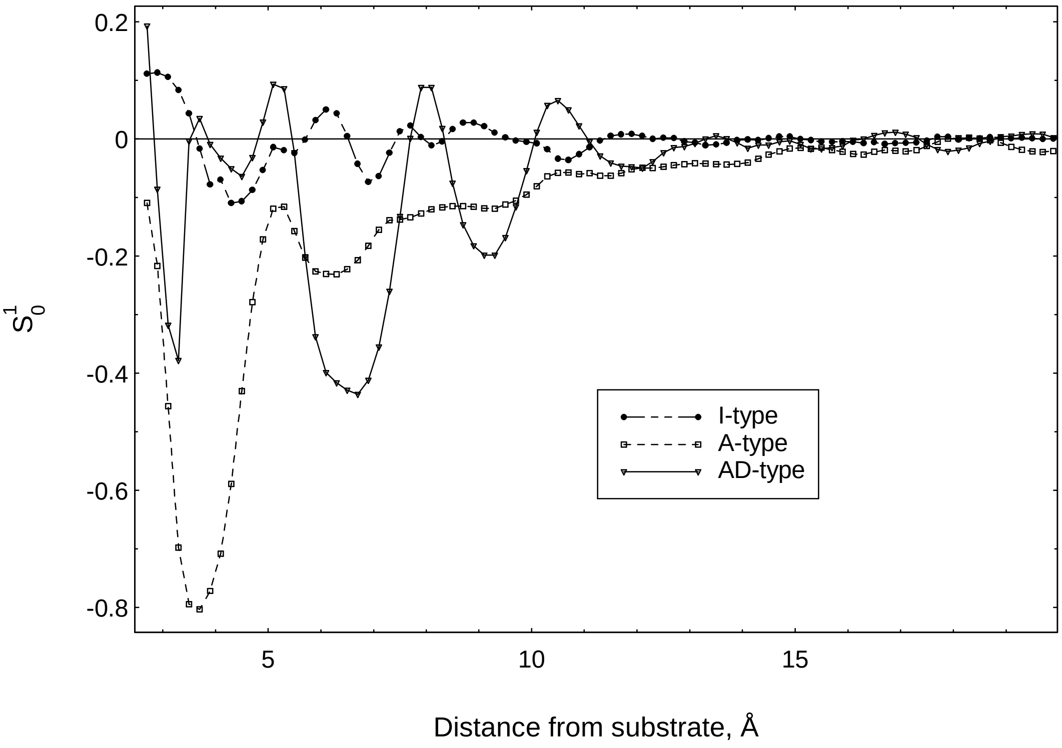

Figure 4-5 Orientational order parameters S_0^1 for the I-, A- (Θ = 30°) and AD-type walls with ε_H = 15 kcal mole^{-1}.

TABLE 4-2. Average density, hydration pressure and integrated order parameter for water confined between A-type walls (H = 40 Å)

ε_H, kcal mole^{-1}	Θ, deg	$\bar{\rho}$, g cm^{-3}	p_h, kbar	Ξ
6.24	30	0.938	-0.37	-0.052
10	30	0.965	-0.21	-0.090
15	30	0.992	-0.09	-0.123
6.24	75	0.982	-0.15	-0.050
10	75	1.007	-0.07	-0.078
15	75	1.040	-0.02	-0.108

As noted in **Chapter 3**, the A-type wall with $\Theta = 30°$ is capable of forming double hydrogen bonds with a water molecule with a total binding energy of $1.4\varepsilon_H$. That is, based on the wall-water interaction strength, the A-type walls can be expected to be more hydrophilic than the I-type walls with the same ε_H. In spite of this, however, the former are found to result in lower p_h (*cf*. Tables 4-1 and 4-2). Moreover, the A-type walls all show attractive p_h and hence they are hydrophobic at all ε_H tried. From Tables 4-1 and 4-2, one can also see that at a given ε_H the average water density between the A-type walls is higher than that between the I-type walls, so that the more attractive hydration forces observed between the A-type walls cannot be explained in terms of density depression.

A comparison of the I- and A-type walls in terms of the internal energy shows that the latter are 0.7 to 1.1 kcal mole^{-1} inferior. The reason can be understood from **Figure 4-6**, which presents the average interaction energy of a water molecule with its surroundings as a function of its separation from the I- and A-type walls with $\varepsilon_H = 15$ kcal mole^{-1}. Both the total interaction energy and its constituents due to the water-water and water-wall interactions are shown. One can see that the residence of a water molecule near the A-type wall is energetically less favorable, mainly because of an appreciable loss in the water-water interaction energy. The energy loss is particularly pronounced in the first hydration layer, where the orientational ordering is strongest and each water molecule has to sacrifice at least one hydrogen bond with its neighbors in order to bind to the wall. The constraints imposed by the orientational ordering upon the freedom of the water molecules to form hydrogen bonds with each other remain important in the second hydration layer and at farther separations. In this separation range, no hydrogen bonds with the wall can be formed, yet the loss of the water-water interaction energy is quite perceptible.

The presence of sharply directional interactions at the wall-water interface affects not only the water-water but also the water-wall contribution to the average interaction energy. From the respective curve in **Figure 4-6**, one can see that the interaction energy of the A-type wall with a typical water molecule in the first hydration layer is only slightly greater in magnitude than the energy of a single hydrogen bond ($\varepsilon_H = 15$ kcal mole^{-1} for the example shown in the figure). This suggests that the too stiff hydrogen bond potential used in this simulation impedes the formation of double hydrogen bonds with the wall. All the above mentioned factors make the A-type walls energetically less favorable compared to the I-type walls. The stronger orientational ordering induced by the A-type walls should also make them unfavorable from the entropic standpoint, too.

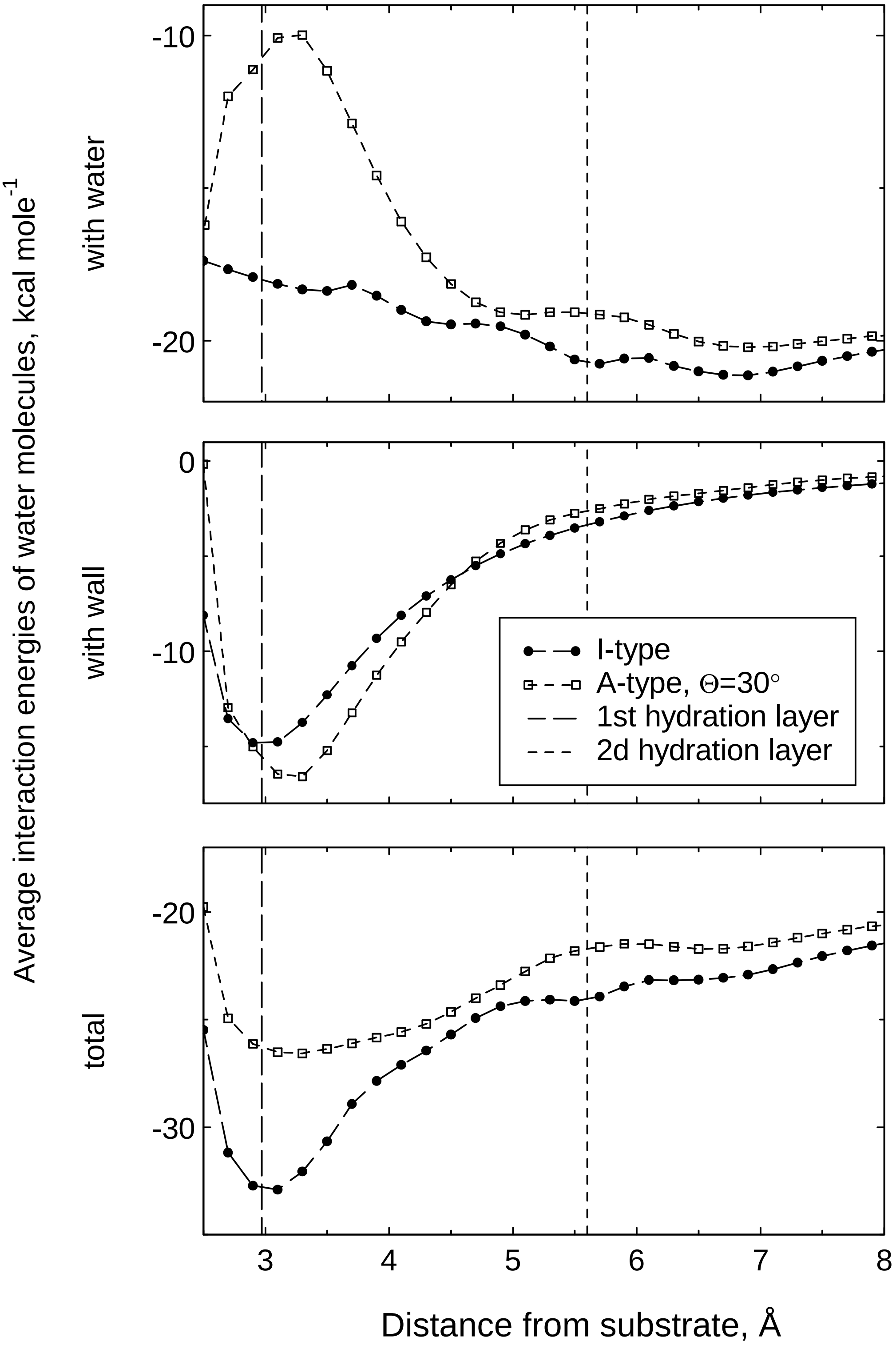

Figure 4-6 Average interaction energy of a water molecule with its surroundings and the individual contributions to this energy for the I-type and A-type (Θ = 30°) walls with ε_H = 15 kcal mole^{-1}.

The increase of the flexibility parameter Θ from 30° to 75° makes all O–H bond orientations with θ_i ranging from 105° to 180° energetically equivalent. This reduces the orientational ordering (see the changes in Ξ in Table 4-2) and affords more orientational freedom for the water molecules in forming hydrogen bonds with their neighbors and the wall. As a consequence, the wall becomes less hydrophobic (or more hydrophilic) which manifests itself in an increase in p_h.

Turning to the calculated average densities in Table 4-2, one can see that the changes in the density and hydration pressure show a same behavior: With increasing ε_H, both $\overline{\rho}$ and p_h increase. At the same time, the intuitive expectation that for hydrophobic confining walls $\overline{\rho}$ should always be lower than ρ_b proves to be fallacious: At $\Theta = 75°$ and $\varepsilon_H \geq 10$ kcal mole^{-1}, the system shows an enhanced $\overline{\rho}$ along with an attractive (hydrophobic) p_h. A similar example has been reported by Besseling[36] in his theoretical work.

4.4 Walls bearing both proton acceptors and proton donors

With the accepted orientation of the lone pairs in the water molecule, an AD-type wall sees the molecule as possessing a V_d symmetry. This means, in particular, that the wall-water potential is invariant with respect to a four-fold inversion axis transformation of the water molecule and the associated change in the sign of the molecular dipole moment. The water-water potential, however, does not possess this symmetry. As a consequence, the whole system may well show a non-vanishing S_0^1 even though the wall itself does not distinguish between the symmetrically related configurations with opposite dipole moments. (Note that similar arguments apply to the I-type surfaces, which show noticeable S_0^1 and Ξ despite the fact that the I-type walls perceive the water molecule as being isotropically symmetric.)

The orientational order generated in water by an AD-type wall can be appreciated from **Figure 4-5** for the case $\varepsilon_H = 15$ kcal mole^{-1} where the magnitude of S_0^1 is greatest. The ordering is seen to be particularly pronounced in the range from 6 to 7 Å and from 8.5 to 9.5 Å, where S_0^1 assumes large negative values. These ranges, however, correspond to minima in the water density distribution $\rho(z)$, while the positive portions of S_0^1 correspond to maxima of ρ(*z*) (**Figure 4-5**). As a consequence, the integrated density-weighted parameter Ξ proves to be fairly small (Table 4-3). As ε_H is decreased, Ξ vanishes.

TABLE 4-3. Average density, hydration pressure and integrated order parameter for water confined between AD-type walls (H = 40 Å, Θ = 75°)

ε_H, kcal mole^{-1}	$\bar{\rho}$, g cm^{-3}	p_h, kbar	Ξ
6.24	1.023	0.05	0.000
10	1.059	0.12	-0.003
15	1.093	0.15	-0.033

For all tried ε_H, $p_h > 0$ and hence the AD-type walls are all hydrophilic. The average density $\bar{\rho}$ is greater than ρ_b for all ε_H. (Table 4-3). An analysis of the energetics of the confined water region in terms of the water-water and water-wall interactions shows that the AD-type walls are intermediate in the water-water interaction energy between the I- and A-type walls with the same ε_H. However, the ability of the AD-type walls to form triple hydrogen bonds with water, with a total binding energy of 3εH, makes this type of wall much more favorable for water, compared to the I- and A-type walls.

Chapter 5: Water confined between self-assembled monolayers

5.1 Water confined between Ag-supported SAMs.

It is known from *ab initio* electronic structure calculations[34,64] that the EG3-OMe tail favors a nearly helical conformation characterized by a *trans-gauche-trans* (*tgt*) configuration of the O-C–C–O bond sequences. A similar conformation is observed experimentally for the poly(ethylene glycol) (PEG) macromolecules in their crystal.[100] On the Ag substrate, the EG3-OMe terminated alkanethiol molecules form an incommensurate crystal-like monolayer structure, in which the EG3-OMe tails are in the all-*trans* planar conformation, as occur in stretched PEG crystals.[101] As shown by our static lattice energy calculations, the driving force behind the transition from the helical to all-*trans* conformation in the EG3-OMe terminated SAM is a substantial increase in the packing density, which forces the EG3-OMe tails to assume a more extended conformation favorable for packing.

The simulation results for the distribution of dihedral angles in the EG3-OMe tails when in contact with water show a noticeable concentration of *gauche* defects close to the chain ends (**Figure 5-1**).[x] The appearance of these defects is partly associated with the formation of hydrogen bonds between the topmost oxygen atoms of the EG3-OMe tails and the water molecules. In the density profiles shown in **Figure 5-2**, the water molecules involved in the hydrogen bonding with the SAM are seen as a shoulder on the low-density edge of the water density distribution $\rho(z)$. The overlap of the shoulder with the profile of the SAM density is indicative of some penetration of water into the SAM, down to the topmost oxygen atoms. Note that the ability of individual water molecules to form hydrogen bonds with the topmost oxygen atoms of the Ag-supported SAM could not be detected in the *ab initio* static energy calculations by Wang *et al.*[64] owing to the neglect of thermal motion of both the water and EG3-OMe molecules.

---

[x] All the dihedral angles in the dry state are sharply peaked at 180 deg, with the width of the peaks being 2-3 degs.

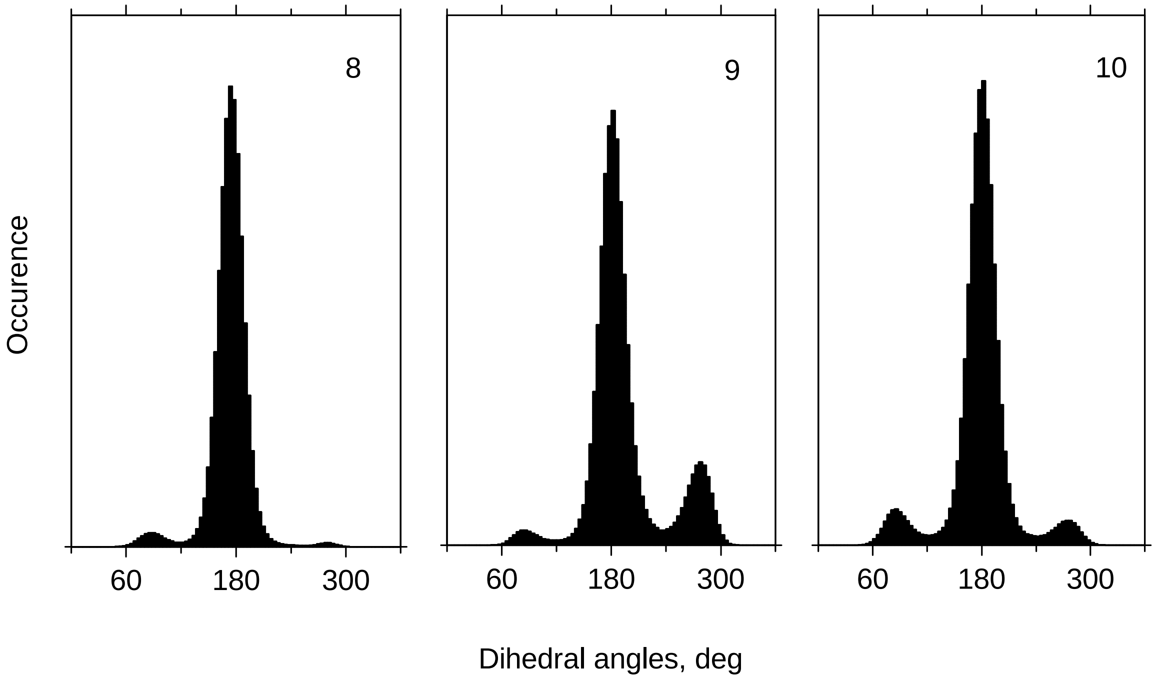

Figure 5-1 Distribution of the three terminal dihedral angles in the EG3-OMe tails for the Ag-supported SAM in contact with water.[xi] The angle numbers, k, correspond to the numbering system[80] in which the dihedrals are numbered in succession from 1 to 10, starting with the C-C-O-C dihedral angle at the junction of the alkanethiol chain and the EG3-OMe tail, and ending by the C–C–O–Me dihedral in the terminal methoxy group.

[xi] In the dry state, all the angles are sharply peaked at 180 deg, with the width of the peaks being 2-3 degs.

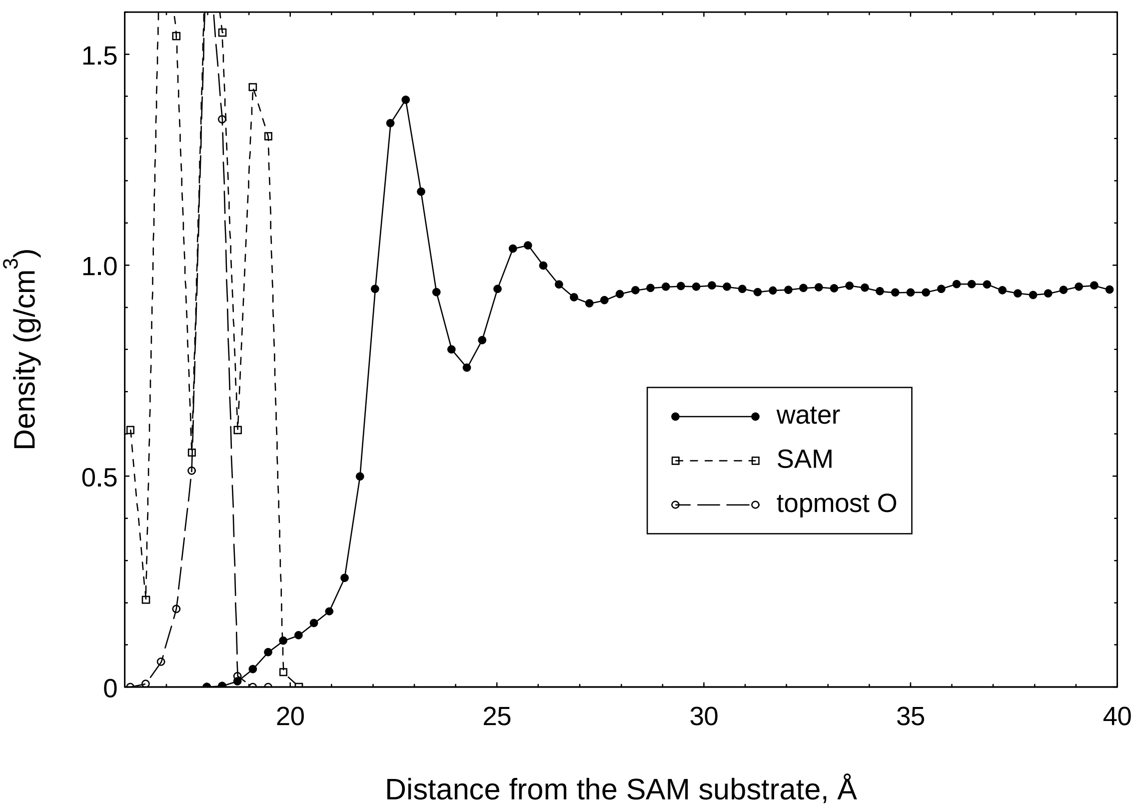

Figure 5-2. Density profiles of water, SAM and topmost oxygen atoms of the methoxy groups near the interface formed by the Ag-supported SAM and water.

Evaluation of the average number of hydrogen bonds formed by water molecules with the SAM during the GCMC run shows however that only 17 % of the EG3-OMe terminated alkanethiol chains are hydrogen bonded to water. About 35 % of these hydrogen bonds enter into bridged intermolecular bonds, in which one water molecule is bound to two different chains in the SAM. Based on the areal density of the SAM and the percentage of the chains involved in hydrogen bonding with water, it is easy to calculate that the areal density of the surface sites supplied by the SAM for hydrogen bonding with water is as low as 0.01 $Å^{-2}$, about seven times less than a lattice-model estimate of the value needed to match bulk water.[36] That is, despite the ability of the SAM to form hydrogen bonds with water, there is no reason to expect that the SAM will show a hydrophilic behavior.

The amphiphilic nature of the SAM surface manifests itself in the orientational distribution of water molecules in the interface region. This can be appreciated from

Figure 5-3, which presents the distance dependence of the orientational order parameter, $S_0^1 = \langle \cos\theta \rangle$, where θ is the angle formed by the molecular dipole moment with the *z* axis. The orientational ordering induced by the SAM is short ranged and affects only the molecules in the first hydration layer ($z < 24$ Å). For the majority of these molecules, corresponding to the main peak of the density distribution, the dipole moments point preferentially outward the SAM ($S_0^1 > 0$), which is typical of hydrophobic surfaces.[43,47] By contrast, the few water molecules that are directly involved in hydrogen bonding with the EG3-OMe chains have their dipole moments pointing inward the SAM, as it occurs near hydrophilic proton acceptor surfaces (see Chapter 4).[102]

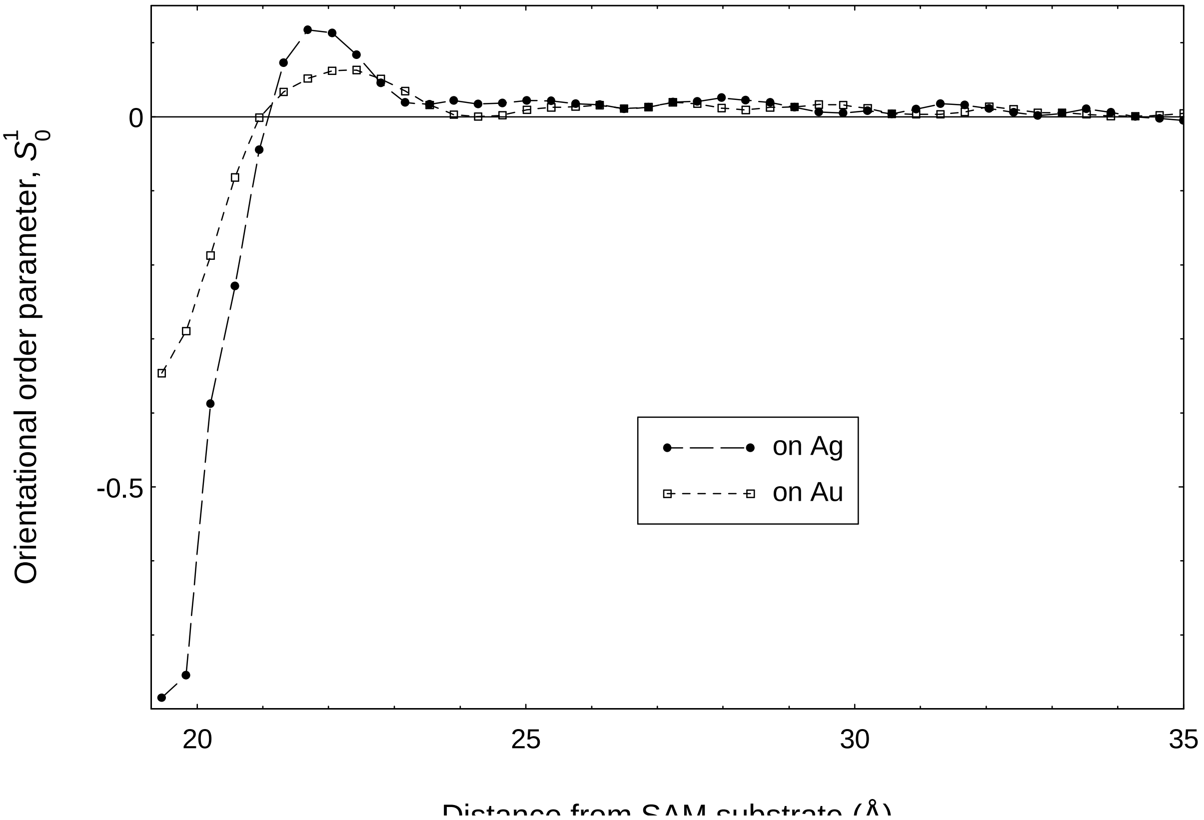

Figure 5-3 Orientational order parameter S_0^1 in water layers adjacent to the Ag- and Au-supported SAMs.

The effect of the SAM on the lateral distribution of water molecules in the adjacent water layers is fairly small. As an example, **Figure 5-4** compares the pair distribution function in the slice centered at the main density maximum with that in water bulk. The differences are a somewhat more pronounced first density peak and a slight shift of the density oscillations to a longer wavelength.

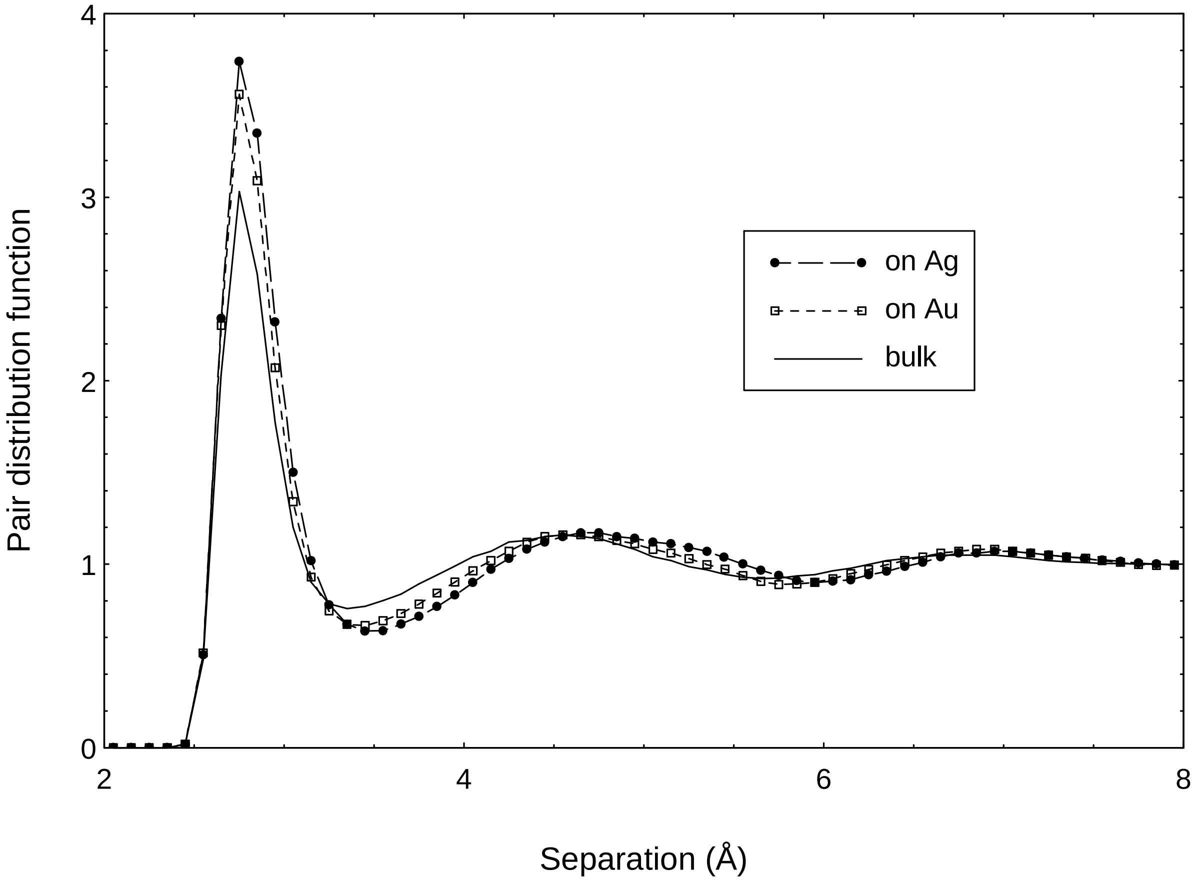

Figure 5-4 Pair distribution functions of water in slices corresponding to the main maximum of the water density profile for the Ag- and Au supported SAMs in comparison with that for bulk water.

Due to the dominance of hydrophobic areas on the SAM surface, the approach of a water molecule to the SAM is, on the average, energetically unfavorable. This can be seen from **Figure 5-5**, which shows the distance dependence of the average interaction energy of a water molecule with its surroundings, $\psi(z)$, *i.e.* the enthalpic part of the local chemical potential of water. At separations near the first density maximum, ψ loses about 2 kcal/mole in magnitude, compared to that in water bulk (**Figure 5-5**). As the molecule comes closer to the SAM surface, the energy loss is first partly compensated by the formation of hydrogen bonds with the SAM and then the magnitude of ψ rapidly drops mainly because of the loss of water-water interactions.

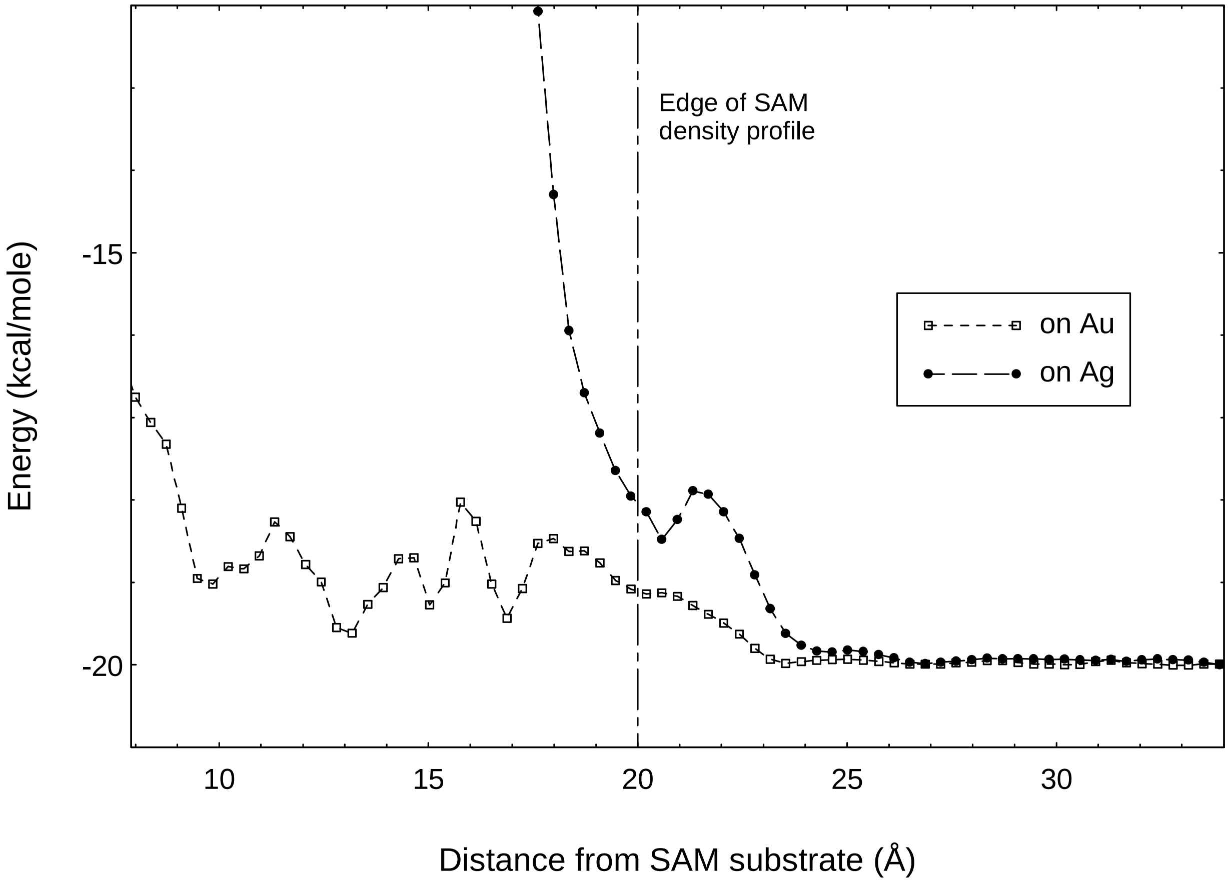

Figure 5-5 Average interaction energy of a water molecule with its surroundings in the SAM/water interface region for the Ag- and Au-supported SAMs.

We now turn to our results for the hydration pressure p^h and mid-point density $\rho_{H/2}$, which are summarized in Table 5.1. In our simulations, we have tried some selected separations H covering the range 60 Å ≤ H ≤ 100 Å. The SAM thickness, h, as determined from the low-density edge of the SAM density distribution (**Figure 5-2**), was about 20 Å and was practically independent of H. So, the thickness of the slit between the SAM surfaces, $H_0 = H - 2h$, ranged from 20 to 60 Å. At all tried $H_0 \leq 32$ Å, the system experienced capillary evaporation (cavitation) typical of water confined between hydrophobic surfaces: Starting with a certain length of the GCMC run, the number of water molecules sharply decreased until nearly all the molecules left the confined region. At higher separations, the system showed attractive p^h and noticeably depressed $\rho_{H/2}$, which is also characteristic of hydrophobic surfaces.[28,29] It is important that the calculated magnitude of p^h substantially exceeds the upper limiting value of p^h due to the pressure disbalance caused by cavitation, $p^h \leq p^b$ (0.13 kbar in our case). Similar results were obtained in simulations of water between structureless hydrophobic surfaces(see Chapter 4).[102] All this means that the interpretation of the hydrophobic attraction solely in terms of cavitation or "drying"[31] can hardly provide a comprehensive description of this phenomenon.

TABLE 5-1: Mid-point density and hydration pressure for water confined between EG3-OMe terminated alkanethiol SAMs

H (Å)	H_0 (Å)	$\rho_{H/2}$ (g/cm^3)[a]	p^h (kbar)[a]
on Ag substrate			
≤ 72	≤ 32	cavitation	
76	36	0.938	–0.51
80	40	0.944	–0.39
100	60	0.974	not converged
on Au substrate			
≤ 58	≤ 18	cavitation	
60	20	–[b]	–0.80
72	32	0.945	–0.43
80	40	0.951	–0.31
100	60	0.964	–0.04

[a] At H ≤ 80 Å, the statistical uncertainty in ρH/2 and ph was estimated to be 0.004 g/cm3 and 0.05 kbar, respectively. At H = 100 Å, the uncertainty in ph was at least 0.1 kbar for the Au-

5.2 Water confined between Au-supported SAMs.

In dry atmosphere, the EG3–OMe terminated alkanethiol SAMs prepared on the Au substrate form a structure, in which the EG3–OMe tails assume a helix-like conformation similar to that observed in isolated OEG molecules and PEG crystal.[24,34,64,100] The lattice of the sulfur head groups in the Au-supported SAMs is dictated by the head group-substrate interactions and is commensurate with the Au(111) lattice.[103] The alkane chains are tilted by ~35° with respect to the surface normal.[104,105] The separation between the sulfur head groups in the SAM is about 5 Å, which is substantially greater than the equilibrium separation between the alkane chains (~4.6 Å).[103]

According to the SFG measurements by Zolk *et al.*,[106] the contact with water causes a substantial conformational disordering and penetration of water into the SAM. This experimental finding is well supported by our computer simulations. The penetration of water molecules deep into the EG3-OMe layer of the SAM can be appreciated from the water and SAM density profiles in **Figure 5-6** and **Figure 5-7**. Note that the water density distribution within the SAM shows maxima that correlate with the positions of the ether oxygen atoms thus demonstrating the tendency of the water molecules to form hydrogen bonds with the EG3–OMe chains. The conformational disordering caused by the water molecules in the SAM can well be seen in the distribution of the dihedral angles in the EG3–OMe tails (**Figure 5-8**). An important result is that the EG3–OMe tails assume, on the average, more extended conformations compared to that observed in the dry SAM. In these conformations, most of the former *gauche* conformers around the C-C bonds give place to *trans* conformers (see dihedrals 3, 6, and 9 in **Figure 5-1**), so that the most populated conformer of the EG3–OMe tails becomes all-*trans*. The tails are in a nearly upright orientation, similar to that observed in the SAM on Ag. The net result of these changes is that the contact with water makes the SAM thickness practically independent of the substrate used (~20 Å, see **Figures 5-2** and **5-6**). Since the areal densities of the sulfur head groups in the Au- and Ag-supported SAMs are related as $(4.6/5.01)^2 \approx 0.84$, the volume density of the former proves to be 16 % lower than that of the latter. It is this difference in density which provides the space for accommodation of water molecules within the Au-supported SAM.

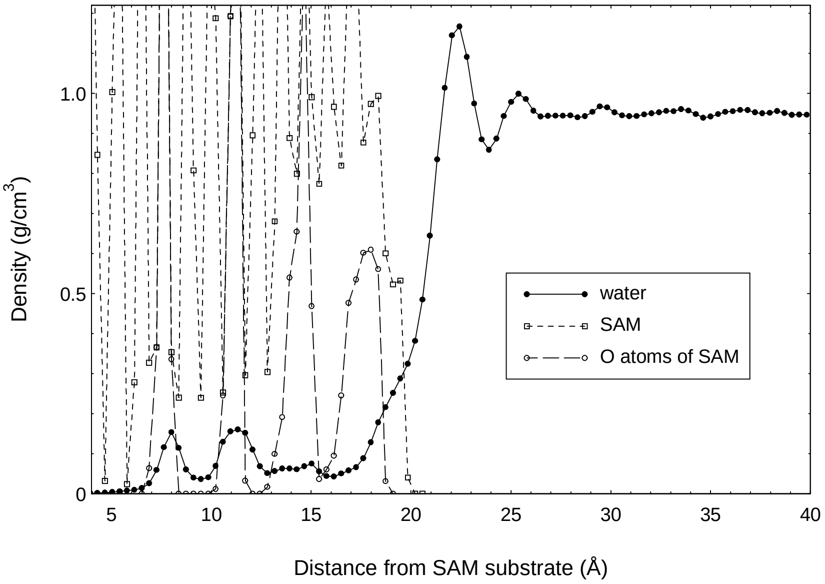

Figure 5-6 Density profiles of water, SAM and oxygen atoms of the EG3-OMe tails near the interface formed by the Au-supported SAM and water.

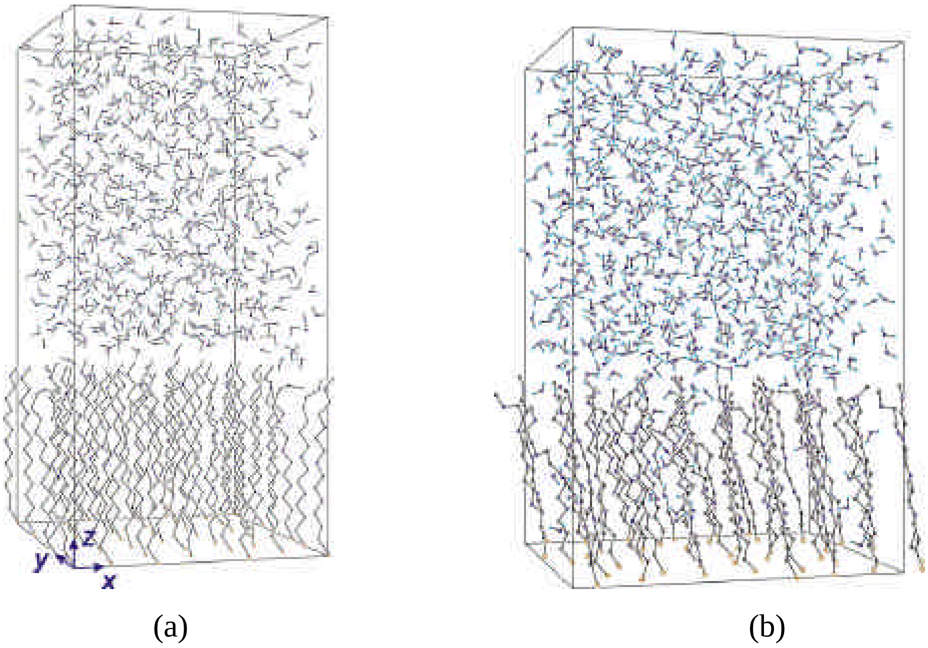

(a) (b)

Figure 5-7 The simulation cells used and a typical configuration of the system for the Ag-supported (a) and Au-supported (b)SAMs. For clarity, the hydrogen atoms in the EG3-OMe terminated alkanethiol molecules are not shown.

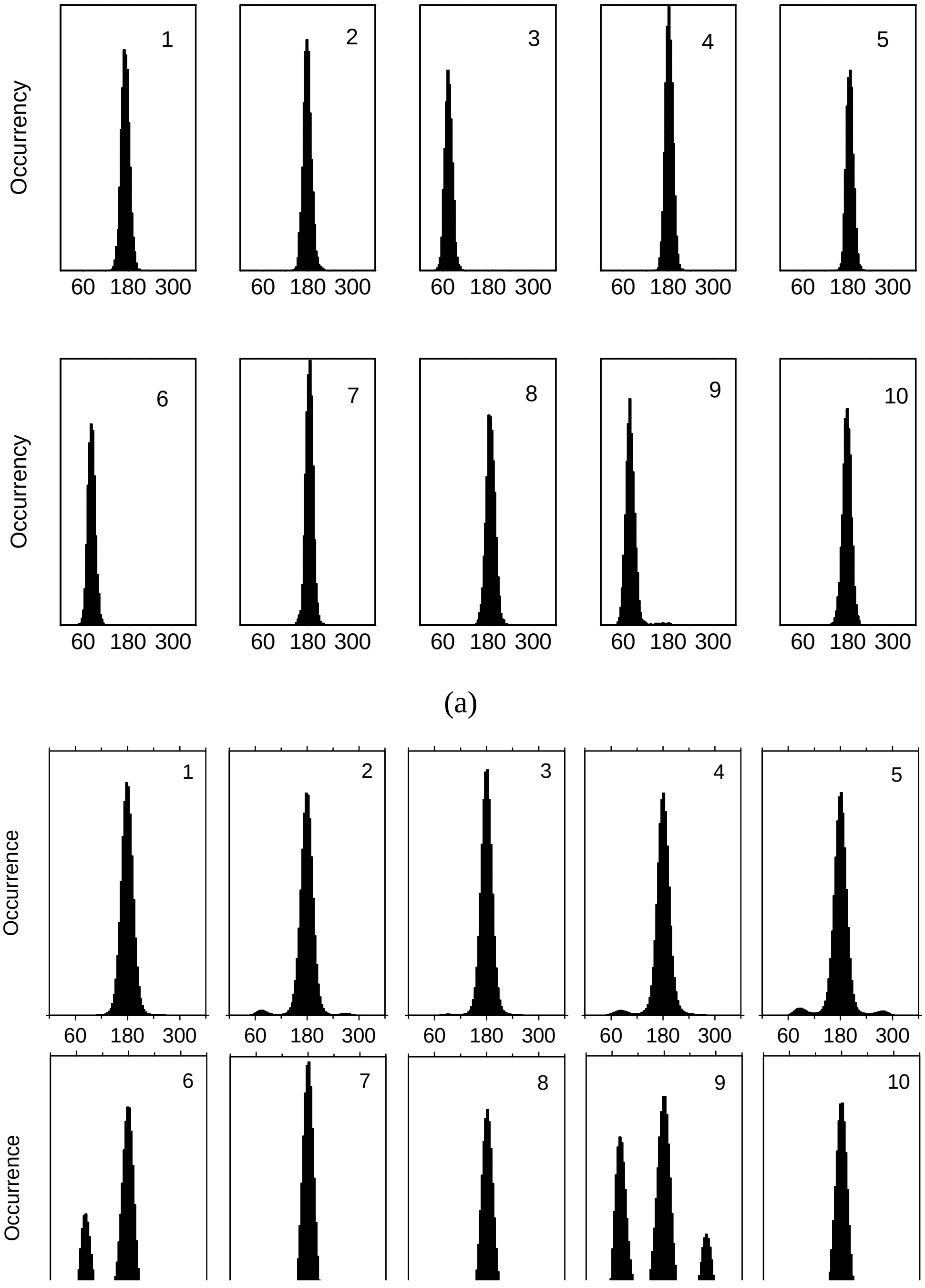

(a)

(b)

Figure 5-8 Distribution of dihedral angles in the EG3-OMe tails for the Au-supported SAM in the dry state (a) and contact with water (b) (see caption to **Figure 5-1** for atom numbering).

To make sure that the above-described structure of the SAM-water interphase region is representative of the equilibrium state of the system, three independent GCMC runs starting from different configurations were carried out. One starting configuration was taken to be the final configuration obtained in our previous studies.[80] The other two configurations were constructed by attaching a slab of bulk water, as simulated using the periodic boundary conditions in all three dimensions, to two different configurations of the SAM, one built up from ideal *tgt* helices and the other from ideal all-*trans* zigzags. After ~10^7 GCMC passes, all the three runs converged to nearly the same structure, as characterized by the distributions of density and dihedral angles.

The loss of stability of the helical *tgt* conformer on going from the dry Au-supported SAM to that in contact with water can be explained in the following way. As shown by the *ab initio* SCF calculations by Wang *et al.*,[64] a perfect close packing of the helical chains on a hexagonal lattice with a period of 5 Å does not allow water molecules to penetrate into the SAM to form hydrogen bonds with the next to the topmost and deeper oxygen atoms. These oxygen atoms can be reached by water molecules only if the EG3-OMe chains assume more extended conformations and nearly upright orientation relative to the substrate surface. That is, the loss in the conformational energy of the EG3-OMe chains is compensated for by the formation of hydrogen bonds between the penetrated water molecules and the three inner oxygen atoms of the chains. Integrating the water density distribution in **Figure 5-6** within the SAM-water interpenetration range (from 5 to 20 Å) we obtain 36 penetrated water molecules per simulation cell, *i.e.* one water molecule per EG3-OMe chain. All of these molecules are involved in hydrogen bonds with the ether oxygen atoms; 44 % of the water molecules are bound to the topmost oxygen atoms and the remaining 56 % to the three deeper oxygens. About 20 % of the hydrogen bonds formed by water with the EG3-OMe chains are bridged ones, and all of these latter are intermolecular.

Compared to the situation near the Ag-supported SAM, the approach of a water molecule to the surface of the SAM prepared on Au is associated with a noticeably smaller loss in the magnitude of ψ (~0.5 kcal/mole for molecules in the vicinity of the first density maximum, see **Figure 5-5**). Because of the conformational disordering of the EG3–OMe chains and a diffuse character of the SAM/water interface, the orienting effect of the SAM on the adjacent water layers is insignificant (**Figure 5-3**). The effect of the SAM on the lateral distribution of water molecules is also insignificant, less than that observed near the Ag-supported SAM (**Figure 5-4**). Thus a remarkable feature of the EG3–OMe terminated SAM on Au is that it perturbs the structure and energetics of the contiguous water layers only slightly.

At all tried separations in the interval 60 Å ≤ H ≤ 100 Å, corresponding to slit widths H_0 between 20 and 60 Å, the hydration pressure p^h is attractive and $\rho_{H/2}$ depressed (Table 5-1). In addition, at H ≤ 58 Å (H_0 ≤ 18 Å) water confined between the Au-supported SAMs shows capillary evaporation. That is, similar to the SAM on Ag, the Au-supported SAM behaves like a hydrophobic surface. It should however be noted that the capillary evaporation between the Au-supported SAMs occurs at a substantially smaller slit width compared to that between the Ag-supported SAMs (18 *vs*. 32 Å). In this respect, the former can be regarded as being less hydrophobic.

The simulation results for the hydration forces operating between the EG3–OMe terminated SAMs can be compared with the recent surface-force measurements by Dicke et al.[65] using scanning force microscopy. The experiments were performed in aqueous solutions of KNO_3 in a concentration range from 0.1 mM to 0.1 M. The Ag-supported SAMs exhibited a hydrophobic attraction practically independent of the ion concentration. The behavior of the Au-supported SAMs was more complicated. At low ion concentrations, the SAMs showed a long-range repulsion, which rapidly weakened with increasing ion concentration. At the highest ion concentration tried (0.1 M), the repulsion of the EG3–OMe terminated SAMs changed to attraction.

While the experimental results for the Ag-supported SAM[107] are in agreement with our GCMC simulations, the data for the Au-supported SAM are not. Since the simulations reproduce only the force that corresponds to ideally pure and non-dissociable water, the discrepancy between the simulation and experiment can well be attributed to the ions present in water. The surface force measurements by Dicke and Hähner[65,66] show that the surface force is only slightly dependent on the electrolyte used and is governed mainly by pH. The electric kinetic studies by Chan et al. confirmed that the EG3-OMe SAM surface is negatively charged at pH > 4.4.[67] That is the interfacial negative charge originates from an asymmetric adsorption of the products of water autodissociation, *viz.* from the preferential adsorption of hydroxide, OH^-, over hydronium, H_3O^+.[108] However, what is important here is that the EG3-OMe SAMs are not unique in exhibiting preferential hydroxide ion adsorption.[67] Combining our simulation results and other experimental[67] and theoretical results[68], we propose a model which can explain the dependence of protein resistance of EG3-OMe SAMs on the gold and silver substrates[24] and the force-distance curve obtained from the AFM measurement.[25,65,66].

As seen from **Figure 5-6** and **5-7**, water molecules penetrate into the EG chains of the SAMs. Kreuzer *et al.* suggested that hydroxide ions adsorbed onto the EG3-OMe SAM form hydrogen bonding with water molecules inside the SAM.[68] The formation of the hydrogen bond not only increases the adsorption energy, but also increases the lateral diffusion barriers, thus reducing the mobility of the hydroxide ions. Direct incorporation of hydroxide ions into the EG chains is not possible because of the repulsive interaction between the negatively charged ion and the partially negatively charged ether oxygen atoms. On the contrary to EG3-OMe SAMs on gold, on surfaces where water molecules cannot penetrate into the film and form hydrogen bonds to the adsorbed ions, hydroxide ions are more mobile and therefore easily displaced by an approaching negatively charged AFM tip. Thus, the electrostatic repulsion would diminish, allowing other bonding forces to dominate and leading to an overall and dominating attractive force.

5.3 Simulation results versus neutron reflectivity measurements

Alon g with the simulations, we performed the neutron reflectivity measurements on the interface formed by the EG3-OMe terminated SAM on Au and deuterated water. The aim was to see whether such measurements can provide direct information about the distribution of density in the SAM/D_2O interface region.[50] The experimental results are shown in **Figure 5-9** as full circles. In the experimental cell used in the measurements, the SAM was prepared on a gold substrate deposited onto a bulk quartz crystal pre-coated with chromium. So, the sample under study represented a multilayer system SiO_2/Cr/Au/SAM/D_2O. The model adopted for the SAM substrate involved a total of five variable parameters: h_{Cr}, h_{Au}, $\sigma_{SiO_2/Cr}$, $\sigma_{Cr/Au}$ and $\sigma_{Au/SAM}$, where h and σ

denote the thickness and interfacial roughness, respectively. The SAM thickness, h_{SAM}, was initially fixed at a value averaged over different experimental measurements with a dry SAM (21.5 ± 1.5 Å).[50] The least-squares parameter fitting performed by minimization of the discrepancy factor

$$\chi^2 = \frac{1}{M-1}\sum_{i=1}^{M}\left(\frac{R_i^{model} - R_i^{observed}}{R_i^{observed}}\right)^2 , \qquad (5.1)$$

with respect to the five substrate parameters resulted in $\chi^2 = 0.052$. The respective model reflectivity of model 1 is shown in **Figure 5-9**.

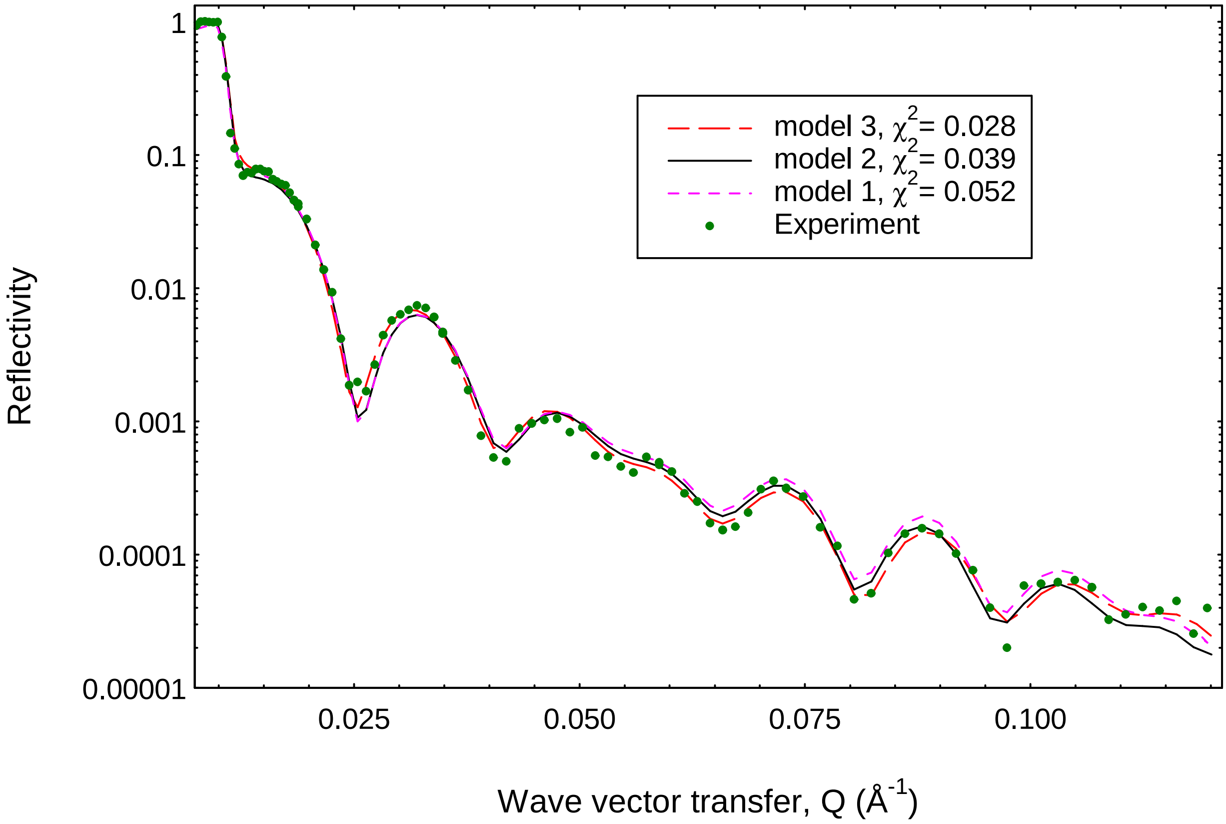

Figure 5-9 Experimental and calculated reflectivities for the Au-supported SAM in contact with deuterated water. Model 1: only thickness and roughness of each layer are considered. Model 2: the swelling of the SAM and penetration of water into the SAM are taken into account. Model 3: fit with an interphase water layer (87 % of bulk density and 40 Å thick) between the SAM and bulk water.

The obvious disadvantage of the model 1 is that it takes no account of the swelling of the SAM in water, which is accompanied by a perceptible increase in the

SAM thickness and, what is very important, in the neutron scattering length density of the EG3-OMe layer due to the penetration of deuterated water. Although the fact of water penetration was detected by the SFG measurements[106], no quantitative estimate for the amount of penetrated water could be obtained. By contrast, all this information can be easily deduced from our computer simulations.

Were the Au/SAM interface ideally smooth ($\sigma_{Au/SAM} = 0$), the contribution of the SAM and adjacent deuterated water to the neutron reflectivity could be calculated quite accurately, by representing the simulated density distribution just as it is shown in **Figure 5-10**, *i.e.* as a set of slices 0.4 Å in thickness. Regrettably, for the real Au/SAM interface, with a roughness of the order of 10 Å, this cannot be done. The reason is that the available methods of incorporating roughness into the calculation of reflectivity are only valid if the roughness is less than the thickness of the relevant layers.[109] This condition is obviously not fulfilled for the 0.4 Å thick slices. To avoid this problem, the simulated density distribution has to be coarsened into a small number of layers whose thickness is comparable with the interfacial roughness (model 2). The distribution shown in **Figure 5-10** is naturally divided into three distinct layers with substantially different scattering length densities:

(I) The alkanethiol layer of the SAM ($0 < z < 6$ Å);
(II) The interpenetration layer (6 Å $< z <$ 20 Å);
(III) The water layer adjacent to the SAM (20 Å $< z <$ 40 Å).

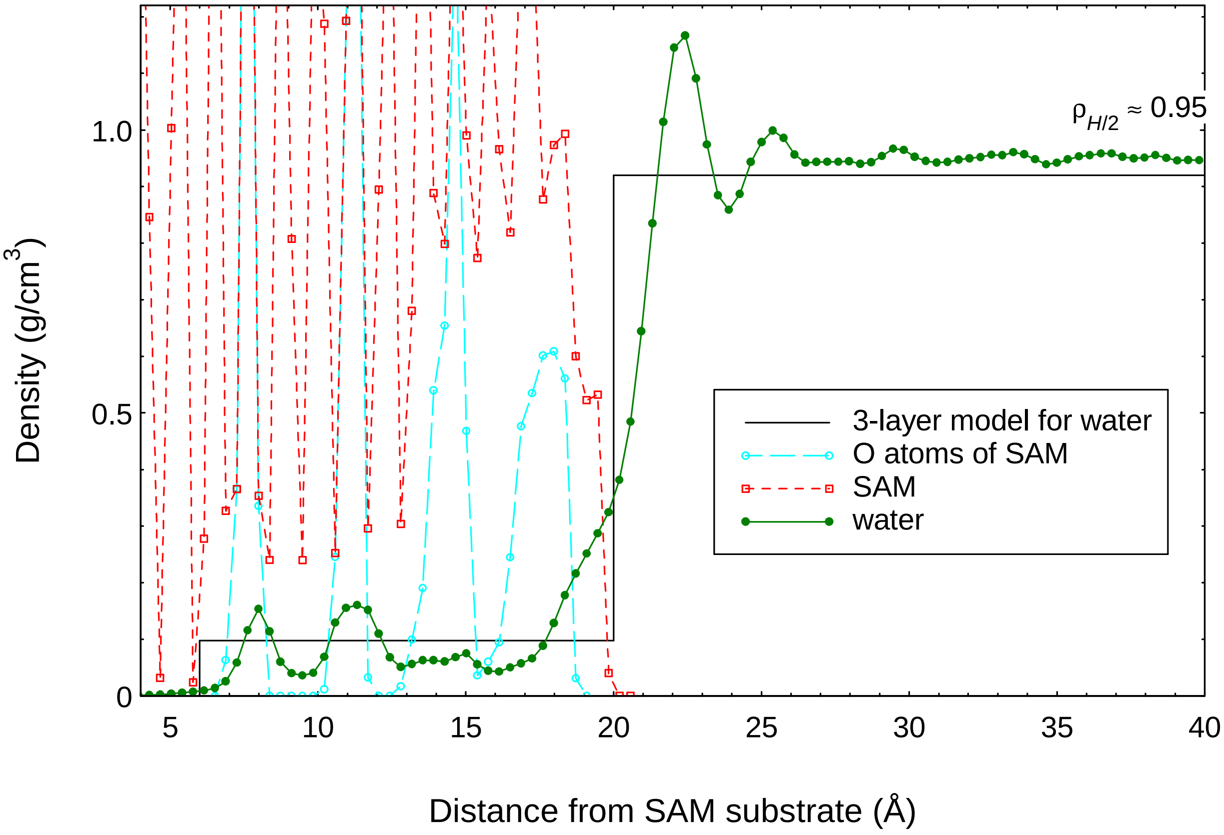

Figure 5-10. Density profiles near the interface formed by Au-supported SAM and water. 'SAM' denotes the density of non-hydrogen atoms.

The averaging of the water density in the respective layers gives $d^{(\mathrm{I})}_{\mathrm{D_2O}}$ = 0, $d^{(\mathrm{II})}_{\mathrm{D_2O}}$ = 9.8 % bulk water density, and $d^{(\mathrm{III})}_{\mathrm{D_2O}}$ = 92 % bulk water density. The latter value should however be corrected for the difference in configuration between the systems used in computer simulations and neutron reflectivity experiments. While the simulations dealt with water confined between two parallel SAMs H = 80 Å apart, the experiments were in essence concerned with semi-confined water formally corresponding to $H \to \infty$. Because of the hydrophobicity of the SAM, the density level of the confined water far from the interface, near the mid-point $z = H/2$, was depressed down to 95 % bulk density (**Figure 5-10**). Were the separation infinite, the mid-point density $d_{H/2}$ would be 100 % and $d^{(\mathrm{III})}_{\mathrm{D_2O}}$ would be higher. Assuming, for simplicity, proportionality between $d^{(\mathrm{III})}_{\mathrm{D_2O}}$ and $d_{H/2}$, we obtain $d^{(\mathrm{III})}_{\mathrm{D_2O}}$ = 0.92/0.95 = 97 %. That is, the

SAM can be considered to be in a practically direct contact with bulk water. (Subsequent calculations of the theoretical neutron reflectivity curve based on the coarse-grained density distribution showed that the 3 % density depression in layer (III) has a negligible effect on the calculated reflectivities and the quality of fit.)

The coarse-grained model of the SAM/water interphase should also be corrected for the difference in the alkane chain length between the simulations ($n = 3$) and experiments ($n = 11$). Considering that the alkanethiol layer I does not swell in water, we estimated its thickness from static lattice energy calculations of the isolated SAM. Minimization of the lattice energy of the SAM with respect to its orientational, translational and conformational parameters resulted in a structure where the (n - 1)-th (*i.e.* 10-th) carbon atom was at a distance of 11.3 Å from the gold substrate. This is just the required thickness of layer I. Note that the calculated thickness of the $S(CH_2)_{10}$ sublayer of the SAM is in agreement with the experimental thickness of the C11OH SAM (13.2 Å).[50] The difference is equal to ~2 Å, which is close to the projection of the terminal $–CH_2–OH$ fragment of the C11OH chain onto the surface normal.

The neutron reflectivity corresponding to the density model derived from our GCMC simulations is shown in **Figure 5-9** as a black solid line (model 2). The discrepancy factor χ^2 calculated for the simulation-based model is 0.039, which is noticeably better than that for the previous model based on the experimental thickness of the dry SAM. The improvement in the description of the experimental neutron reflectivity is particularly pronounced in the wave vector transfer range between 0.05 and 0.1 $Å^{-1}$. In general, the agreement of the simulation-based model with experiment can be regarded as fairly good considering the fact the model involves only five adjustable (substrate) parameters and no assumptions whatever concerning the density distribution in the SAM/water interphase region. The improvement in the quality of fit occurring on going from the "dry" to penetrable SAM model well demonstrate the utility of the simulations in interpreting neutron reflectivity data.

Further improvement in the quality of fit was achieved by extending the simulation-based model to include an "interphase water" (IW) layer between the SAM and bulk water (model 3). Both the thickness and density of this layer were treated as variables, so that the total number of adjustable parameters increased to seven. The minimization of the discrepancy factor with respect to the seven variable parameters resulted in $\chi^2 = 0.028$ and the neutron reflectivity curve shown in **Figure 5-9**. The IW layer proved to be 40 Å thick and to have a density of 87 % bulk water density, even less than that of ice (92 %). The physical meaning of this result is still unclear. Based on our own simulation results and the available literature on computer simulation of water near various surfaces, it is difficult to imagine that the so strong density depression over the so extended separation range can originate from the true effect of the SAM on the adjacent water region. A likely reason of the observed density depression is the presence of air nanobubbles at the SAM/water interface, similar to those observed by Ishida and other authors.[110-114] The surmisable role of air nanobubbles is confirmed by the experimentally observed differences in neutron reflectivity between SAM/D_2O interfaces formed by degassed and non-degassed D_2O.[50]

Conclusions

In this work, water molecules near model organic surfaces and hydration forces between them were investigated using the grand canonical Monte Carlo (GCMC) technique.

In **Chapter 1**, we discussed the meaning of ‘hydrophobic’ and ‘hydrophilic’ in terms of interfacial tension, water contact angle, and hydration force. It is concluded that the hydration force can be used as a criterion for ‘hydrophilic’ or ‘hydrophobic’, if the interfacial tension is a monotonic function of the surface-to-surface separation. Thus, if the hydration force is used as criteria, it must be investigated at large separations, where the oscillations in the interfacial tension decay.

In **Chapter 3**, an atomistic force field fitted to *ab initio* MP2 level energies and geometries of 1,2-dimethoxyethane (EG1) and EG1-water complexes[91] was tested for transferability to methoxy terminated tri(ethylene glycol) (EG3) and its complexes with water. The test was based on a comparison of the force field predictions for EG3 and EG3-water complexes with the respective results of recent *ab initio* calculations using density functional theory (DFT).[34] The force field well reproduced the structure and stability sequence of EG3 and EG3-water conformers but yielded noticeably higher EG3-water binding energies. Most of the difference in binding energy was associated with differences between the *ab initio* methods used in parametrization (MP2) and testing (DFT) of the force field. The agreement between the force field and *ab initio* DFT predictions can be improved by introducing an additional fitting parameter, like dielectric permittivity, which attenuates the electrostatic terms of the EG3-water potential. However, the MD simulation by Bedrov *et al.*[91] showed that the use of a slightly weaker EG1-water interaction potential yields an immiscible system, contrary to experimental evidence. Based on this result, we employed the original force field in the simulations of water and tri(ethylene glycol) terminated alkanethiol (EG3-OMe) SAMs.

In **Chapter 4,** we studied the hydration forces between structureless flat walls. Most attention was given to large wall-to-wall separations, where the force oscillations due to the water layering effects decayed and the sign of the hydration pressure can be used as a criterion for the hydrophilicity/hydrophobicity of the walls. For the wall with the weakest interaction with water (ε = 0.46 kcal mole^{-1}), we observed capillary evaporation at $H \leq 58.4$ Å and a strong attraction due to density depression at larger H. In the latter case, the magnitude of hydration force, p_h substantially exceeded bulk pressure, p_b (the upper limiting pressure due to evaporation), which cast some doubt on the treatment of capillary evaporation as the main source of hydrophobic attraction.

Our results for the hydrophilic walls are, in some respects, opposite to the findings reported by Forsman *et al.*.[33] In contrast to the cited work,[33] we found that the inclusion of orientation dependent terms in the water-wall interaction potential added an attractive contribution to the hydration force by making the confined region less favorable for water from both the entropic and energetic points of view. While the loss in entropy can be well understood in terms of the surface-induced orientational ordering and confinement of the librational motion of water molecules, the reasons of the energy loss are not so apparent. One is the reduction of the water-water contribution to the internal energy due to the disturbance of the hydrogen bonding network natural for water. Another reason has to do with constraints imposed by the directionality of the hydrogen bond upon the ability of water molecules to form multiple hydrogen bonds with the surface. In the model potentials used in describing the water-surface interaction, the orientation dependence of the hydrogen bond energy reflects not only the intrinsic trend of the hydrogen bond to linearity but also the flexibility of the surface groups involved in the hydrogen bonding, *i.e.* the ability of these groups to adapt their orientations to the approaching water molecules. The confinement of this ability should obviously be energetically unfavorable.

In **Chapter 5** we simulated the hydration forces operating between the EG3-OMe terminated SAMs on the Au and Ag substrates. As far as we know, this is a first simulation study of the water-mediated forces between organic surfaces, based on a realistic molecular model and force field. Despite the experimentally observed water wettability of the SAMs (the water contact angle being ~65° for both SAMs on Au and Ag substrates[24]), the effect of the SAMs on confined water is typical of hydrophobic surfaces. The main manifestations of hydrophobicity are, first, capillary evaporation experienced by water at small separations and, second, an attractive hydration pressure in conjunction with a noticeably reduced water density level between the SAMs.

The simulations described in this paper suggest that the fundamental difference between the Ag- and Au-supported SAMs is the lower areal density of the latter. Due to this difference, the Au-supported SAM is penetrable for water, while the SAM prepared on Ag is not. The penetration of water deep into the Au-supported SAM is accompanied by conformational disordering and redistribution of conformer populations, such that the helical conformation practically disappears and the most populated conformer of the EG3-OMe tails becomes all-*trans*.

The simulations showed that the effect of the Au-supported SAMs on the structure of the adjacent water layers is remarkably small. In view of this finding, the protein resistance of the SAM can hardly be ascribed to a protective coat of structured water, as is frequently speculated in the chemical and biological literature to explain the force preventing colloid particles, macromolecules or surfaces from direct contact. The hydration force cannot explain the protein resistance: Both the Au- and Ag-supported SAMs behave as a hydrophobic surface and attract each other.

We proposed a model which can explain the AFM results by Dicke *et al*[65,66] and the dependence of protein resistance on substrate[24]. Electrokinetic studies by Chan *et al*. showed that EG3-OMe SAMs has charging patterns which are attributed to preferential hydroxide ion adsorption as observed on other non-ionic SAMs.[67] In cases of surfaces, which trap water molecules inside, such as gold-supported EG3-OMe SAMs, the trapped water molecules form hydrogen bonds with the hydroxide ions at the SAM-water interface and reduce the mobility of the hydroxide ions.[68] As a result, the EG3-OMe SAM on gold repels a negatively charged AFM tip in aqueous environment. Contrary, on silver-supported EG3-OMe and n-alkanethiol SAMs, which are not penetrable for water, hydroxide ions are mobile and easily displaced by the AFM tip, and other bonding forces will be dominant. As a consequence, these surfaces attract the AFM tip or protein molecules in aqueous environment.

References

(1) Gregory, R. B. *Protein-Solvent interactions*; Marcel Dekker, Inc.: New York, **1995**.

(2) Robinson, G. W.; Zhu, S.; Singh, S.; Evans, M. V. *Water in biology, chemistry and physics: experimental overviews and computational methologies*; World Scientific: Singapore, New Jersey, London, Hong Kong, **1996**.

(3) Vogler, E. A. *Advances in Colloid and Interface Science* **1998**, 74, 69.

(4) Vogler, E. A. *Water in Biomaterials Surface Science*; John Wiley & Sons, Ltd., **2001**.

(5) Ball, P. H_2O: *A biography of water*; Weidenfeld & Nicolson: London, **1999**.

(6) Chaplin, M., '*Water structure and behavior*' http://www.sbu.ac.uk/water/, **2003**.

(7) Stanley, H. E.; Buldyrev, S. V.; Canpolat, M.; Havlin, S.; Mishima, O.; Sadr-Lahijany, M. R.; Scala, A.; Starr, F. W. *Physica D* **1999**, 133, 453.

(8) Stanley, H. E.; Buldyrev, S. V.; Canpolat, M.; Meyer, M.; Mishima, O.; Sadr-Lahijany, M. R.; Scala, A.; Starr, F. W. *Physica A* **1998**, 257, 213.

(9) Soper, A. K.; Bruni, F.; Ricci, M. A. *J. Chem. Phys*. **1997**, 106, 247.

(10) Nezbeda, I.; Slovak, *J. Mol. Phys.* **1997**, 90, 353.

(11) Palma, M. U.; Biagio, P. L. S.; Bulone, D.; Palma-Vittorelli, M. B. *Hydrogen Bond Networks*; Kluwer Academic Publishers: Dordrecht Hardbound, **1994**.

(12) Israelachvili, J.; Wenerstroem, H. *Nature* **1996**, 379, 219.

(13) Vogler, E. A. *In Water in Biomaterials Surface Science*; Morra, M., Ed.; John Wiley & Sons, Ltd., **2001**.

(14) Israelachvili, J. *Intermolecular and Surface Forces*; Academic Press: London, **1992**.

(15) Lyklema, J. *Fundamentals of Interface and Colloid Science I: Fundamentals*; Academic: London, **1991**.

(16) Lyklema, J. *Fundamentals of Interface and Colloid Science II: Solid-Liquid Interfaces*: London, **1991**.

(17) Leckband, D.; Israelachvili, J. *Quarterly Reviews of Biophysics* **2001**, 34, 105.

(18) Verwey, E. J.; Overbeek, J. T. G. *The theory of the Stability of Lyophobic Colloids*; Elsevier: Amsterdam, **1948**.

(19) Ulman, A. *Chem. Rev.* **1996**, 96, 1533.

(20) Swalen, J. D.; Allara, D. J.; Andrade, J. D.; Chandross, E. A.; Garoff, S.; Israelachvili, J.; McCarthy, T. J.; Murray, R.; Pease, R. F.; Rabolt, J. F.; Wynne, K. J.; Yu, H. *Langmuir* **1987**, 3, 932.

(21) Dubois, L. H.; Nuzzo, R. G. *Annu. Rev. Chem.* **1996**, 43, 437.

(22) Ulman, A. *An Introduction to Ultrathin Organic Films*; Academic Press: Boston, **1991**.

(23) Prime, K. L.; Whitesides, G. M. *J. Am. Chem. Soc.* **1993**, 115, 10714.

(24) Harder, P.; Grunze, M.; Dahint, R.; Whitesides, G. M.; Laibinis, P. E. *J. Phys. Chem. B* **1998**, 102, 426.

(25) Feldman, K.; G. Haehner; Spencer, N. D.; Harder, P.; Grunze, M. *J. Am. Chem. Soc* **1999**, 121, 10134-10141.

(26) Allen, M. P.; Tildesley, D. J. *Computer Simulation of Liquids*; Oxford Science Publications, **1986**.

(27) Svensson, B.; Woodward, C. E. *J. Chem. Phys.* **1994**, 100, 4575.

(28) Forsman, J.; Joensson, B.; Woodward, C. E. *J. Phys. Chem*: **1996**, 100, 15005.

(29) Forsman, J.; Joensson, B.; Woodward, C. E.; Wennerstroem, H. *J. Phys. Chem. B* **1997**, 101, 4253.

(30) Wallqvist, A.; Berne, B. J. *J. Phys. Chem.* **1995**, 99, 2893.

(31) Lum, K.; Chandler, D.; Weeks, J. D. *J. Phys. Chem*. B **1999**, 103, 4570.

(32) Luzar, A.; Bratko, D.; Blum, L. *J. Chem. Phys.* **1987**, 86, 2955.

(33) Forsman, J.; Woodward, C. E.; Joensson, B. *Langmuir* **1997**, 13, 5459.

(34) Wang, R. L. C.; Kreuzer, H. J.; Grunze, M. *Phys. Chem. Chem. Phys*. **2000**, 2, 3613.

(35) Evans, R.; Marconi, U. M. B. *J. Chem. Phys.* **1987**, 86, 7138.

(36) Besseling, N. A. M. *Langmuir* **1997**, 13, 2113.

(37) Valleau, J. P.; Gardner, A. A. *J. Chem. Phys.* **1987**, 86, 4162.

(38) Grigera, J. R.; Kalko, S. G.; Fischbarg, J. *Langmuir* **1996**, 12, 154.

(39) Joensson, B. *Chem. Phys. Lett.* **1981**, 82, 520.

(40) Marchesi, M. *Chem. Phys. Lett.* **1983**, 97, 224.

(41) Matsuoka, O.; Yoshimine, M.; Clementi, E. *J. Chem. Phys.* **1976**, 64, 1351.

(42) Stillinger, F. H.; Rahman, A. *J. Chem. Phys.* **1972**, 57, 1281.

(43) Lee, C. Y.; McCammon, J. A.; Rossky, P. J. *J. Chem. Phys.* **1984**, 80, 4448.

(44) Du, Q.; Freysz, E.; Shen, Y. R. *Science* **1994**, 264, 826.

(45) Scatena, L. F.; Brown, M. G.; Richmond, G. L. *Science* **2001**, 292, 908.

(46) Kjellander, R.; Marcelja, S. *Chem. Phys. Lett.* **1985**, 120, 393.

(47) Lee, S. H.; Rossky, P. J. *J. Chem. Phys.* **1994**, 100, 3334.

(48) Wallqvist, A. *Chem. Phys. Lett. 1990*, 165, 437.

(49) Cheng, L.; Fenter, P.; Nagy, K. L.; Schlegel, M. L.; Sturchio, N. C. *Phys. Rev. Lett.* **2001**, 87, 156103.

(50) Schwendel, D.; Hayashi, T.; Steitz, R.; Schreiber, F.; Dahint, R.; Pertsin, A.; Grunze, M. *Langmuir* **2002**.

(51) Besseling, N. A. M.; Lyklema, J. *Pure & Appl. Chem.* **1995**, 67, 881.

(52) Sakurai, M.; Tamagawa, H.; Ariga, K.; Kunitage, T.; Inoue, Y. *Chem. Phys. Lett* **1998**, 289, 567-571.

(53) Booth, M. J.; Duh, D.-M.; Haymet, A. D. J. *J. Chem. Phys.* **1994**, 101, 7925.

(54) Spohr, E. *J. Chem. Phys.* **1997**, 106, 388.

(55) Israelachvili, J. N. *Surface Science Reports* **1992**, 14, 109.

(56) Israelachvili, J. N.; Adams, G. *J. Chem. Soc. Faraday Trans. I* **1977**, 74, 975.

(57) Tsao, Y.-H.; Evans, D. F.; Wennerstroem, H. *Science* **1993**, 262, 547.

(58) Yoon, R.-H.; Flinn, D. H.; Rabinovich, Y. I. *J. Colloid and Interface Sci.* **1997**, 185, 363.

(59) Pashley, R. M. *J. Colloid Interface Sci.* **1981**, 83, 531.

(60) Pashley, R. M. *J. Colloid Interface Sci.* **1981**, 80, 153.

(61) Yaminsky, V. V.; Ninham, B. W. *Langmuir* **1993**, 9, 3618.

(62) Postma, J. P.; Berendsen, H. J. C.; Haak, J. R. *Faraday Symp. Chem. Soc.* **1982**, 17, 55.

(63) Jeon, S. I.; Lee, J. H.; Andrade, J. D.; Gennes, P. G. D. *J. Colloid and Interface Sci.* **1991**, 142, 149.

(64) Wang, R. L. C.; Kreuzer, H. J.; Grunze, M. *J. Phys. Chem B.* **1997**, 101, 9767.

(65) Dicke, C.; Haehner, G. *J. Phys. Chem. B* **2002**, 106, 4450.

(66) Dicke, C.; Haehner, G. *J. Am. Chem. Soc.* **2002**, 124, 12619.

(67) Chan, M.; Schweiss, R.; Werner, C.; Grunze, M. submitted **2003**.

(68) Kreuzer, H. J.; Wang, R. L. C.; Grunze, M. *J. Am. Chem. Soc.* **2003**, submitted.

(69) Metropolis, N.; Rosenbluth, A. W.; Rosenbluth, M. N.; Teller, A. H. *J. Chem. Phys.* **1953**, 21, 1087.

(70) Mezei, M. *Molecular Physics* **1987**, 61, 565.

(71) Mezei, M. *Molecular Physics* **1980**, 40, 901.

(72) Binder, K.; Ceperley, D. M.; Hansen, J. P.; Kalos, M. H.; Landau, D. P.; Levesque, D.; Mueller-Krumbhaar, H.; Stauffer, D.; Weis, J. J. *Monte Carlo Methods in Statistical Physics*; Springer-Verlag: Berlin Heidelberg New York, **1979**.

(73) Pertsin, A. J.; Grunze, M. *Langmuir* **1994**, 10, 3668.

(74) Pertsin, A. J.; Hahn, L.; Grossmann, H. P. *J. Comput. Chem.* **1994**, 15, 1121.

(75) Deitrick, G. L.; Scriven, L. E.; Davis, H. T. *J. Chem. Phys.* **1989**, 90, 2370.

(76) Swendsen, R. H.; Wang, J.-S. *Phys. Rev. Lett.* **1987**, 58, 86.

(77) Shelley, J. C.; Patey, G. N. *J. Chem. Phys*. **1995**, 102, 7656.

(78) Fenter, P.; Eigenberger, P.; Li, J.; III, N. C.; Bernasek, S.; Scoles, G.; Ramanaranan, T. A.; Liang, K. S. *Langmuir* **1991**, 9, 1082.

(79) Camilone, N.; Chidsey, C. E. D.; Liu, G. Y.; Scoles, G. J. *J. Chem. Phys.* **1993**, 98, 4843.

(80) Pertsin, A. J.; Grunze, M. *Langmuir* **2000**, 16, 8829.

(81) Pertsin, A. J.; Kitaigorodsky, A. I. *The Atom-Atom Potential Method Applications to Organic Molecular Solids*; Springer, **1987**.

(82) Jorgensen, W. L. *J. Am. Chem. Soc.* **1981**, 103, 335.

(83) Shelley, J. C.; Patey, G. N. *Molecular Physics* **1996**, 88, 385.

(84) Ewald, P. *Ann. Phys.* **1921**, 64, 253.

(85) Smith, G. D.; Jaffe, R. L.; Yoon, D. Y. *J. Phys. Chem.* **1993**, 97, 12752-12759.

(86) Sorensen, R. A.; Liau, W. B.; Kesner, L.; Boyd, R. H. *Macromolecules* **1988**, 21, 200.

(87) *Handbook of Chemistry and Physics*; Weast, R. C., Ed.; The Chemical Rubber Co., **1964**.

(88) Hautman, J.; Klein, M. *Mol. Phys.* **1992**, 75, 379.

(89) Heyes, D. M.; Swol, F. v. *J. Chem. Phys*. **1981**, 75, 5051.

(90) Pertsin, A. J.; Grunze, M.; Garbuzova, I. A. *J. Phys. Chem. B* **1998**, 102, 4918

(91) Bedrov, D.; Pekny, M.; Smith, G. D. *J. Phys. Chem. B* **1998**, 102, 996.

(92) Smith, G. D.; Borodin, O.; Bedrov, D. *J. Comput. Chem.* **2002**, 23, 1480.

(93) Bedrov, D.; Borodin, O.; Smith, G. D. *J. Phys. Chem. B* **1998**, 102, 5683.

(94) Pertsin, A. J.; Hahn, J.; Grossmann, H. P. *J. Comput. Chem.* **1994**, 15, 1121.

(95) Hautman, J.; Klein, M. *J. Chem. Phys.* **1989**, 91, 4994.

(96) Hautman, J.; Klein, M. L. *J. Chem. Phys.* **1990**, 93, 7483.

(97) Nuzzo, R. G.; Zegarski, B. R.; Dubois, L. H. *J. Am. Chem. Soc.* **1987**, 109, 733.

(98) Jorgensen, W. L.; Chandrasekhar, J.; Madura, J. D.; Impey, R. W.; Klein, M. L. *J. Chem. Phys.* **1983**, 79, 926-935.

(99) Hermans, J.; Pathiaseril, A.; Anderson, A. *J. Am. Chem. Soc.* **1988**, 110, 5982.

(100) Takahashi, Y.; Tadokoro, H. *Macromolecules* **1973**, 6, 672.

(101) Takahashi, Y.; Sumita, I.; Tadokoro, H. *J. Poly. Sci.* **1973**, 11, 2113.

(102) Hayashi, T.; Morikawa, Y.; Nozoye, H. *J. Chem. Phys*. **2001**, 114, 7615.

(103) Dubois, L. H.; Zegarski, B. R.; Nuzzo, R. G. *J. Chem. Phys.*, **1983**, 98, 678.

(104) Fenter, P.; Eisenberger, P.; Fisher, A. J.; Ismail, O. *Phys. Rev. Lett.* **1995**, 70, 2447.

(105) Laibinis, P. E.; Whitesides, G. M.; Allara, D. L. *J. Am. Chem. Soc.* **1991**, 113, 7152.

(106) Zolk, M.; Eisert, F.; Pipper, J.; Herrwerth, S.; Eck, W.; Buck, M.; Grunze, M. *Langmuir* **2000**, 16, 5849.

(107) Dicke, C.; Feldman, K.; Eck, W.; Herrwerth, S.; Haehner, G. *Polymer Prepr.* **2000**, 41, 1444.

(108) Karraker, K. A.; Radke, C. *J. Adv. Colloid. Interfaces.* **2002**, 96, 231.

(109) Nevot, L.; Croce, P. *Revue Phys. Apll.* **1980**, 15, 761.

(110) Ishida, N.; Inoue, T.; Miyahara, M.; Higashitani, K. *Langmuir* **2000**, 16, 6377.

(111) Ishida, N.; Sakamoto, M.; Miyahara, M.; Higashitani, K. *Langmuir* **2000**, 16, 5681.

(112) Tyrrell, J. W. G.; Attard, P. *Phys. Rev. Lett.* **2001**, 87, 176104.

(113) Tyrrell, J. W. G.; Attard, P. *Langmuir* **2002**, 18, 160.

(114) Carambassis, A.; Jonker, L. C.; Attard, P.; Rutland, M. W. *Phys. Rev. Lett.* **1998**, 80, 5357.

Acknowledgements

First, I would like to thank Prof. Dr. Michael Grunze, my supervisor. Without his kind invitation, continual understanding and financial support, provision of interesting topics and helpful discussions, I would not have had the opportunity to finish my Ph. D here in Heidelberg. Also I am grateful to him for providing me with the chance to attend international and national symposiums.

I would like to thank Prof. Dr. Joachim P. Spatz for his kind agreeing to be my supervisor.

I would like to thank Prof. Dr. Alexander J. Pertsin for a lot of advices on computer simulation and his critical reading of this thesis. I really appreciate his encouragement, patience, and crushing jokes. His attitude to science really impressed me. I will never delete about 800 e-mails we exchanged between Heidelberg and Moscow from my hard disk.

Special thanks must go to Dr. Reiner Dahint, our group leader, in Heidelberg. His adequate advices on our work and humor are acknowledged. I also have to thank him for providing me a room, when I came to Germany one day earlier.

I must thank Dr. Dirk Schwendel for working together and giving me a lot of jokes and ideas concerning chemistry. His many helps in my life in Germany are unforgettable.

I also acknowledge the helps from my friends in our institute, Dr. Berthold Völkel, Dr. Karin Heister, and Dr. Claudia Gries. I thank them for introducing me German cultures and taking me to restaurants and Kinos.

My thanks go to Dr. Andreas Eisele, the administrator of our network and ‘music server’ APC-SV1 for many helps on the maintenance of the network and a lot of discussions about music and jogging.

I thank my colleague Sabina Tatur for telling me many things about Poland and other countries and for very interesting and stimulating conversation between us.

I thank Ulf Fritz for giving me ‘very useful’ computer software, Without him, maybe I would have been still interested in working in computer software companies!

Thanks to Dr. Meik Ranft for giving me many advice on computers and software in the early stage of the course of my Ph. D.

I would like to thank Dr. Marco Maccarini for many discussions about water-solid interfaces and nanobubbles.

I also would like to thank my Chinese and Taiwanese friends, Dr. Yang Jie Yong and Yian Tai for their help and hospitality. I really enjoyed the wonderful meals Yian cooked. Thanks to Russian friends Dr. Andrey Chaporenko and Dr. Yan Zubavichus for nice conversations on differences in our cultures as well as science.

I would like to say thank you to Wouter Roos and Dr. Tamas Haraszti for showing and explaining their interesting works to me.

I thank the member of "Team APC". Since I had never played football in Japan, it was really good experience. I would like to thank Dr. Alexander Lampert for teaching me bicycle sports.

A special "Danke!" to Frau Edeltraud Boczek for everything she did for me. And many thanks to Robert Läufer for his helpful administrative works. Especially I thank Frau Inge Corre. It is amazing that she convinced Frau Anita Pidde to share her apartment with me, before I came here.

Many thanks to Peter Jeschka for his help in the administration of our network and the maintenance of our computers. Many helps and encouragements from Günter Meinusch must be acknowledged.

I am very indebted to Dr. Shuzo Tokumitsu for teaching me how to get Japanese foods in Germany and for bringing us to many wineries.

Very special thanks must go to 'Meine Deutsche Mutter' Frau Anita Pidde for her help during my stay in Eppelheim. She took care of many things, when I started living in Germany. I will never forget your hospitality and I want to visit you, at least, once a year after my Ph. D.

I would like to thank Japanese wine friends in Germany, Mr. Sasai and Keller Meister Mr. Nakatani, for inviting me to their wine party in Frankfurt many times.

Many thanks to my friends in Japan (Shinsuke Kubo, Kensuke Kimura, Masayuki Komine, Akira Isogai, Takeshi Kuwabara, Tomonao Matsushita, Tomoya Sugisawa, Tomomi Sano, Naoko Takenaga, Naoyuki Otani, the members of the tennis club in Sony Information System Solutions, and so on…) for sending me encouraging and stimulating e-mails from Japan.

I thank Sanwa Electronic Co. Ltd for financial support during my Ph. D. course. I thank also the staffs of the company for giving me encouraging e-mails and coming to our wedding ceremony. I'm really looking forward to working with you.

A special mention must go to my parents for supporting me through my Ph. D.

And Yoko, for her love, dedication, and belief in me. Also for cooking wonderful meals! Without her continual support and encouragement, it would not have been possible for me to finish my Ph. D.

Tomohiro Hayashi

Ich erkläre hiermit, daß ich die vorliegende Dissertation selbst verfaßt und mich dabei keiner anderen als der von mir bezeichneten Quellen und Hilfsmittel bedient habe. Ich habe an keiner anderen Stelle ein Prüfungsverfahren beantragt oder die Dissertation in dieser oder anderer Form bereits anderweitig als Prüfungsarbeit verwendet oder einer anderen Fakultät als Dissertation vorgelegt.

Heidelberg, den 20.03.2003

Tomohiro Hayashi

Address:
tomo@sanwa-hs.co.jp
tomohiro_hayashi@hotmail.com
http://tomohitoh.tripod.com